Title

Stability Constants Important to the Understanding of Plutonium in Environmental Waters - Hydroxy and Carbonate Complexation of PuO{sub 2}{sup +}

Author

Bennett, D.A.

Publication Date

1990-04-01

LBL-28963

Lawrence Berkeley Laboratory
UNIVERSITY OF CALIFORNIA

Stability Constants Important to the Understanding of Plutonium in Environmental Waters—Hydroxy and Carbonate Complexation of PuO_2^+

D.A. Bennett
(Ph.D. Thesis)

April 1990

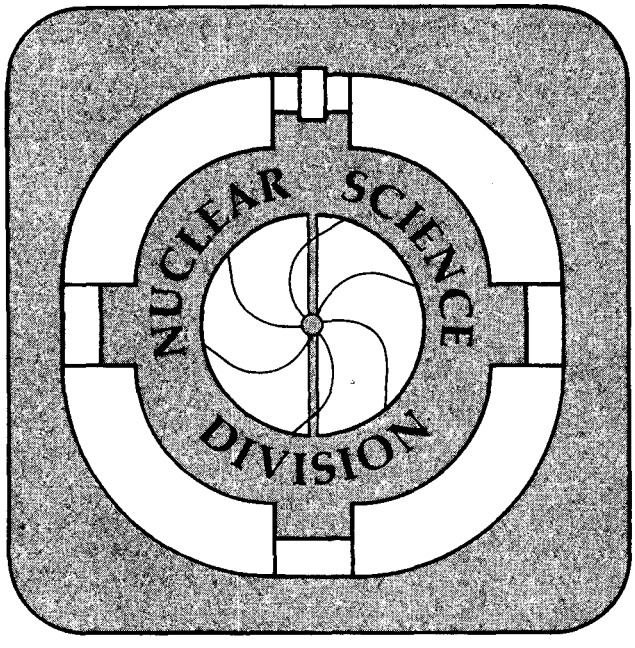

Prepared for the U.S. Department of Energy under Contract Number DE-AC03-76SF00098.

DISCLAIMER

LBL-28963

Stability Constants Important to the Understanding of Plutonium in Environmental Waters-Hydroxy and Carbonate Complexation of PuO_2^+

Dianne Angelo Bennett

Ph. D. Thesis

Department of Chemistry
University of California
Berkeley, CA 94720

and

Nuclear Science Division
Lawrence Berkeley Laboratory
Berkeley, CA 94720

April 20, 1990

This work was supported in part by the Yucca Mountain Project, Nevada Operations Office, U.S. Department of Energy Office of Civilian Radioactive Waste Management, Lawrence Livermore National Laboratory under contract W-7405-ENG-48, and Director, Office of Energy Research, Division of Nuclear Physics of the Office of High Energy and Nuclear Physics of the U.S. Department of Energy under contract DE-AC03-76SF00098.

Stability Constants Important to the Understanding of Plutonium in Natural Waters--Hydroxy and Carbonate Complexation of PuO_2^+

Dianne Angelo Bennett

ABSTRACT

The formation constants for the reactions $PuO_2^+ + H_2O = PuO_2(OH) + H^+$ and $PuO_2^+ + CO_3^{2-} = PuO_2(CO_3)^-$ were determined in aqueous sodium perchlorate solutions by laser-induced photoacoustic spectroscopy. The molar absorptivity of the PuO_2^+ band at 569 nm decreased with increasing hydroxide concentration. Similarly, spectral changes occurred between 540 and 580 nm as the carbonate concentration was increased. The absorption data were analyzed by the non-linear least-squares program SQUAD to yield complexation constants. For the hydrolysis reaction at 0.1 M ionic strength, log $^*\beta_{11}(0.1) = -9.73 \pm 0.10$, and for the first carbonate complexation constant at 0.5 M ionic strength, log $\beta_{11}(0.5) = 4.60 \pm 0.04$. Using the specific ion interaction theory, both complexation constants were extrapolated to zero ionic strength: for hydrolysis, log $^*\beta_{11}(0) = -9.73 \pm 0.10$, and for carbonate complexation, log $\beta_{11}(0) = 5.10 \pm 0.06$. These thermodynamic complexation constants were combined with the oxidation-reduction potentials of Pu to obtain Eh versus pH diagrams.

Dedication

This thesis is dedicated with special thanks to those people who have helped me develop as a scientist and human being:

- My parents, Jim and Louise Angelo, who have continually given me encouragement and support and recently the babysitting necessary to finish these experiments.

- My research advisor, Dr. Darleane Hoffman, who provided me with unique scientific opportunities and gave me the freedom to choose among them.

- Dr. David Forkey and Dr. John Russell of California State University, Sacramento, who introduced my to the frustrations and rewards of research.

- My son, Mick, who has brought me the joys of motherhood.

- Last but not least, my husband, Michael, whose support, encouragement, and periodic pep talks have made this accomplishment possible.

Acknowledgements

The author is grateful to the other members of the LBL Heavy Ion Radiochemistry Group (D. C. Hoffman, D. M. Lee, M. J. Nurmia, K. E. Gregorich, R. A. Hendersen, J. D. Leyba, H. L. Hall, and G. T. Seaborg) and collaborators (H. Nitsche, R. A. Torres, P.A. Baisden, R. J. Silva, C. E. A. Palmer, R. Russo, J. E. Andrews, and P. Robouch) for their assistance.

This work was supported in part by the Yucca Mountain Project, Nevada Operations Office, U.S. Department of Energy Office of Civilian Radioactive Waste Management, Lawrence Livermore National Laboratory under contract W-7405-ENG-48, and Director, Office of Energy Research, Division of Nuclear Physics of the Office of High Energy and Nuclear Physics of the U.S. Department of Energy under contract DE-AC03-76SF00098.

The author wishes to thank the U.S. Department of Energy's Heavy Element Production Program at Oak Ridge National Laboratory for the ^{242}Pu.

Contents

List of Figures

List of Tables

Chapter 1

INTRODUCTION

Currently, the growth of commercial nuclear power has slowed in the United States for a variety of reasons. One of these reasons is the concern over the possible hazard to future generations from the radioactive wastes generated from the operation of nuclear power plants. In response to this concern, the U. S. is developing strategies for long-term storage and isolation of nuclear wastes for perhaps hundreds of thousands of years [1.1]. Because it is difficult to conduct experiments which simulate this length of time or the complex chemical systems of

the radioactive waste effluents, computer modelling is used to predict behavior [1.2]. The reliability of these models depends strongly on the accuracy of the modelling data base. Recently, Congress selected the Yucca Mountain area at the Nevada Test Site as an underground repository for radioactive wastes. Therefore, chemical and geochemical characterization of this site is needed.

The behavior of plutonium during long-term storage is especially important in planning the repository. There are two possible waste forms for plutonium. The "spent" fuel element of commercial nuclear waste is stored directly, since reprocessing of commercial fuel is not currently allowed in the U. S.. Defense-related wastes are reprocessed, and it is proposed that the plutonium is reduced to its highly stable oxide form ($PuO_{2(S)}$) which is fixed in a solid matrix such as borosilicate glass, a ceramic, or a synthetic "rock". Either waste form can then be encapsulated in a multiple barrier system which provides further protection beyond that inherent in the geology, hydrology, and geochemistry of the repository itself. These multiple barriers are

designed to ensure containment of the radionuclides in the repository site and further reduce the risk of migration into the biosphere. There are five primary considerations in planning a multiple barrier system:

1. a waste form of high stability;
2. containment of the waste form in a canister and packing materials of high corrosion resistance and durability;
3. engineered or artificial overpack around the canister which has high sorptive properties for the radionuclides which might be released by dissolution of the canister and waste form;
4. the geologic medium itself including its geochemical and hydrological properties;
5. the distance to population centers and water supplies.

However, when the time frame of isolation spans hundreds of thousands of years, rupture of the barriers and contact of the waste with natural waters might be possible. This interaction could result in a slow leaching and dissolution process where the solubility of plutonium in environmental waters is largely determined by hydrolysis and

carbonate complexation [1.3-5]. The formation constants for these processes are of particular importance to the thermodynamic data base of the Yucca Mountain region because the natural waters in this vicinity are slightly basic (pH range 6.9 - 7.7), carbonate rich (120 - 170 ppm), and oxidizing (Eh = 700 mV). Table 1.1 lists the composition of Yucca Mountain groundwater.

Table 1.1: Composition of groundwater in the vicinity of Yucca Mountain [1.6]

Element	Range (mg/l)
Ca	1-20
Mg	0.05-2
Na	45-95
K	1-5
Li	0.05-0.4
Fe	0.01-0.05
Mn	0.01-0.03
Al	0.004-0.03
Si	20-30
Species	
HCO_3^-	120-170
Cl^-	5.5-7.7
SO_4^{2-}	18-28
NO_3^-	0.6-10
F^-	1.0-4.5
O_2	1.8-6.4
pH	6.9 to 7.7
Eh	600 to 800 mV

Plutonium has four principal oxidation states in aqueous solution: Pu^{3+}, Pu^{4+}, PuO_2^+, PuO_2^{2+}. The solution conditions (pH, Eh, salinity, complexing anions, etc.) govern which oxidation state or states will be

predominant. In 1982, B. Allard calculated the solubility and speciation of plutonium in the pH range 5-11 under four different atmospheres with varying CO_2 compositions, considering formation of hydroxy and carbonate complexes only [1.3]. The results of Allard's calculations are shown in Figure 1.1. In the pH range of 6 to 8, $Pu(OH)_4$ is calculated to be the major soluble species in solution. PuO_2^+ is predicted to dominate the overall solubility from pH 5-6 and PuO_2^+ carbonate complexes play a varying role at pH values above 8. It is also important to note that the calculated overall solubility of plutonium is independent of the carbonate concentration.

This predicted behavior of plutonium contradicts the results of several solubility experiments. Solubilty studies have shown that the pentavalent oxidation state is the predominant soluble species under a wide variety of environmental conditions. Bondietti and Reynolds determined that 95% of the soluble plutonium existed as PuO_2^+ and PuO_2^{2+} in neutral 0.1 mM carbonate solution [1.7]. Nelson found PuO_2^+ to be the principal oxidation state in sea water, lake water, and bicarbonate

solutions [1.8]. Rai, Serne, and Swanson discovered that solutions in equilibrium with PuO_2 solid contain PuO_2^+ as the dominant species under oxic conditions at pH below 7 [1.9]. These findings were further verified by Nitsche [1.10,11] and Edelstein [1.10], who also demonstrated that the presence of carbonate increases the overall solubility of plutonium by as much as 4000 times (see Table 1.2).

Table 1.2: Solubility study illustrating the increased solubility of plutonium in the presence of carbonate [1.10]

Initial species	Solubility in moles/liter		Increased solubility in the presence of carbonate
	0.1 M $NaClO_4$	Yucca Mtn grdwater	
+4	3×10^{-8}	2×10^{-6}	67
+5	2×10^{-9}	8×10^{-6}	4000
+6	1×10^{-7}	3×10^{-5}	300

Measurement of the hydrolysis ($*\beta_n$) and carbonate complexation (β_n) constants of PuO_2^+ should provide the additional input parameters necessary to resolve the discrepancy between Allard's calculations and results of the solubility experiments. These reactions and the corresponding stability constants are described in Eq. 1.1 and 1.2, respectively. Because the hydrogen ion dependence is found in the numerator of Eq. 1.1b, it is distinguished with an asterisk.

$$PuO_2^+ + n\,H_2O \rightleftharpoons (PuO_2(OH)_n)^{1-n} + n\,H^+ \qquad (1.1a)$$

$$*\beta_n = [(PuO_2(OH)_n)^{1-n}]\,[H^+]^n / [PuO_2^+] \qquad (1.1b)$$

$$PuO_2^+ + n\,CO_3^{2-} \rightleftharpoons (PuO_2(CO_3)_n)^{1-2n} \qquad (1.2a)$$

$$\beta_n = [(PuO_2(CO_3)_n)^{1-2n}] \,/\, [PuO_2^+]\,[CO_3^{2-}]^n \qquad (1.2b)$$

It might seem unusual that these fundamental reactions have not been measured for PuO_2^+. There are several reasons for this fact. The primary reason is that PuO_2^+ is thermodynamically unstable with respect to disproportionation in acidic solutions [1.12,13] as described by Eq. 1.3,

$$2\,PuO_2^+ + 4\,H^+ \rightleftharpoons Pu^{4+} + PuO_2^{2+} + 2\,H_2O \qquad (1.3)$$

Once disproportionation begins and a mixture of oxidation states is simultaneously present, additional reactions can also occur which are shown by Eqs. 1.4 and 1.5 [1.14].

$$PuO_2^+ + Pu^{3+} + 4\,H^+ \rightleftharpoons 2\,Pu^{4+} + 2H_2O \qquad (1.4)$$

$$PuO_2^+ + Pu^{4+} \rightleftharpoons PuO_2^{2+} + Pu^{3+} \qquad (1.5)$$

The combined effect of the reactions described by Eqs. 1.3, 4, and 5, is an overall increase in the concentrations of Pu^{3+}, Pu^{4+} and PuO_2^{2+} and depletion of PuO_2^+ in acidic solution [1.16].

Historically, plutonium chemistry has been conducted under acidic conditions where the pH was less than 1 and the plutonium concentrations were much greater than 10^{-3} M. PuO_2^+ is an unstable species under these conditions and, consequently, was treated as an unimportant oxidation state of plutonium. However, under environmental conditions, the pH is near neutral and plutonium concentrations are limited by solubility products in the $<10^{-9}$ range [1.3]. These conditions favor the pentavalent oxidation state and help explain the predominance of PuO_2^+ in the previously mentioned solubility

experiments. Therefore, it is very important to understand the complexation behavior of PuO_2^+ , particularly with anionic species commonly found in natural waters (OH^-, CO_3^{2-}, F^-, HPO_4^{2-}, SO_4^{2-}). Schematic 1 illustrates a potential migration mechanism at Yucca Mountain where hydroxy and carbonate complexation strongly influence the solubility of plutonium in natural waters.

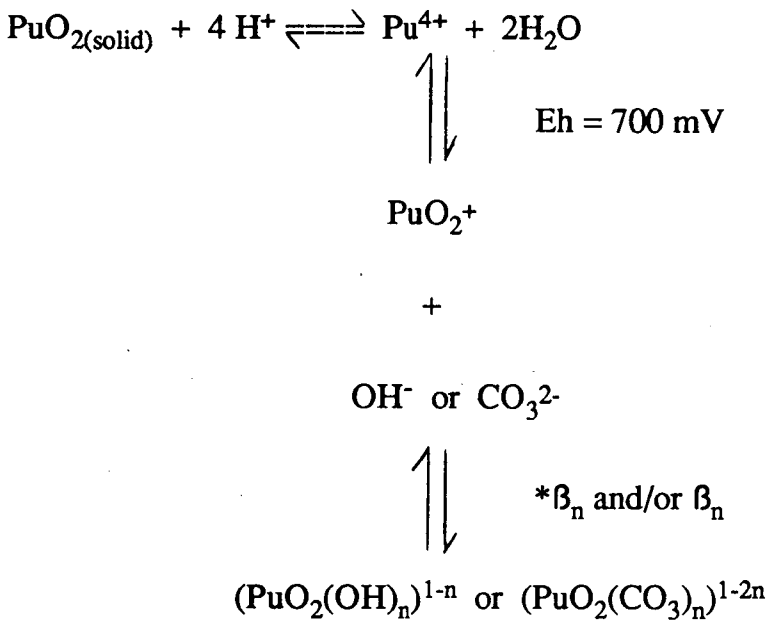

Schematic 1

References

1.1 Hoffman, D. C. and Choppin, G. R.: Chemistry Related to the Isolation of High-Level Nuclear Waste. J. Chem. Educ.. 63, 1059-1064 (1986).

1.2 Cross, J. E., Ewart, F. T., Tweed, C. J.: Thermochemical Modelling with Application to Nuclear Waste Processing and Disposal. UKAEA Report AERE-R12324, United Kingdom (1987).

1.3 Allard, B.: Solubilities of Actinides in Neutral or Basic Solutions. In: Actinides in Perspective, (N. Edelstein, ed.) Pergamon Press, New York, pp. 553-580 (1982).

1.4 Skytte Jensen, B.: The geochemistry ofRadionuclides with Long Half-lives. Riso Nat. Lab., Riso-R-430 (1980).

1.5 Grenthe and Ferri: Actinide Speciation in Groundwater Systems. Proc. OECD/NEA Workshop on Near-field Phenomena in Geological Repositories for Radioactive Waste, Seattle, (1981).

1.6 Daniels, W. R., *et at.*: "Summary Report on Geochemistry of Yucca Mountain and Environs," Los Alamos Nat. Lab. report La-9328-MS December (1982).

1.7 Bondietti, E. A. and Reynolds, S. A.: Field and Laboratory Observations on Plutonium Oxidation States. Proc. Actinide-sediment Reactions Working Meeting, (L. L. Ames, ed.), Batelle Northwest Lab., USDOE Rep. BNWL-2117, pp 505-537 (1977).

1.8 Nelson, D.: Workshop on Environmental Chemistry of Plutonium. Savannah River, April 1-2, 1980.

1.9 Rai. D., Serne, R. J., Swanson, J. L.:Solution Species of Plutonium in the Environment. J. Environ. Qual., 9, 417-420 (1980).

1.10 Nitsche, H. and Edelstein, N. M.: Solubilities and Speciation of Selected Transuranium Ions. A Comparison of a Non-complexing Solution with Groundwater from the Nevada Tuff Site. Radiochim. Acta. U39U, 23-33 (1985).

1.11 Nitsche, H.: Effects of Temperature on the Solubility and Speciation of Selected Actinides in Near-neutral Solution. Inorg. Chim. Acta 127, 121-128 (1987).

1.12 Gevantman, L. H. and Kraus, K. A.: Chemistry of Plutonium(V). Stability and Spectrophotometry. In: The Transuranium Elements, IV-14B. (Seaborg, Katz, and Manning, eds.) McGraw Hill, New York, pp. 500-519 (1949).

1.13 Rabideau, S. W.: The Kinetics of the Disproportionation of Plutonium(V). JACS 79, 6350- 6353 (1957).

1.14 Connick, R. E.: Mechanism of the Disproportionation of Plutonium(V). JACS 71, 1528-1533 (1949).

1.15 Connick, R. E., Kasha, M., McVey, W. H., and Sheline, G. E.: The +5 Oxidation State of Plutonium. MDDC-749, July 6, 1944.

1.16 Silver, G. L.: Suggestion for the Determination of Plutonium Valencies in Aqueous Solutions. Radiochem. Radioanal. Letts., 9 (5-6), 315-320 (1972).

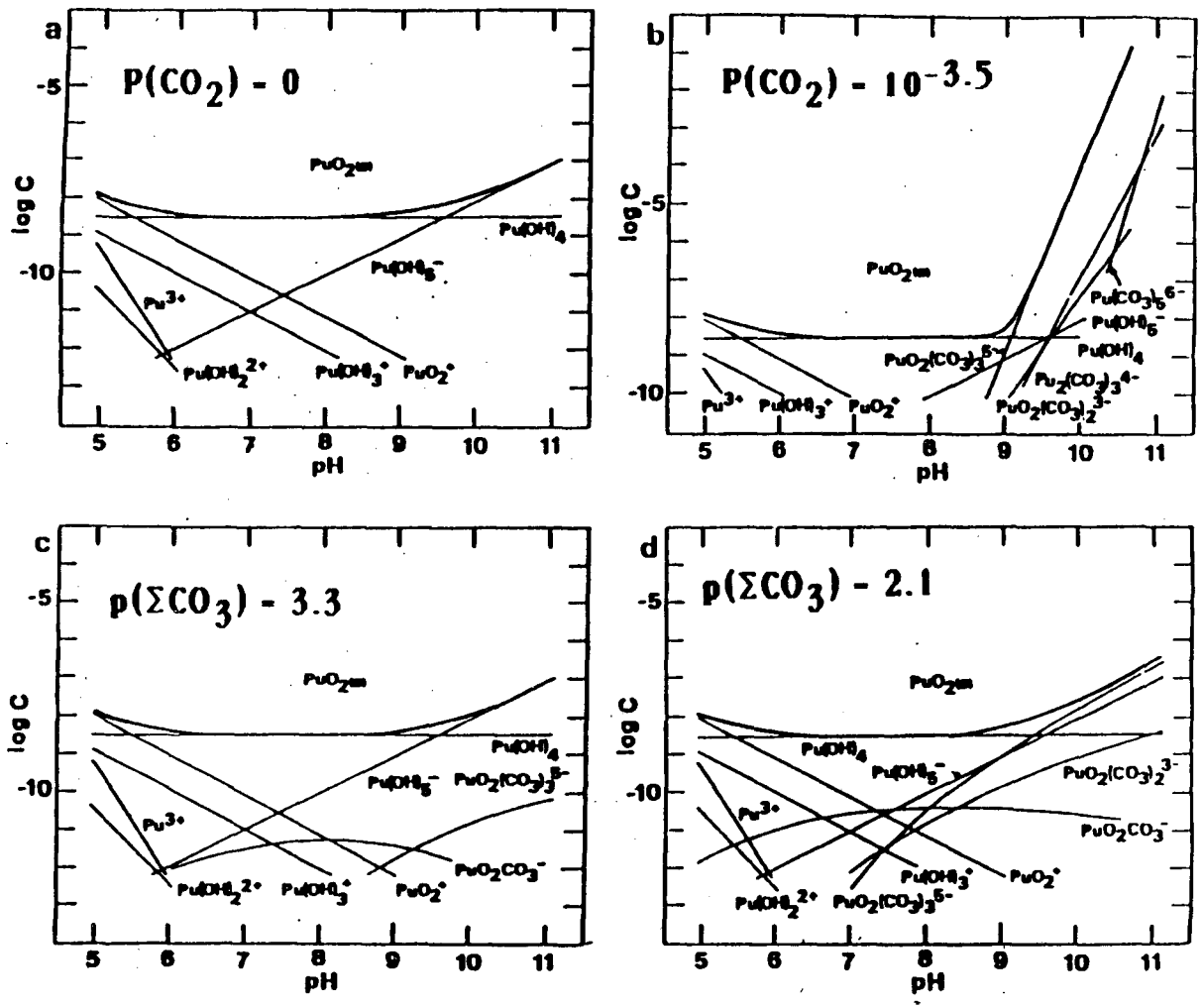

Figure 1.1 Estimated solubilities of plutonium at various partial pressures of CO_2 [1.3].

Chapter 2

PREPARATION OF PuO_2^+

The pentavalent oxidation state of plutonium was discovered in 1944 [2.1]. Sulfur dioxide water was added to a characteristic orange-pink solution of PuO_2^{2+}. Immediately after addition of the reducing agent, the solution turned nearly colorless. After standing for several minutes the solution slowly turned yellow-green, indicating reduction to the 4^+ oxidation state. When this reduction was followed visually with a spectroscope, a unique absorption spectrum was observed during the colorless stage which featured a narrow band at 569 nm. The

pentavalent oxidation state was further verified through a quantitative determination of the electron change involved in the reduction.

The ideal PuO_2^+ stock solution for the hydroxy and carbonate complexation experiments should contain only PuO_2^+, $HClO_4$, and $NaClO_4$ and have a pH ≈ 3 to stabilize against disproportionation [2.2-5]. Sodium perchlorate is used as the background electrolyte because perchlorate does not interact with PuO_2^+ [2.6]. Since the initial discovery of PuO_2^+, several methods of preparation have been developed. One group of methods for preparing PuO_2^+ involves the reduction of a PuO_2^{2+} solution with various reducing agents, such as sulfur dioxide [2.1], hydroxylamine hydrochloride [2.7], sodium nitrite [2.7], and sodium iodide [2.8]. These methods are undesirable because they do not give quantitative reduction or the oxidized reducing agent has to be removed from the PuO_2^+ solution with an organic extractant.

Electrochemical techniques offer an alternate method of oxidation and reduction which allow the preparation of a pure PuO_2^+ solution free of unwanted species. Riglet [2.9] recently completed a critical evaluation

of the published redox potentials for plutonium. The conclusions from survey are summarized in Table 2.1, the formal potential of the PuO_2^{2+}/ PuO_2^{+} couple is 0.941 ± 0.005 V at 25°C.

Table 2.1: Formal potentials of plutonium couples in volts at 25°C in 1M $HClO_4$ [2.9].

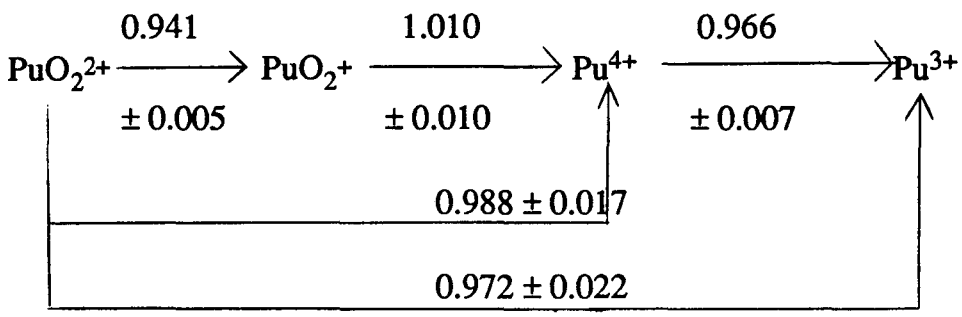

Based on this information, Cohen measured the current-voltage curves for the oxidation-reduction reactions of plutonium ions [2.10]. As shown in Figure 2.1, PuO_2^{+} solutions can only be prepared by reduction of PuO_2^{2+}. The oxidation of Pu^{4+} at a platinum anode yields PuO_2^{2+} because of the high overpotential of the PuO_2^{+} / Pu^{4+} couple of about +1.95 V vs

NHE which is necessary to form the plutonium-oxygen bonds. Consequently, it is especially difficult to get this oxidation to go to completion.

As part of this research, the method described in Section 2.1.1 was developed which combined chemical oxidizing agents and elctrochemical reduction to routinely prepare pure PuO_2^+ solutions.

2.1 Experimental Details

2.1.1 Reagents

The plutonium stock solution was prepared from $^{242}PuO_2$ powder supplied through the United States Department of Energy's Heavy Element Production Program at Oak Ridge National Laboratory. This isotope of plutonium was selected to minimize the effects of radiolysis. The plutonium was purified via anion exchange chromatography [2.12] according to the following procedure: approximately 350 mg of PuO_2 powder was dissolved in 10M HCl with a few drops of concentrated HF,

and this solution was passed through a 1.5 cm x 11cm anion exchange column (Bio-Rad AG-1-X8, 200-400 mesh, chloride form). At this point, the plutonium was in the 4+ oxidation state and orange in color. The plutonium and its daughters (uraniun, neptunium, and americium) were absorbed on the resin while cationic and monovalent anionic species passed through. The column was washed twice with 10 M HCl to remove any residual non-absorbed material. The plutonium was then eluted from the column with a 7:1 solution of 10 M HCl:5 M HI by volume. As the Pu^{4+} was reduced to Pu^{3+} by the I^-, a band of the characteristic blue-violet color was observed which then passed through the column. This plutonium fraction was collected, and an aliquot was analyzed by spark emission spectroscopy for elemental purity. The spectrochemical analysis is shown in Table 2.3.

Table 2.3: Spectrochemical analysis of of plutonium from the plutonium stock solution*.

Element	Micrograms per sample	Element	Micrograms per 100 μg Sample
Al	< 0.05	Mo	< 0.01
Am	< 0.1	Na	< 1
Ca	< 0.03	Nd	< 0.1
Cd	< 0.5	Ni	< 0.01
Ce	< 0.1	Pb	< 0.1
Co	< 0.05	Pu	100
Cr	< 0.01	Si	< 0.01
Dy	< 0.05	Sm	< 0.05
Eu	< 0.01	Sn	< 0.1
Fe	< 0.01	Sr	< 0.01
K	< 1	Yb	< 0.01
La	< 0.01	Y	< 0.01
Mg	0.05	Zn	< 0.1
Mn	< 0.01	Zr	< 0.01

*Results marked with < indicate element was not detected within limit of detection.

An aliquot was also assayed by alpha pulse-height-analysis (PHA). This assay revealed 99.7% of the total mass was ^{242}Pu with the balance consisting primarily of ^{239}Pu. Approximately, 0.005 ppm of ^{238}Pu

contamination by weight contributed 26% of the alpha count rate.

The plutonium solution was evaporated to dryness and treated with fuming nitric and perchloric acids to destroy any organic residue, such as resin fines. The plutonium was converted to a 2 M perchloric acid medium. The concentration was measured by liquid scintillation counting (LSC) to be 10 mg of ^{242}Pu/ml.

PuO_2^+ stock solutions were prepared as necessary. An aliquot of plutonium stock solution was boiled down and fumed with 1 ml of concentrated $HClO_4$ to near dryness. The resulting solution of PuO_2^{2+} was diluted in NaOH and the pH was adjusted to 3. The PuO_2^{2+} was electrochemically reduced to PuO_2^+ at a platinum electrode by applying 778 mV vs NHE [2.10]. The oxidation state purity was verified spectrophotometrically by comparison with previously reported spectra [2.2,11]. A typical spectrum for each of the four oxidation states is shown in Figures 2.2 -2.5. The measured molar extinction coefficients for the spectrometer used in this work are listed in Table 2.2. Because Pu^{3+}, Pu^{4+}, and PuO_2^{2+} have molar absorptivities 2 to 36 times greater

than PuO_2^+, it is easy to assess the purity of a PuO_2^+ solution.

The concentration of the PuO_2^+ stock solutions was approximately 4.5 x 10^{-4} M.

Table 2.2 Measured molar absorptivities of Pu^{3+}, Pu^{4+}, PuO_2^+, and PuO_2^{2+} at selected wavelengths.

	Molar absorptivity (M^{-1} cm^{-1})			
Wavelength (nm)	Pu^{3+}	Pu^{4+}	PuO_2^+	PuO_2^{2+}
600	39	2	2	1
470	3	58	2	9
569	34	4	19	2
830	5	14	4	550

2.1.2 Equipment

The pH was measured with a micro-combination electrode (Beckman, Model 39522) and a digital pH meter (Orion Research, Model 601A). The saturated KCl solution in the pH electrodes was replaced with saturated NaCl/AgCl to prevent clogging of the junction by $KClO_4$. The electrode was standardized wilth NBS traceable buffers of pH 4.00, 7.00, and 10.00 (25°C, EM Science) at the beginning and end of each day.

The three-electrode electrochemical cell consisted of the following: a 2.4 cm x 4.5 cm quartz cell with lucite lid, platinum grid working electrode (40 mesh), single junction platinum coil auxiliary electrode (3 M $NaNO_3$), and single junction Ag/AgCl reference electrode (sat'd NaCl/AgCl). Figure 2.6 is an illustration of the electrochemical cell. The junction for the auxiliary and reference electrode was a sintered glass frit (Vycor). The reference electrodes were made by reducing the surface of a silver wire in a NaCl solution ($AgCl(s) + e^- \rightleftharpoons Ag(s) + Cl^-$; $E° = 0.222$ V) and then calibrating the assembled electrode with a saturated calomel electrode (SCE). The average potential for the reference electrodes was 207.5 mV vs NHE.

A Princeton Applied Research Model 264A Polarographic Analyzer/Stripping Voltammeter was used for the oxidations and reductions.

A Model 200 Guided Wave Spectrometer was used for all conventional absorption spectrophotometric measurements. The spectrometer was equipped with a 1200 line/mm grating, Si type detector, and 0.063 mm exit slit. Solutions were measured in a 1 cm UV-quartz cuvette.

A Beckman Model LS5801 liquid scintillation counter was used to measure the plutonium concentrations by assay of the gross alpha activity ^{242}Pu (E = 4.90 MeV). The LSC was calibrated with an ^{243}Am (E = 5.28 MeV) secondary standard and all measurements were made in triplicate. The alpha spectrometry system included a Au/Si surface barrier detector coupled to a multi-channel analyzer.

References

2.1 Connick, R. E., Kasha, M., McVey, W. H., and Sheline, G. E.: The +5 Oxidation State of Plutonium. Metallurgical Project Report CN-1912, July 6, 1944.

2.2 Gevantman, L. H. and Kraus, K. A.: Chemistry of Plutonium(V). Stability and Spectrophotometry. In: The Transuranium Elements, IV-14B. (Seaborg, Katz, and Manning, eds.) McGraw Hill, New York, pp. 500-519 (1949).

2.3 Rabideau, S. W.: The Kinetics of the Disproportionation of Plutonium(V). JACS 79, 6350- 6353 (1957).

2.4 Connick, R. E.: Mechanism of the Disproportionation of Plutonium(V). JACS 71, 1528-1533 (1949).

2.5 Madic, C., Begun, G. M., Hobart, D. E., and Hahn, R. L.: Raman Spectroscopy of Neptunyl and Plutonyl Ions in Aqueaous Solution: Hydrolysis of Np(VI) and PU(VI) and Disproportionation of Pu(V). Inorg. Chem. 23, 1914-1921 (1984).

2.6 Hartley, F. R., Burgess, C., and Alcock, R.: Solution Equilibria, John Wiley and Sons, Inc., New York, pp 26 (1980).

2.7 Hindman, J. C. and Ames, D. P.: Metallurgic Project Rep. CN-2068, Sept. 1, 1944.

2.8 Kraus, K. A., Dam, J. R., and Moore, G. E.: Clinton Lab. Rep. CL-P-395, March 15, 1945.

2.9 Riglet, C.: The Chemistry ofNeptunium and other Actinides in Carbonate Solution, Ph.D. Thesis, University of Paris 6 (1989).

2.10 Cohen, D.: Electrochemical Studies of Plutonium Ions in Perchloric Acid Solution. J. Inorg. Nucl. Chem. 18, 207- 210 (1961).

2.11 Cohen, D.: The Absorption Spectra of Plutonium Ions in Perchloric Acid Solutions. J. Inorg. Nucl. Chem. 18, 211-218 (1961).

2.12 Hoffman, D. C.: Purification of Plutionium via Anion Exchange Chromatography. In: Radiochemistry of Plutonium,

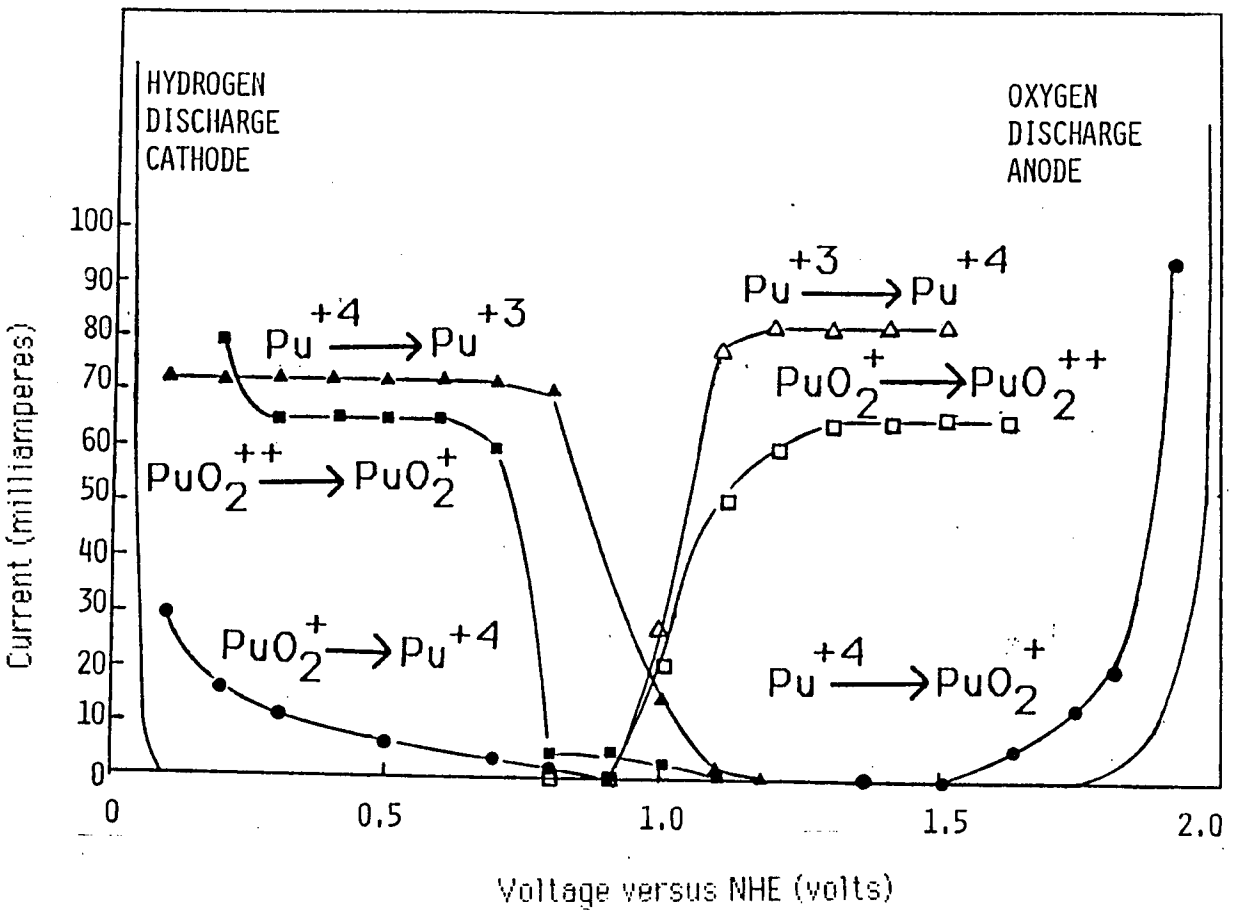

Figure 2.1 Current-voltage curves versus NHE for plutonium ions in 1 M $HClO_4$ at 25°C [2.11].

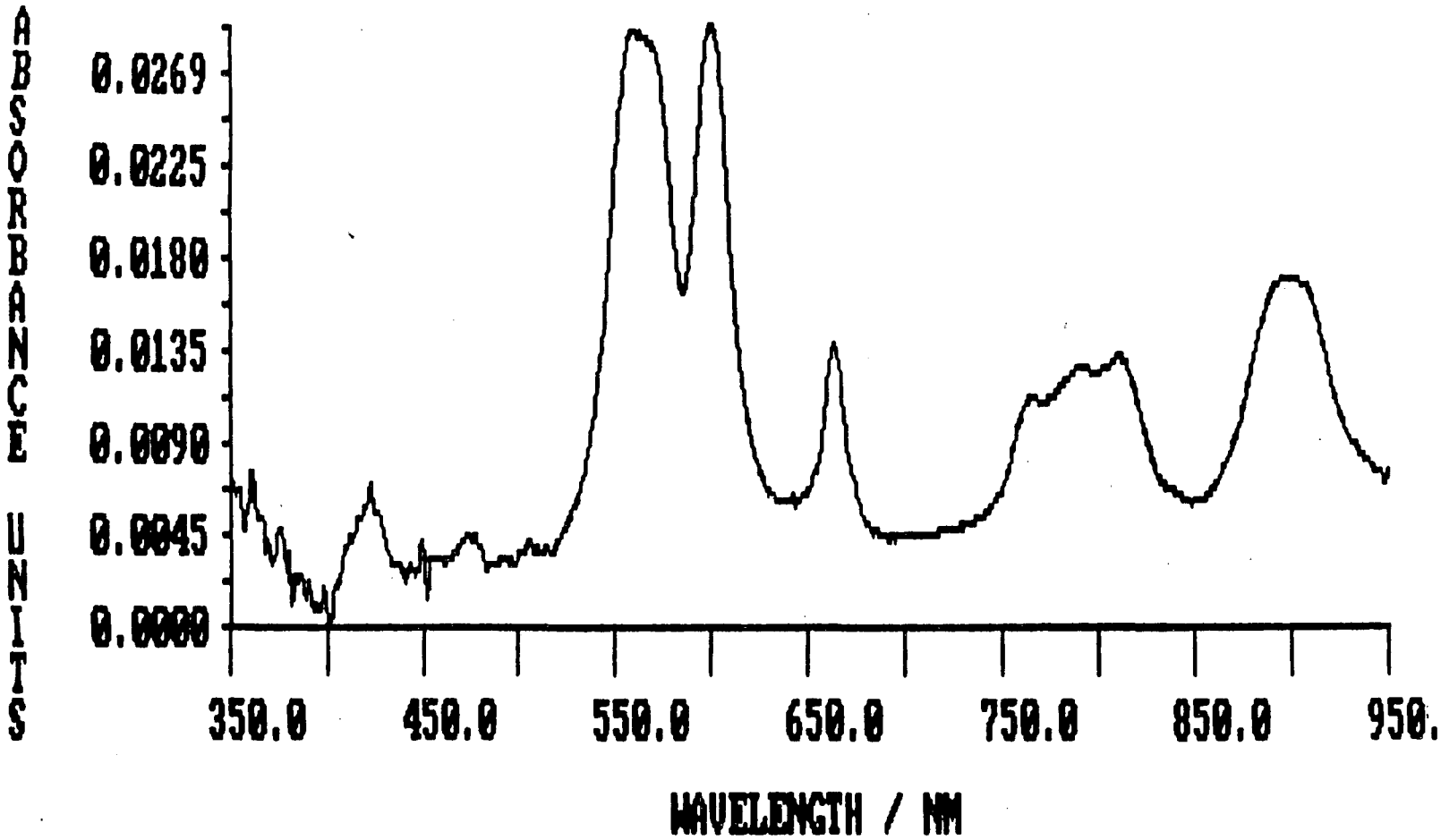

Figure 2.2 Absorption spectrum of Pu^{3+} measured on Guided Wave spectrometer.

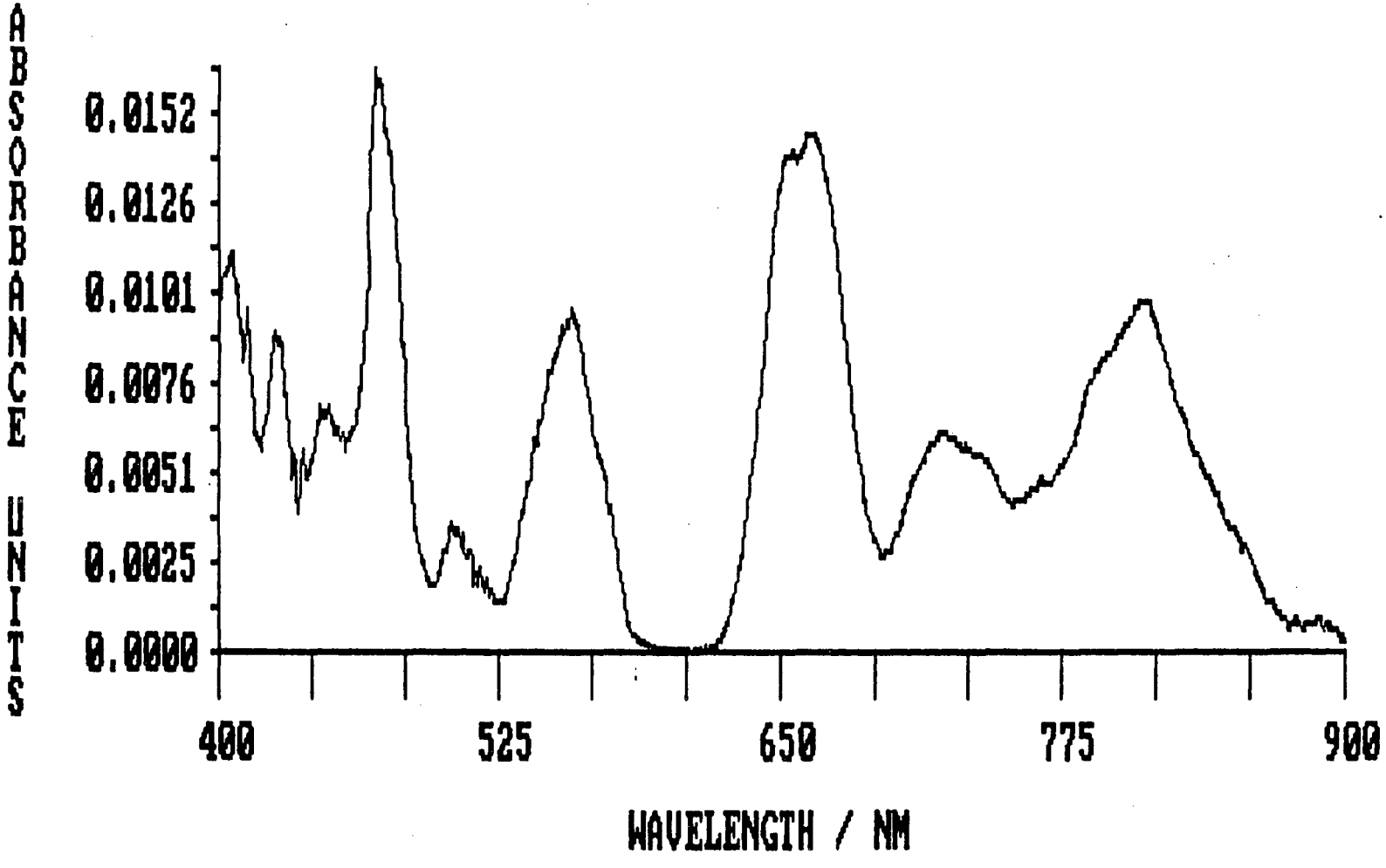

Figure 2.3 Absorption spectrum of Pu^{4+} measured on Guided Wave spectrometer.

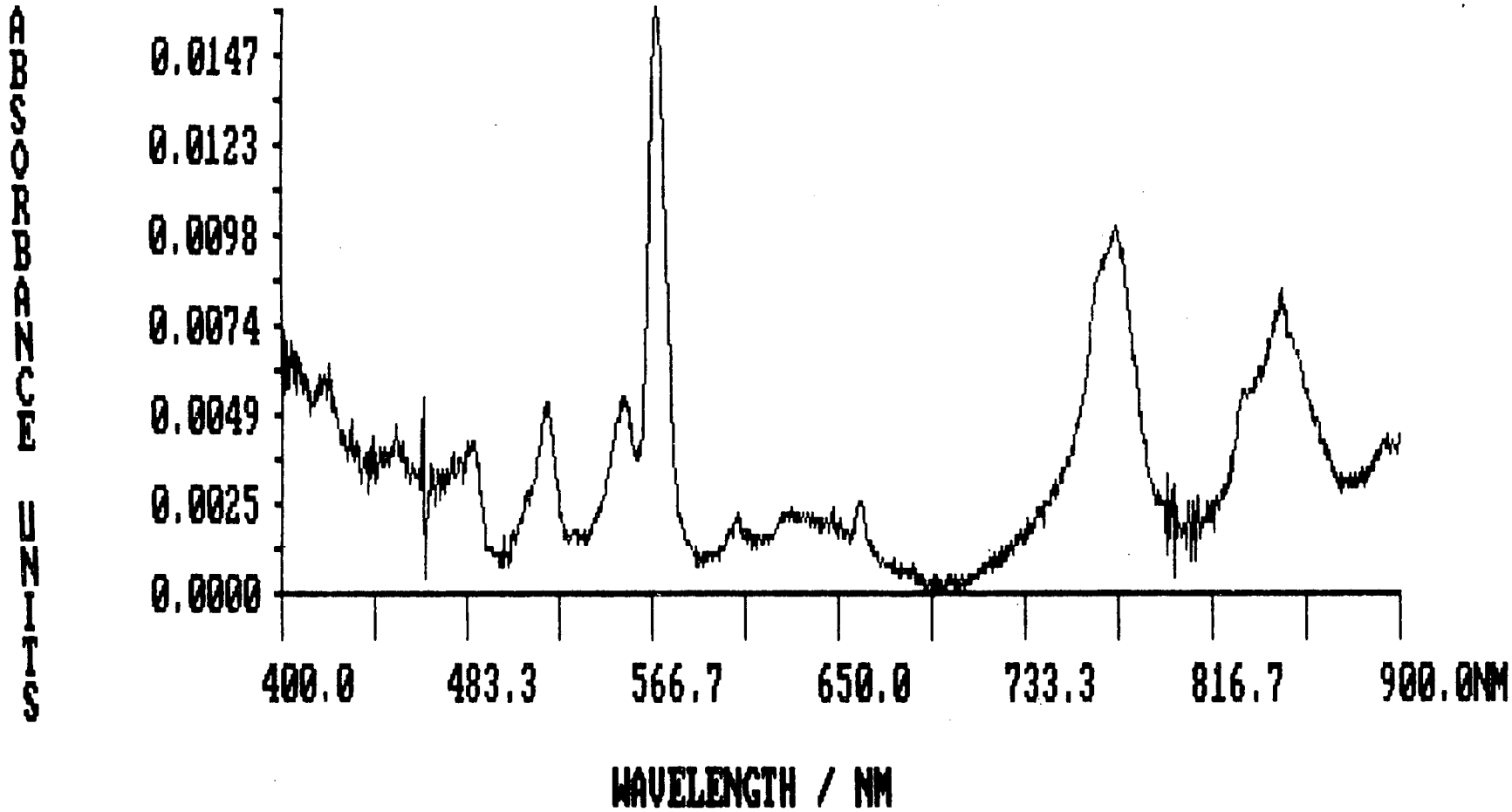

Figure 2.4 Absorption spectrum of PuO_2^+ measured on Guided Wave spectrometer.

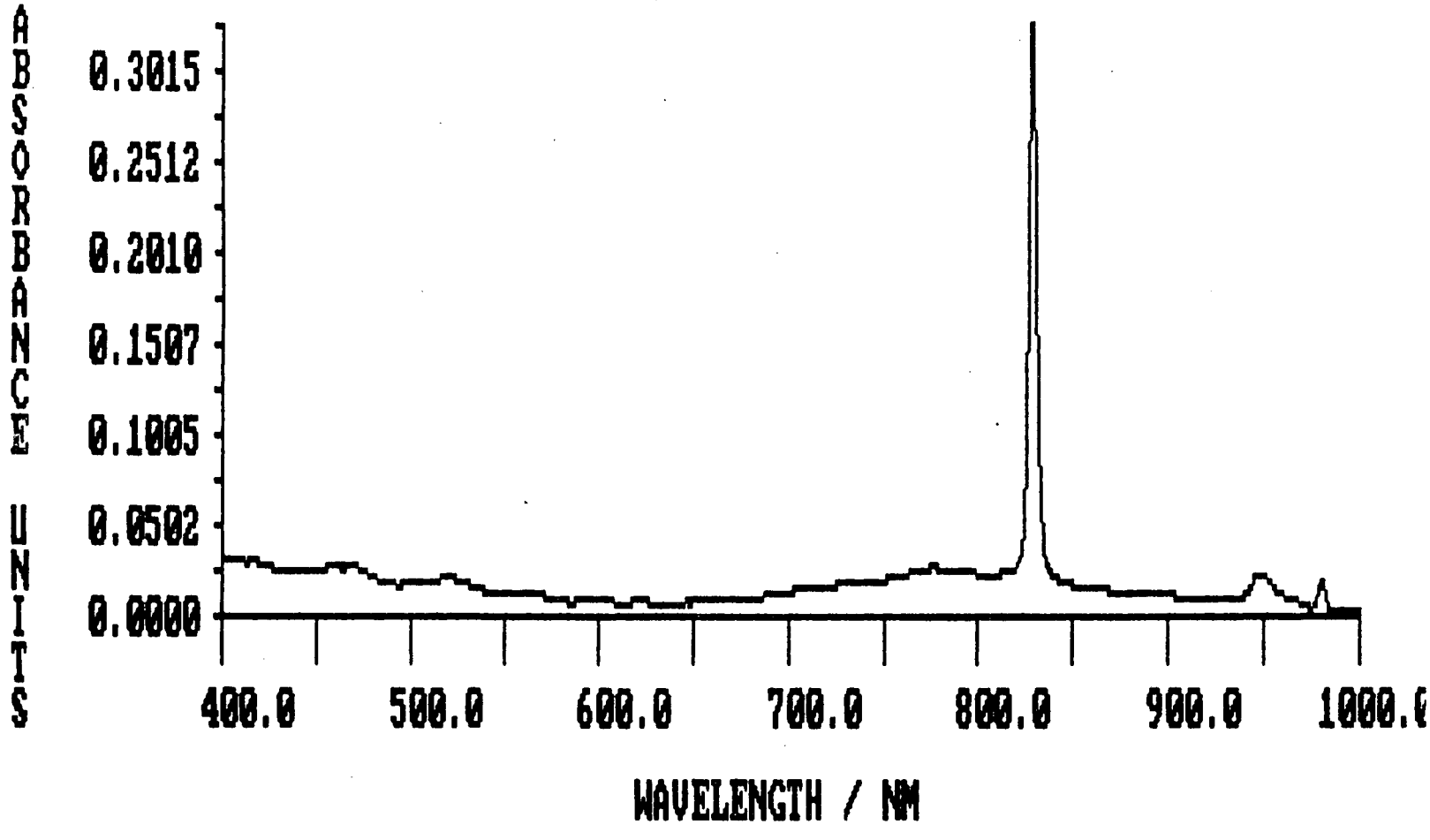

Figure 2.5 Absorption spectrum of PuO_2^{2+} measured on Guided Wave spectrometer.

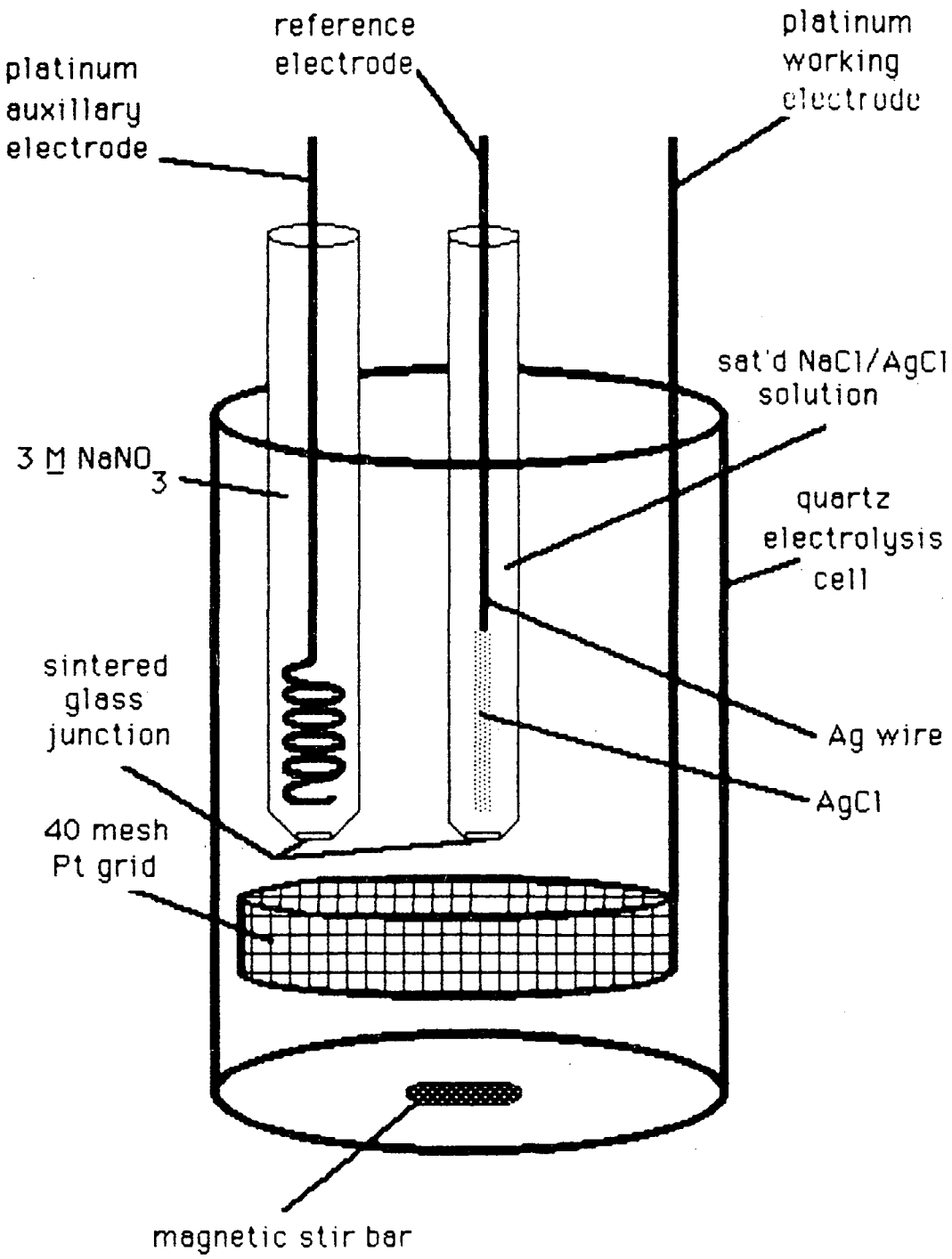

Figure 2.6: Schematic of electrolysis cell

Chapter 3

Development of a Laser-Induced Photoacoustic Spectroscopy (LIPAS) System

We chose the spectrophotometric method of measurement because it allows a direct, non-invasive determination of the PuO_2^+ speciation. Initial experiments were attempted with a conventional absorption spectrometer which utilized fiber optic cables. Unfortunately, this

technique did not have the sensitivity necessary to overcome the combination of the low molar absorptivity ($\leq 19\ M^{-1}cm^{-1}$) and low solubility ($K_{sp} \leq 10^{-10}$) of PuO_2^+ and its complexes [3.1-3]. Laser induced photoacoustic spectrometry (LIPAS) was selected as an alternate method because it offers an increased sensitivity of 100-1000 times that of conventional absorption spectroscopy [3.4-9]. Since LIPAS systems are still in the developmental stage and not commercially available, it had to be constructed [3.25].

3.1 The Photoacoustic Technique

Photoacoustic spectrometry (PAS) is inherently more sensitive than conventional spectrophotometry because it relies on the direct measurement of absorbed photon energy, rather than the difference between incident and transmitted radiation as measured conventionally. In LIPAS, some of the absorbed photon energy from a pulsed laser is converted via non-radiative decay to an acoustic wave. This is known as the laser photoacoustic effect; it is illustrated in Figure 3.1. Because the actinide absorption bands in the visible and near-infrared region are

parity-forbidden f-f transitions, radiationless de-excitation is favored. Therefore, the laser photoacoustic technique is particularly suitable for actinides.

3.2 History of Photoacoustics

The 'photoacoustic' effect was first reported by Alexander G. Bell in 1880 [3.10]. Bell used sunlight as a light source and, after the discovery, referred to the effect as 'optoacoustics'. This term was subsequently confused with the acousto-optic effect employed by laser modulators. In 1973, Rosencwaig introduced the term 'photoacoustics" [3.11] which has been readily adopted.

Bell's initial discovery was followed by widespread interest and the photoacoustic effect was observed in solids, gases, and to a lesser extent liquids [3.12-15]. Simple gas cells, precursors to modern gas microphones, were designed and constructed. However, quantitative measurements were not possible because signal detection depended on human hearing. This inability to make precise measurements resulted in a temporary loss of interest in photoacoustics [3.16].

During the late 1930's and early 1940's, the photoacoustic effect gained renewed interest as a technique for gas analysis by absorption of infared radiation (IR). However, gas chromatography and IR spectrometry superseded infrared photoacoustic spectroscopy a short time later.

Since the early 1970's, photoacoustics and related fields have advanced rapidly. One of the first applications was to successfully measure absorption spectra from highly efficient light scattering materials [3.17,18]. Photoacoustic spectroscopy using the gas microphone cell has remained popular, but other detection methods have been developed to improve the technique's versatility. The new detection methods include piezoelectric transducers to form highly sensitive acoustic detectors [3.19] and photothermal techniques which rely on the interaction of light with thermally induced refractive index gradients, such as thermal lensing [3.20] and photothermal deflection [3.21,22]. While photothermal deflection has been shown to be the theoretically most sensitive method of detection [3.23], piezoelectric detection offers the advatage of simplicity, with sensitivity approaching

that of photothermal deflection [3.19,24].

In 1983, the application of the photoacoustic technique to actinide speciation was first described by Schrepp et. al. [3.25]. Their system consisted of a pulsed dye laser light source with piezoelectric detection of the light absorbed by actinide solutions in quartz spectrophotometric cells. This early work demonstrated the potential of the approach for determining uranium speciation among different oxidation states at levels well below the range of conventional spectrophotometry. Subsequently, other actinides (Am^{3+}, Am^{4+}, Pu^{4+}, Np^{4+}, NpO_2^+, and NpO_2^{2+}) have been measured in the concentration range of 10^{-5} to 10^{-8} M for a variety of chemical conditions [3.16,26-29].

3.3 Theory of Laser Induced Photoacoustic Detection

As illustrated in Figure 3.1, the photoacoustic effect occurs when the absorption of electromagnetic radiation in a sample results in localized heating. The heat energy is transmitted to the surrounding matter through two mechanisms: 1) diffusion and 2) the thermoacoustic (or thermoelastic) process. The thermoacoustic process is nondissipative,

and the speed of energy transfer is governed by the speed of sound in the material. The distance of appreciable energy transfer is limited by the dimensions of the sample. For weak absorption, Tam has described the generation of a photoacoustic pulse with a simplified theory [3.24]. This theory is based on the assumption that the duration of the laser pulse, τ , is much shorter than one millisecond, so that thermal diffusion is negligible. The acoustic pulse production can then be described for two boundary conditions depending on whether the laser beam radius is smaller, R_s, or larger, R_L, than the distance travelled by the acoustic pulse, $v\tau$, where v is the sound velocity in the medium. The general concepts for the two boundary conditions are decribed below. For a rigorous theoretical treatment of pulsed photoacoustic generation refer to the following references 3.24,31-33.

Case 1: $R_s < v\tau$

The photoacoustic source can be considered as a long cylindrical medium with length l. The energy absorbed by the medium, E_{abs}, per laser pulse is given by

$$E_{abs} = E_0(1 - e^{-\alpha l}) \tag{3.1}$$

where E_0 is the input energy per pulse and

α is the optical absorption coefficient.

For weakly absorbing species, $\alpha l << 1$ and the absorbed energy can be approximated by

$$E_{abs} \approx E_0 \alpha l \tag{3.2}$$

Since it is assumed that nonradiative relaxation predominates in the medium, then the thermal energy is given by

$$E_{th} \approx E_{abs} \approx E_0 \alpha l \tag{3.3}$$

Knowing the specfic heat at constant pressure, C_p, the increase in temperature, ΔT, of the illuminated volume can be calculated from

$$E_{th} = C_p V \Delta T \rho \tag{3.4}$$

where V is the illuminated volume ($V = \pi R^2 l$) and

ρ is the density of the condensed material.

Combining Eqs. 3.3 and 3.4 gives the rise in temperature

$$\Delta T = E_0 \alpha / \pi R^2 C_p \rho \tag{3.5}$$

The initial adiabatic, isobaric expansion, ΔR, of the source with radius, R_s, immediately after the laser pulse, is given by

$$\pi(R_S + \Delta R)^2 l - \pi R_S^2 l = \beta V \Delta T \qquad (3.6)$$

where ß is the volumetric expansion coefficient. Expanding Eq. 3.6 and assuming $\Delta R << R_s$ gives

$$\Delta R \approx 1/2\, R \beta \Delta T \qquad (3.7)$$

Inserting the expression for ΔT from Eq. 3.5 into Eq. 3.7, Eq. 3.8 is obtained

$$\Delta R = (\beta E \alpha) / (2\pi \rho C_p \nu \tau) \qquad (3.8)$$

The peak displacement, $U_S(r)$, at a distance, r, from the photoacoustic source (assuming r<<l) varies as $r^{-1/2}$ because of the conservation of acoustic energy [3.30].

$$U_S(r) = \Delta R (R_S/r)^{1/2} = (\beta E \alpha) / (2\pi \rho C_p (\nu \tau r)^{1/2} \qquad (3.9)$$

The peak acoustic pressure, $P_S(r)$, at position, r, is approximately related to the acoustic displacement, $U_S(r)$, by

$$P_S(r) \approx [\rho U_S(r)] / \tau \qquad (3.10)$$

Substituting Eq. 3.9 into Eq. 3.10, we obtain the peak photoacoustic pressure observed at r for a small source radius,

$$P_S(r) \approx (\beta E \alpha^2) / [2\pi C_p (\nu\tau)^{3/2} r^{1/2}] \quad (3.11)$$

Eq. 3.11 is similar in form to the more rigorous estimate given by Patel and Tam [3.19] in Eq. 3.12

$$P(r,t) \approx \pm [(\beta E \alpha) / (\pi C_p \tau^2)] [(\nu\tau) / (2\pi r)]^{1/2} \quad (3.12)$$

Case 2: $R_L > \nu\tau$

This condition can also be treated simply by assuming that the heated volume does not have time to expand isobarically immediately after the laser pulse. Instead, a pressure increase, P_O, appears immediatley at the surface of the irradiated volume following the laser pulse:

$$P_O = \rho\nu^2 \beta \Delta T \quad (3.13)$$

where $\rho\nu^2$ is the bulk modulus of the medium. Following the substitution for ΔT

$$P_O = (\rho v^2 \beta E \alpha) / (\pi R_L^2 \rho C_p) \qquad (3.14)$$

The peak acoustic pressure, P_L, for the cylindrical wave varies as $r^{-1/2}$. therefore

$$P_L(r) = P_O(R_L/r)^{1/2} = (\beta v^2 E \alpha) / (\pi R_L^{3/2} C_p r^{1/2}) \qquad (3.15)$$

A comparison of Eq. 3.11 and 3.15 shows that when the laser beam radius is large the photoacoustic pulses exhibit the lowest intensity. This relationship is not surprising since the contributions from different positions in the large source case do not sum together coherently. These equations also indicate that acoustic pressure varies linearly with the laser pulse energy.

Tam has summarized the results of more rigorous treatments of pulsed photoacoustic generation which are based on thermal expansion and electrostriction [3.24,31-33]. All show a strong resemblance to Eq. 3.11 and 3.15, indicating the simple model is valid.

The performance of our LIPAS system can be evaluated from theory. A typical beam radius under operational conditions is approximately 0.1 cm. Therefore, this system falls in the large beam radius case where $R_L > \nu\tau$. Substituting some of the system typical values into Eq. 3.15 gives a value for the maximum possible peak pressure, P_{max}, produced from 10 nanosecond laser pulse which is 3 cm away from the region of optical absorption at λ = 503 nm, in a water medium.

P_{max} = 3.0 g cm^{-1} s^{-2} = 3.0 x 10^{-4} atm

where α = 2.5 x 10^{-4} cm^{-1}, water absorption at 503 nm

ν = 1.5 x 10^5 cm s^{-1}

E = 1.5 x 10^{-3} J

ß = 2.57 x 10^{-4} K^{-1}

C_p = 4.179 J g^{-1} K^{-1}

r = 3.0 cm

R_L = 0.1 cm.

In order to utilize this pressure pulse, it must be detected. We selected piezoelectric transducers for the reasons discussed in Section 3.2. These pressure sensitive detectors are made of lead zirconate titanate (PZT 5A). This artificially grown material has the property of being able to generate electrical charges when certain crystal faces are subjected to mechanical stressing. Thus, the voltage output of the PZT transducer is proportional to the pressure of the acoustic wave which is related to the concentration of the absorbing species. However, the P_{max} value is the approximate intensity of the acoustic wave near the bottom face of the quartz cuvette (refer to Figure 3.6). In order to calculate the detector voltage output, the propagation losses must be taken into account. The primary losses are caused by the reflection of a portion of the acoustic wave as it crosses the boundary between one medium and another, as illustrated in Figure 3.2. The total losses, L_T, can be assessed by treating each medium as exhibiting a specific acoustic impedance, Z, which can be calculated according to Eq. 3.16.

$$Z = \rho v \tag{3.16}$$

Eq. 3.17 describes the portion of the acoustic wave, ∂, which successfully

propagates the boundary between medium 1 and medium 2 [3.34]

$$\partial = 4(Z_1 Z_2)/(Z_1 + Z_2) \qquad (3.17)$$

The density and acoustic wave velocity of the materials used in our LIPAS system are listed in Table 3.1 along with their respective acoustic impedances [3.14,15,35,36]. The portion which successfully propagates, S, across the boundaries shown in Figure 3.2 are summarized in Table 3.2.

Table 3.1: Density and acoustic wave velocity of materials used in LIPAS cell assembly

Material (g/cm^2s)	Density (g/cm^3)	Acoustic wave velocity (cm/s)	Acoustic impedence
water	1 [3.14]	1.5×10^5 [3.35]	1.5×10^5
quartz	2.2 [3.14]	5.97×10^5 [3.35]	1.311×10^6
epoxy*	1.3 [3.14]	1.9×10^5 [3.35]	2.47×10^5
Ag epoxy*	2.7 [3.14]	6.4×10^5 [3.35]	1.73×10^6
PZT 5A	7.75 [3.15]	4.35×10^5 [3.36]	3.37×10^6

*Glycerine and aluminum data used for epoxy and Ag epoxy, respectively, because of the lack of information on the optical coupling.

Table 3.2: Portion of acoustic wave which successfully propagates the boundaries in the LIPAS cell assembly

Boundary	Portion of acoustic wave which successfully propagates the boundary between two media
1) water/quartz	0.368
2) quartz/epoxy	0.53
3) epoxy/quartz	0.53
4) quartz/Ag epoxy	0.98
5) Ag epoxy/PZT 5A	0.9

Portion which successfully propagates, S = (1) x (2) x (3) x (4) x (5) = 0.0912

The portion of the acoustic wave that manages to propagate across all four boundaries is the product of the losses at each boundary as described in Eq. 3.18.

$$S = \Sigma \beta_i \; ; \qquad (3.18)$$

For our LIPAS system, S = 0.091. This value is a lower limit since the quartz/epoxy/quartz boundaries will form a good acoustic contact. If the successful propagation at boundaries (2) and (3) equals 0.97, then S = 0.31. Therefore, the value of S lies in the range $0.091 < S < 0.31$. The pressure, P_p, generated by the acoustic wave at the piezoelectric transducer is

$$P_p = S P_{max} \tag{3.19}$$

Therefore, $P_p \geq 0.27$ g cm^{-1} s^{-2} or 2.7×10^{-5} atm.

This pressure pulse is converted to an electrical signal by the piezoelectric transducer. The longitudinal piezoelectric effect (where the charge is collected at the transducer face where the force is applied) produces a charge, q, which is directly proportional to the force, F, sustained [3.37]

$$q = k_{33} d_{33} F \tag{3.20}$$

where k_{33} is the longitudinal coupling factor [3.36] and d_{33} is the piezoelectric constant quantitatively relating charge, density, and stress. The subscript (33) describes the direction of the electric field and the

stress and is illustrated in Figure 3.3.

The charge generated by the transducer can be easily converted to a voltage, V

$$V = q / C \tag{3.21}$$

C is the transducer capacitance which is defined as follows

$$C = \epsilon_o \epsilon_r A / H \tag{3.22}$$

where ϵ_o is the dielectric constant of free space (F m^{-1})

ϵ_r is the relative dielectric constant

H is the transducer thickness (cm)

A is the transducer surface area (cm^2).

Combining Eqs. 3.20 through 3.22 and using the usual substitution of pressure and area for force, the output voltage of a piezoelectric transducer in response to a normal incident pressure wave is

$$V = k_{33} d_{33} H P_{max} / \epsilon_o \epsilon_r \tag{3.23}$$

Typical values for the PZT-5A transducer material employed in the detection system are

$k_{33} = 0.710$

$d_{33} = 374 \times 10^{-12}\ m.V^{-1}$

$H = 0.6\ cm$

$\epsilon_o = 8.85 \times 10^{-12}\ F.m^{-1}$

$\epsilon_r = 1700$

Substituting these values in Eq. 3.23, the output voltage from the transducer is 2.8×10^{-6} V.

This result compares quite favorably with the signal level actually measured, about 3×10^{-6} V. This agreement confirms that the simple theory represented by Eq. 3.15 is a good description of the photoacoustic detection system.

3.4 The LIPAS Equipment

A block diagram of our photoacoustic spectrometer is shown in Figure 3.4. A Nd:YAG laser (Spectra-Physics, Model DCR-3) pulsed at 20 Hz pumps a tunable dye-laser (Spectra-Physics, Model PDL-2), which excites the sample. We used the laser dye Coumarin 540-A (Exciton) to

provide a light of suitable wavelengths for exciting the PuO_2^+ absorption band at 569 nm. Coumarin 540-A has a usable tuning range from ≈525 - 600 nm when dissolved in methanol and pumped with the 355 nm third harmonic of the Nd:YAG laser beam. The useful life of the dye was extended by adding ≈1 g of 1,4-diazobicyclo(2,2,2)octane to the dye-methanol solution [3.38]. As shown in Figure 3.5, most laser dyes have a narrow tuning range which limits the spectral region that can be measured. Because the laser must be turned off to change laser dyes, it is very important to have a dye which adequately spans the wavelength region of interest. This feature of the LIPAS system is one of its major drawbacks.

A photodiode (United Detector Technology, Model PIN-10DFP) that has a flat spectral response from 450 to 950 nm monitors the intensity of each dye-laser pulse. Solutions are placed in a 1 cm square uv-quartz cell. The cell is bonded to a quartz cylinder (1 cm diameter x 1 cm long) with uv-cured epoxy, which is bonded in turn to a cylindrical piezoelectric transducer (Vernitron PZT-5A, 1.5 cm diameter x 6 mm) with silver reflective epoxy. We placed the PZT inside an anodized

aluminum box (≈0.03 cm^2) to shield it as much as possible from electrical noise. A LEMO connector in the wall of the aluminum box provides electrical contact between PZT leads and the associated measurement electronics. The entire cell-detector assembly (Figure 3.6) attaches to a precision X-Y-Z translator that is rigidly fixed to the laser table. Locating pins on the bottom of the cell-detector assembly allow it to be removed from and reattached to the X-Y-Z translator without altering the geometry with respect to the laser beam.

The detector signal is amplified and shaped with a charge-sensitive pre-amp((ORTEC, Model 142C) and differentiating amplifier (ORTEC, Model 570) with a 1 μs shaping time. Figure 3.7 shows the amplified photoacoustic pulse from our spectrometer. A gated integrator (Stanford Research, Model SR250) samples the amplitude of the photoacoustic pulse ≈20μs after the laser trigger with a gate width of ≈1 μs. A second gated integrator measures the photodiode signal from each laser pulse in order to correct for both the pulse-to-pulse power variations at a fixed wavelength as well as the variations in laser power with wavelength that arise from the dye gain.

The acquisition of a spectrum involves stepping the dye-laser monochromator to the desired starting wavelength, averaging the signal from enough laser pulses to give sufficient signal-to-noise (S/N), stepping to the next wavelength, and repeating the process untill the stopping wavelength is reached. An IBM-PC controls the monochromator through an IEEE-488 interface (National Instruments, Model GPIB-PC2A); it measures the voltages from the gated integrators on a pulse-by-pulse basis with an A/D-I/O board (Data Translation, Model DT-2801A). The control program allows three channels of data from two PZT detectors and one photodiode. Therefore, with a second cell-detector assembly and associated electronics, background-corrected spectra can be obtained in real time by placing a reference solution in the laser path. Since this cell arrangement demonstrated no real advantage over a single-beam technique, all the data for this study were acquired in a single-beam arrangement with off-line background substraction.

Reference spectra were measured for each solution. The only difference between the reference and sample solutions was the presence

or absence of plutonium. As shown in Figure 3.8, the absorption spectrum of water is relatively strong and steadily increases at wavelengths above 500 nm. Because the measurements for this work were made in a region where the water absorption exhibits a steep increase, background subtraction is especially important. Particulary, since the weakly absorbing species is at low concentrations where the photoacoustic signal from water is comparable to or greater than the PA signal of the species of interest.

The PAS spectra over the wavelength range 530 to 590 nm were acquired after adjusting the incident laser power to 1.5 mJ/pulse at the Coumarin 540-A dye gain maximum (≈555 nm). The dye laser produces a nominal 10 ns full width at half maximum (FWHM) Gaussian pulse. We adjusted the size of the laser beam to cover an area of ≈0.03 cm^2 at the cell. All specra were obtained by averaging 100 pulses/wavelength at a spectral resolution of 0.25 nm. All measurements were made at ambient temperature (≈24°C).

Spectra-Calc (Galactic Industries) software was used to manipulate the spectral data. This general purpose spectroscopic software package

has features such as zooming, scaling, spectral subtraction, and overlay capabilities which allow multiple spectra to be conveniently averaged and/or compared.

3.5 Photoacoustic spectra of Pu^{4+}, PuO_2^{+}, and PuO_2^{2+}

The photoacoustic spectra of Pu^{4+}, PuO_2^{+}, and PuO_2^{2+}, their corresponding reference spectra, and the resulting background subtracted spectra are shown in Figures 3.9, 10, and 11, respectively. Each oxidation state of plutonium was measured at multiple concentrations between 1×10^{-4} and 1×10^{-6} M. From these spectra, Beer's Law plots of Pu^{4+}, PuO_2^{+}, and PuO_2^{2+} were made to demonstrate the linear behavior of the LIPAS system, as shown in Figure 3.13, 14, and 15, respectively. A signal to noise ratio (S/N) of 3 can be described as the detection limit of a spectrometer. When the detection limit is multiplied by the molar absorptivity, the sensitivity (α) is obtained. These results are summarized in Table 3.3 where the consequences of a large water

background are also shown. The molar absorptivity of PuO_2^{2+} is almost 10 times greater than that of Pu^{4+}, but the background from water absorption is approximately 100 times greater at the absorbance maxima (830.7 nm) of PuO_2^{2+} than the absorbance maxima (469.7 nm) of Pu^{4+} (see Figure 3.8). Consequently, their sensitivities are approximately equal ($\approx$ 86 ppm).

Table 3.3 Results of Pu^{4+}, PuO_2^{+}, and PuO_2^{2+} on LIPAS system

	Pu^{4+}	PuO_2^{+}	PuO_2^{2+}
Absorbance Maximum (nm)	469.7	569.2	830.7
Molar Absorptivity ($M^{-1}cm^{-1}$)	58	19	550
[Pu] @ S/N = 3	3.7E-07	2.4E-06	3.5E-07
α (cm^{-1})	2.1E-05	4.6E-05	1.9E-04
Sensitivity	88	720	84

References

3.1 Allard, B.: Solubilities of Actinides in Neutral or Basic Solutions. In: Actinides in Perspective, (Edelstein ed.) Pergamon Press, New York, pp. 553-580 (1982).

3.2 Connick, R. E., Kasha, M. McVey, W. H., and Sheline, G. E.: The Pentaposive Oxidation State of Plutonium. In: The Transuranium Elements, IV-14B, (Seaborg, Katz, and Manning, eds.) McGraw Hill, New York, pp 2227-240 (1949).

3.3 Cohen, D.: The Absorption Spectra of Plutonium Ions in Perchloric Acid Solutions. J. Inorg. Nucl. Chem. 18, 211-218 (1961).

3.4 Russo, R. E., Silva, R. J., Bucher, J. J., and Edelstein, N. M.: Measurements of Actinide Speciation at Ultralow Solution Concentrations Using Photoacoustic Spectroscopy. Lawr. Liv. Nat. Lab. Report (1986).

3.5 Sawada, T., Oda, S., Shimizu, H., and Kamada, H.: Laser-induced Photoacoustic Spectroscopy of some Rare Earth Ions in Aqueous Solutions. Anal. Chem. 51, No. 6, 688-690 (1979).

3.6 Klenze, R. and Kim, J. I.: Direct Speciation of Transuranium Elements in Natural Aquatic Systems by LIPAS. Radiochim. Acta 44/45, 77-85 (1988).

3.7 Beitz, J. V., Bowers, D. L., Doxtader, M. M., Maroni, V. A., and Reed, D. T.: Detectioon and Speciation of Transuraniumm Elements in Synthetic Groundwater via Pulsed-Laser Excitation. Radiochim. Acta 44/45, 87-93 (1988).

3.8 Pollard, P. M., Liezers, M., McMillan, J. W., Philips, G., Thomason, H. P., Ewart, F. T.: Some Actinide Speciation Using LIPAS. Radiochim. Acta 44/45, 95-101 (1988).

3.9 Moulin, C., Delorme, N., Berthoud, T., Mauchien, P.: Dopuble Bean Thermal Lens Spectroscoppy for Actinide Detection and Speciation. Radiochim. Acta 44/45, 103-106 (1988).

3.10 Bell, A. G., Am. J. Sci. 20, 305 (1880).

3.11 Rosencwaig, A., Opts. Comm., Photoacoustic Spectroscopy of solids. 7 (4), 305 (1973).

3.12 Tyndall, J., Proc. Royal. Soc. London, 31, 307 (1881).

3.13 Preece, W. H., Proc. Royal, Soc. London, 31, 506 (1881).

3.14 Bell, A. G., Phil. Mag. 2, 510 (1881).

3.15 Roentgen, W. C., Phil. Mag. 11, 308 (1881).

3.16 Ewart, F. T., Liezers, M., McMillan, J. W., Pollard, P. M., and Thomason, H. P.: The Development of a Laser Induced Photoacoustic Facility for Actinide Speciation. AERE-R 12875 (1988).

3.17 Rosencwaig, A.: Photoacoustic Spectroscopy of Biological Materials. Science 181, 657 (1973).

3.18 Rosencwaig, A.: Photoacoustic Spectroscopy--A New Tool for Investigation of Solids. Anal. Chem. 47, No. 6 (1975).

3.19 Patel, C. K. N. and Tam, A. C.: Pulsed Optoacoustic Spectroscopy of Condensed Matter. Rev. Mod. Phys. 53, No. 3 (1981).

3.20 Hu, C. and Whinnery, J. R.: New Thermooptical Measurement Method and a Comparison with Other Methods. Appl. Opts. 12 (1), 72-79 (1973).

3.21 Boccara, A. C., Fournier, D., and Badoz, J.: Thermo-optical spectroscopy: Detection by the "mirage effect". Appl. Phys. Lett. 36 (2), 130-132 (1980).

3.22 Fournier, D., Boccara, A. C., Badoz, J.: Photothermal deflection Fourier transform spectroscopy: a tool for high-sensitivity absorption and dichroism measurements. Appl. Opts. 21 (1), 74-76 (1982).

3.23 Jackson, W. B., Amer, N. M., Boccara, A. C., and Fournier, D.: Photothermal deflection spectroscopy and detection. Appl. Opts. 20 (8), 1333-1344 (1981).

3.24 Tam, A. C.: Applications of photoacoustic sensing techniques. Rev. Mod. Phys. 58 (2), 381-430 (1986).

3.25 Schrepp,, W., Stumpe, R., Kim, J. I., and Walther, H.: Oxidation-State-Specific Detection of Uranium in Aqueous Solution by Photoacoustic Spectroscopy. Appl. Phys. B 32, 207-209 (1983).

3.26 Berthoud, T. Mauchien, P., Omenetto, N., and Rossi, G.: Determination of Low Levels of Uranium(VI) in Water Solutions by means of the Laser-induced Thermal Lensing Effect. Anal. Chim. Acta 153, 265-269 (1983).

3.27 Stumpe, R., Kim, J. I., Schrepp, W., and Walther, H.: Speciation of Actinide Ions in Aqueous Solution by Laser-Induced Pulsed Photoacoustic Spectroscopy. Appl. Phys. B 34, 203-206 (1984).

3.28 Russo, R. E., Silva, R. J., Bucher, J. J., and Edelstein, N. M.: Measurments of Actinide Speciation at Ultralow Solution Concentrations Using Photoacoustic Spectroscopy. Lawr. Liv. Nat. Lab. Report (1986)

3.29 Doxtader, M. M., Maroni, V. A., Beitz, J. V., and Heaven, M.: Materials Research Soc. Symposia Proceedings 84, 173 (1987).

3.30 Landau, L. D. and Lifshitz, E. M.: 'Fluid Mechanics', Chapt. 8, (Sykes and Reid, translators and eds.) Pergamon Press, Oxford (1959).

3.31 Brueck, S. R. J., Kildal, H., and Belanger, L. J.: Photo-acoustic and Photo-refractive Detection of Small Absorptions in Liquids. Opts. Comm. 34 (2), 199-204 (1980).

3.32 Lai, H, M. and Young, K.: Theory of the Pulsed Optoacoustic Technique. J. Acoust. Soc. Am. 72 (6), 2000-2007 (1982).

3.33 Heritier, J. M.: Electostrictive Limit and Focusing Effects in Pulsed Photoacoustic Detection. Opts. Comm. 44 (4), 267-272 (1983).

3.34 Silk, M. G.: Ultrasonic Transducers for Nondestrictive Testing, Adam Hilger Ltd., London (1984).

3.35 CRC Handbook of Chemistry and Physics (Weast and Astle, eds.) CRC Press, Florida (1986).

3.36 'Five Modern Piezoelectric Ceramics', Vernitron Ltd., Bedford, Ohio Bulletin 66011/F (9176).

3.37 Spescha, G. and Volle, E.: 'Piezoelectric Measuring Instruments', P. Ballanta, Raterschen (1971).

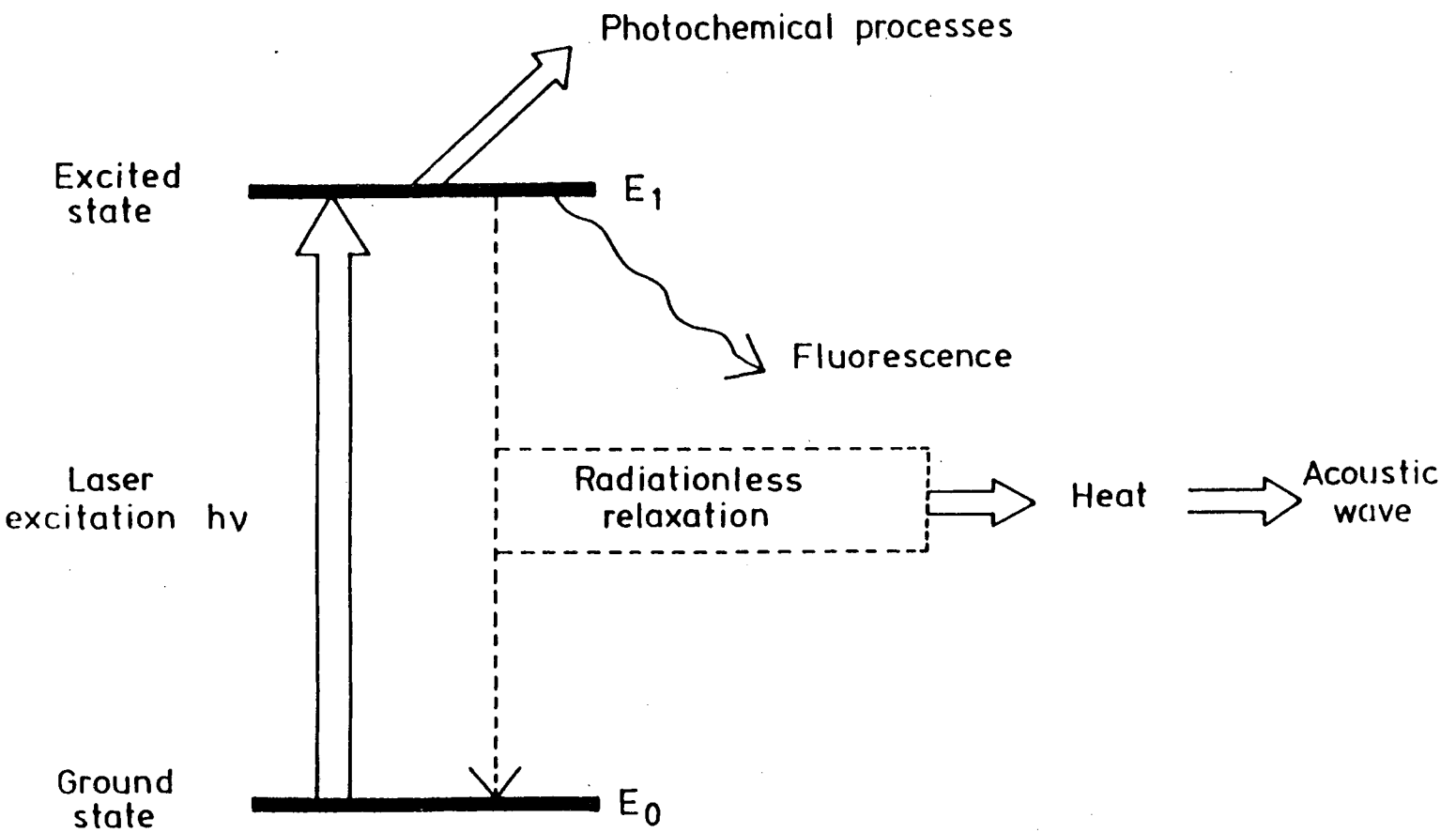

Figure 3.1 The Photoacoustic Process

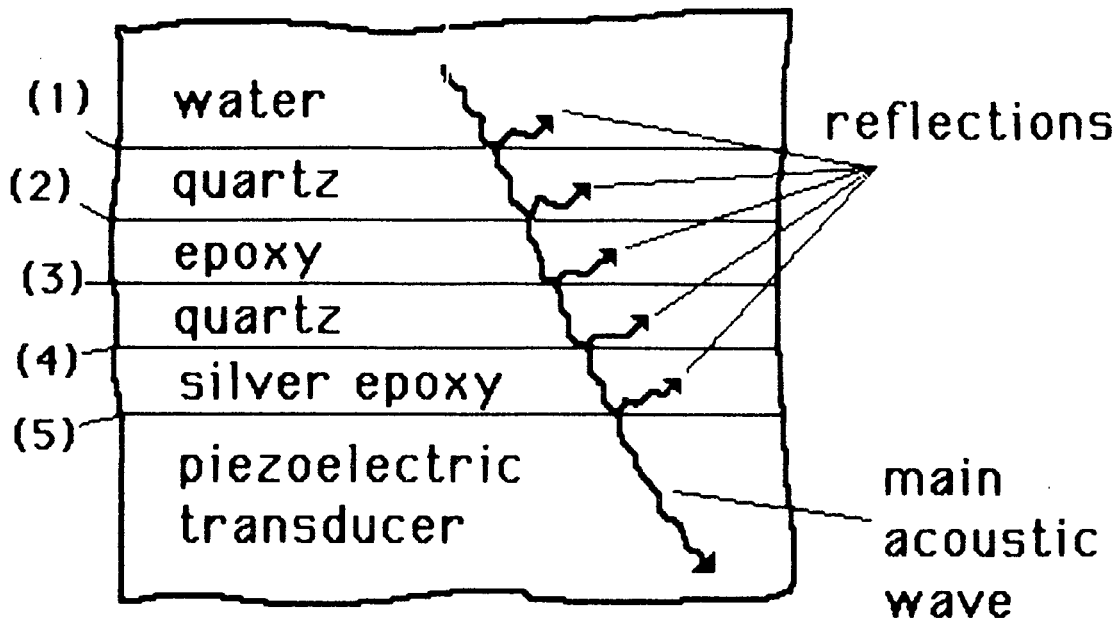

Figure3.2: Acoustic losses in the cell assembly detection system.

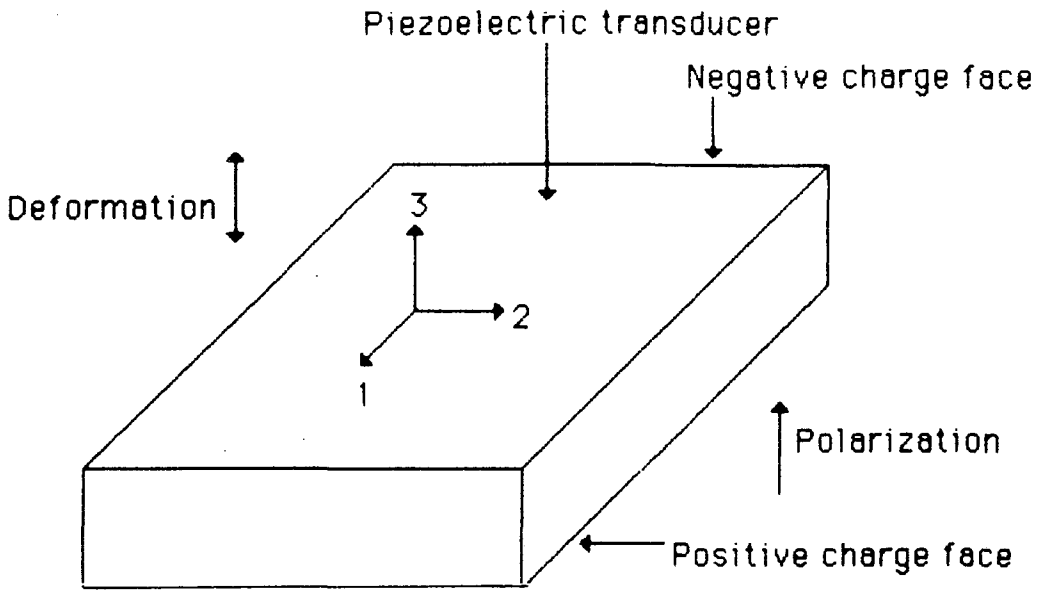

Figure 3.3: The planes of a piezoelectric transducer

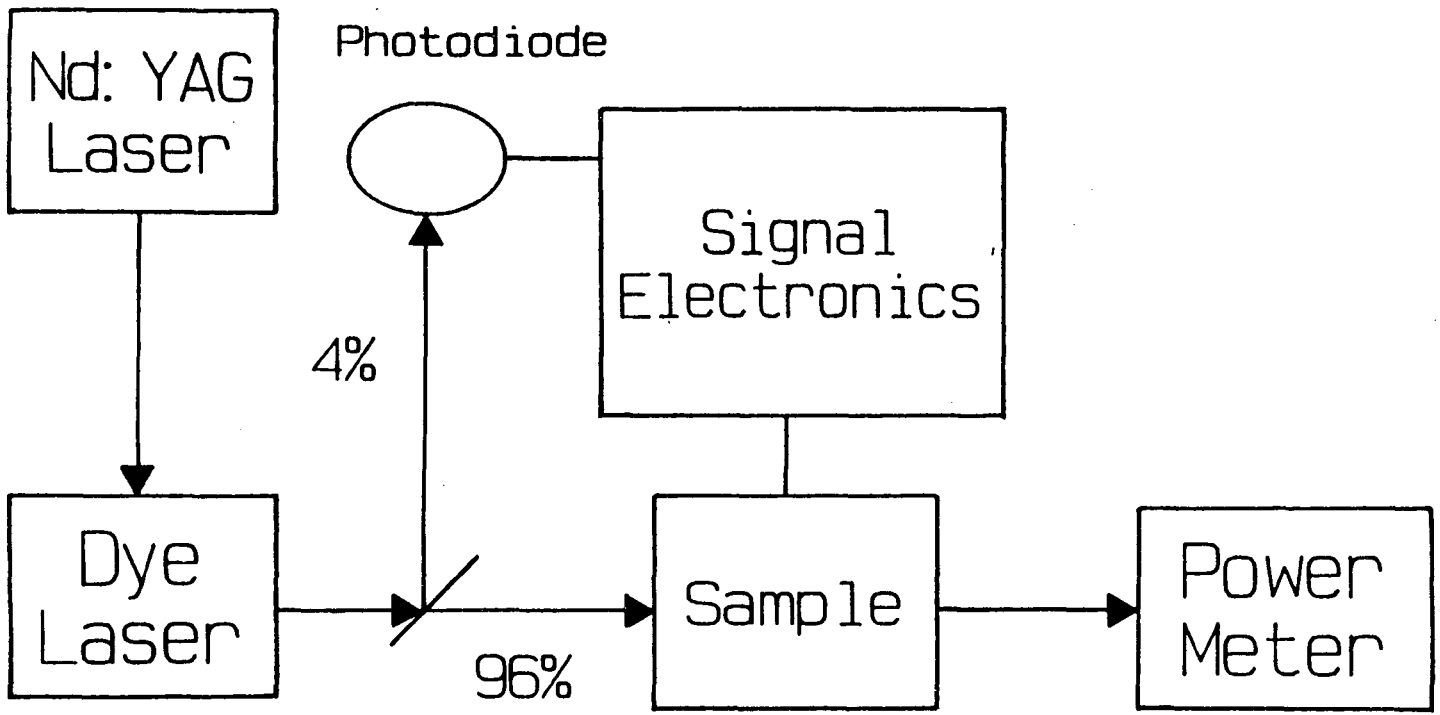

Figure 3.4 Block Diagram of our Laser Induced Photoacoustic Spectrometer System.

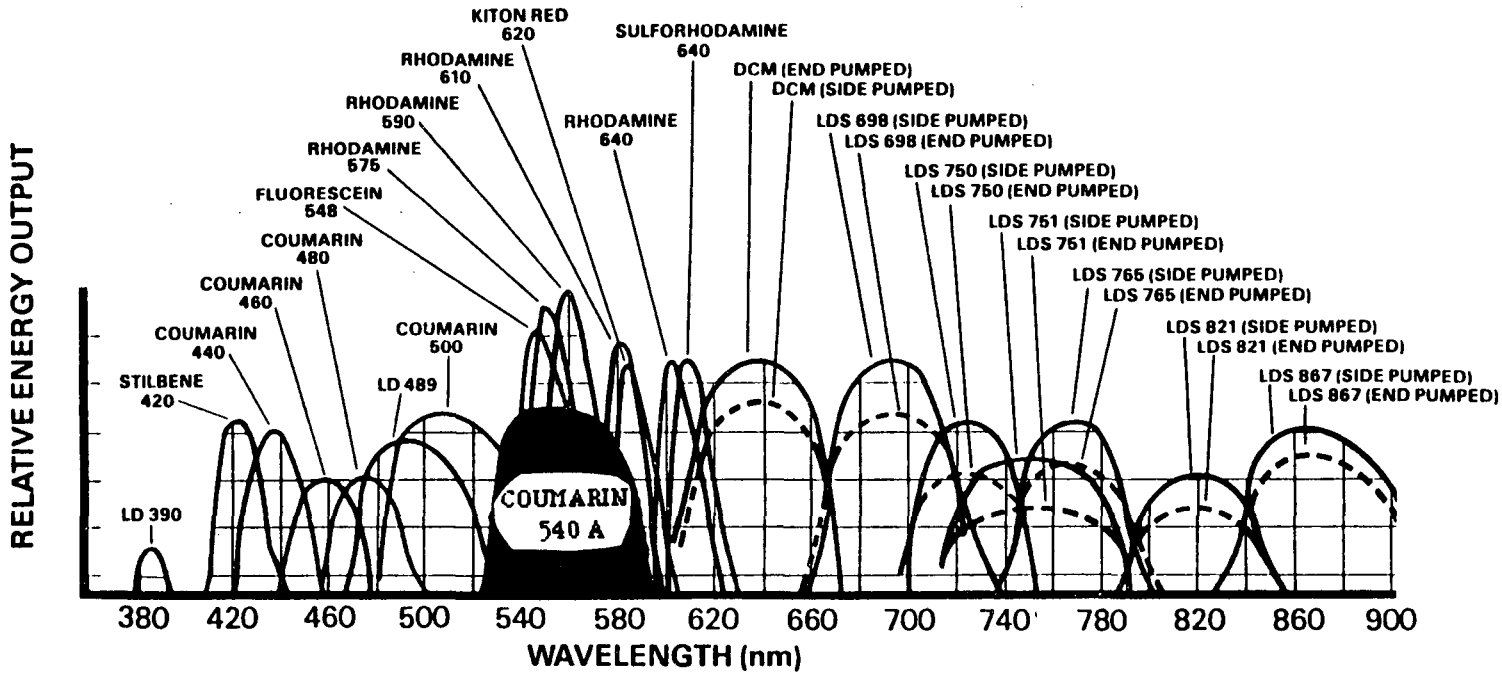

Figure 3.5 Laser dye gain curves for Nd:YAG pumped laser dyes.

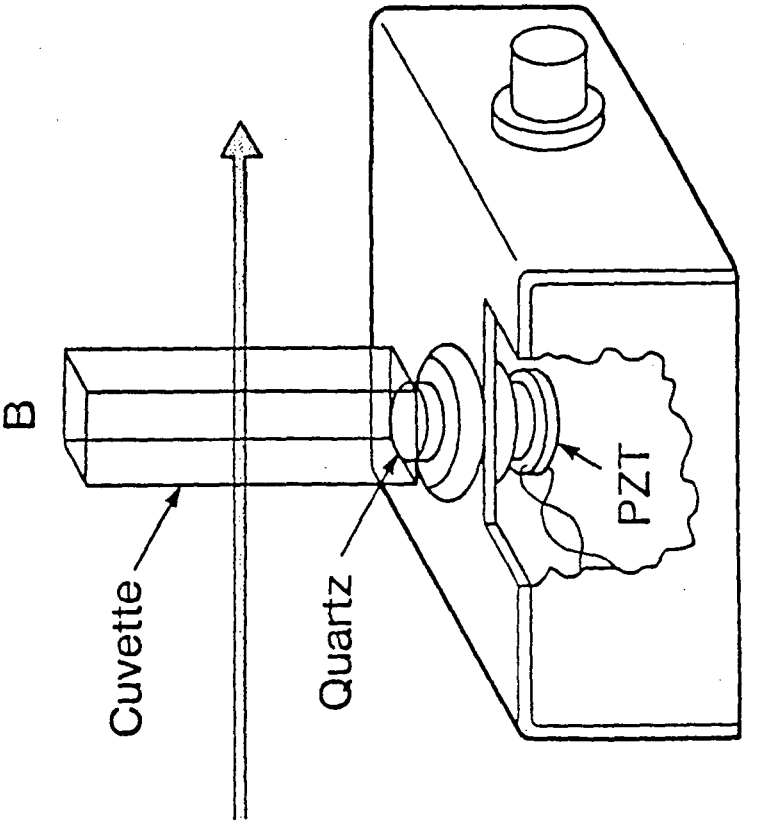

FIGURE 3.6 Cell assembly of detection system.

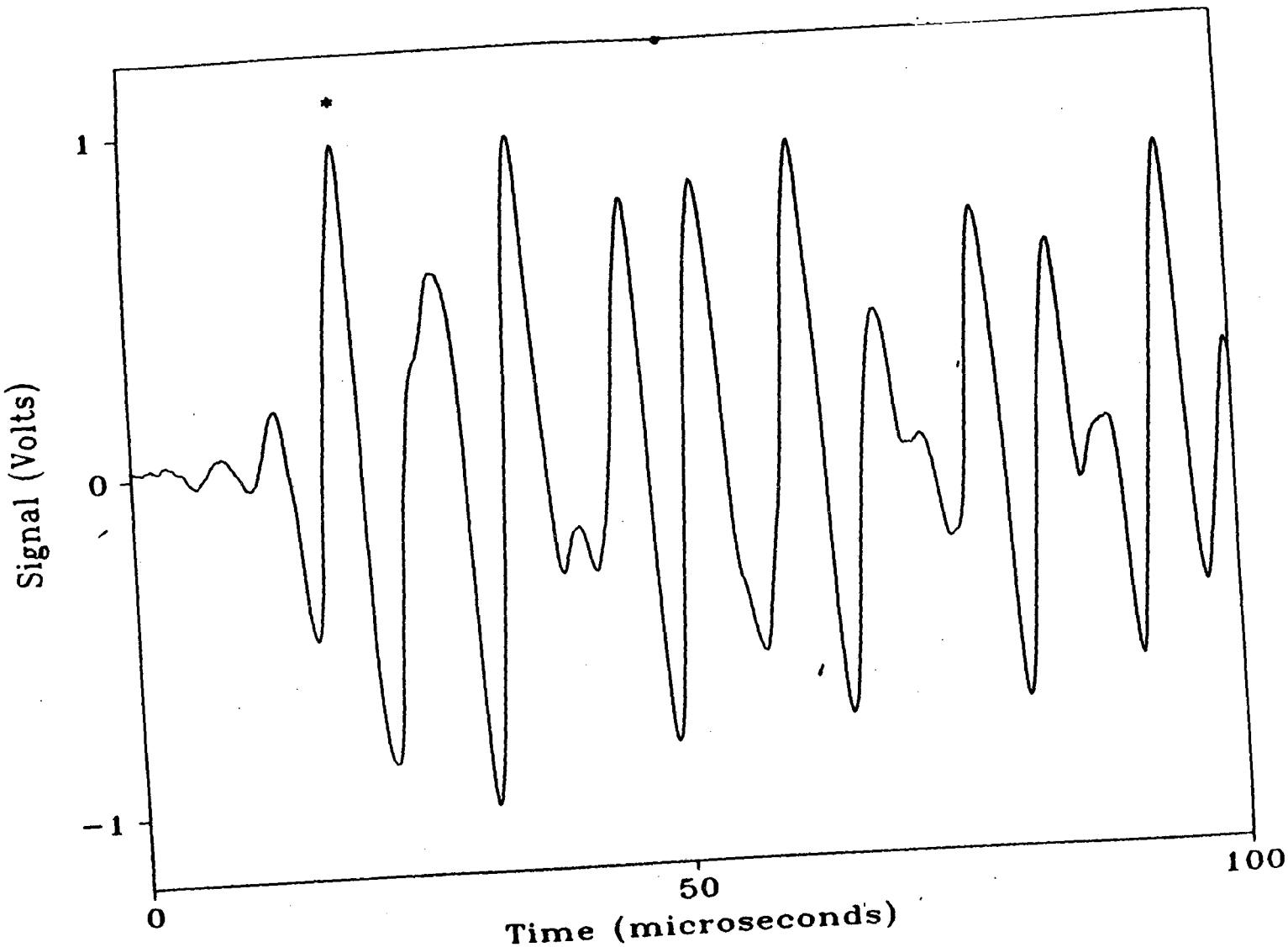

Figure 3.7 Amplified photoacoustic signal with the * indicating the position of the gate.

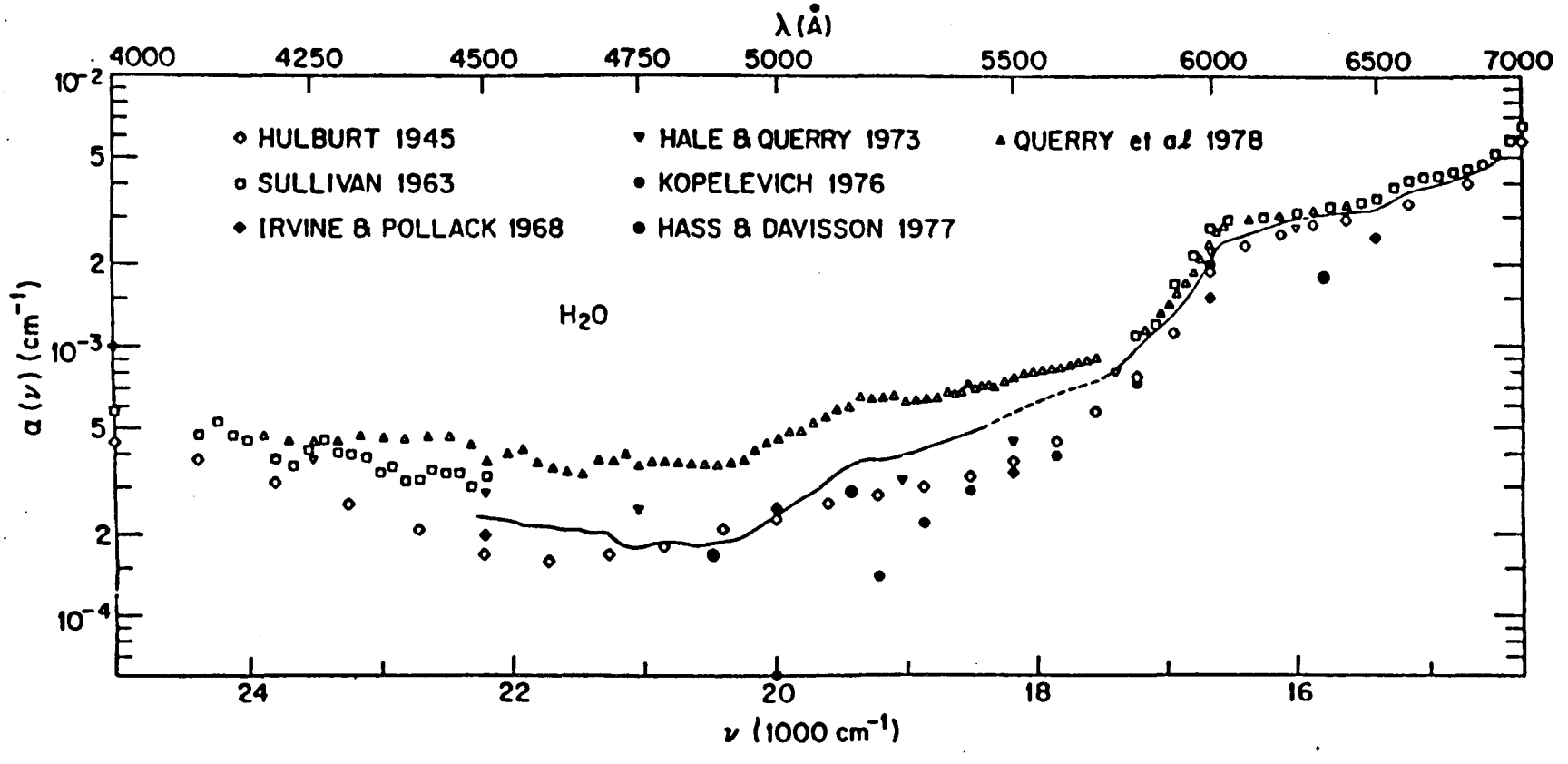

Figure 3.8 The absorption spectrum of water.

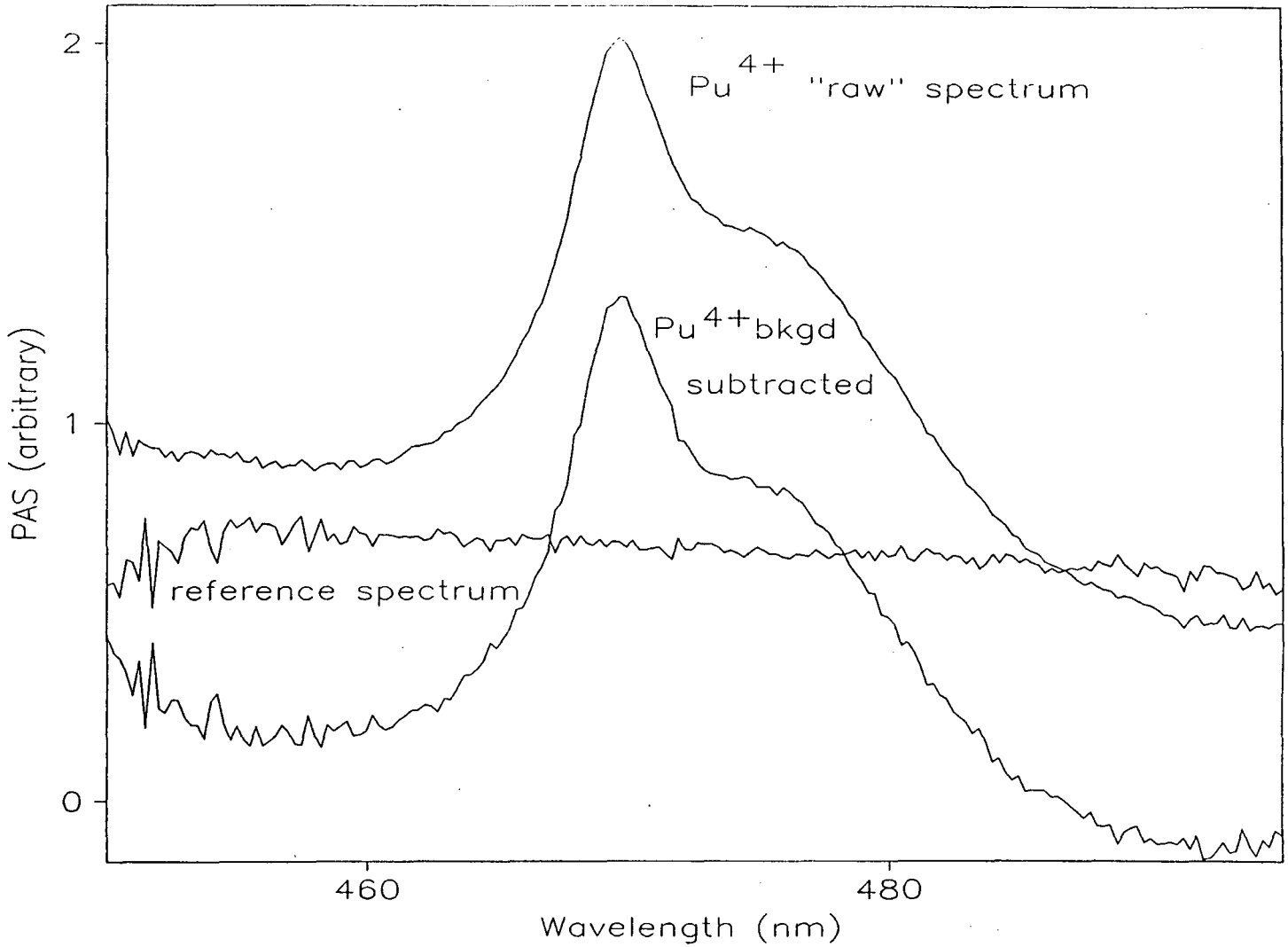

Figure 3.9 PAS spectra of Pu^{4+}.

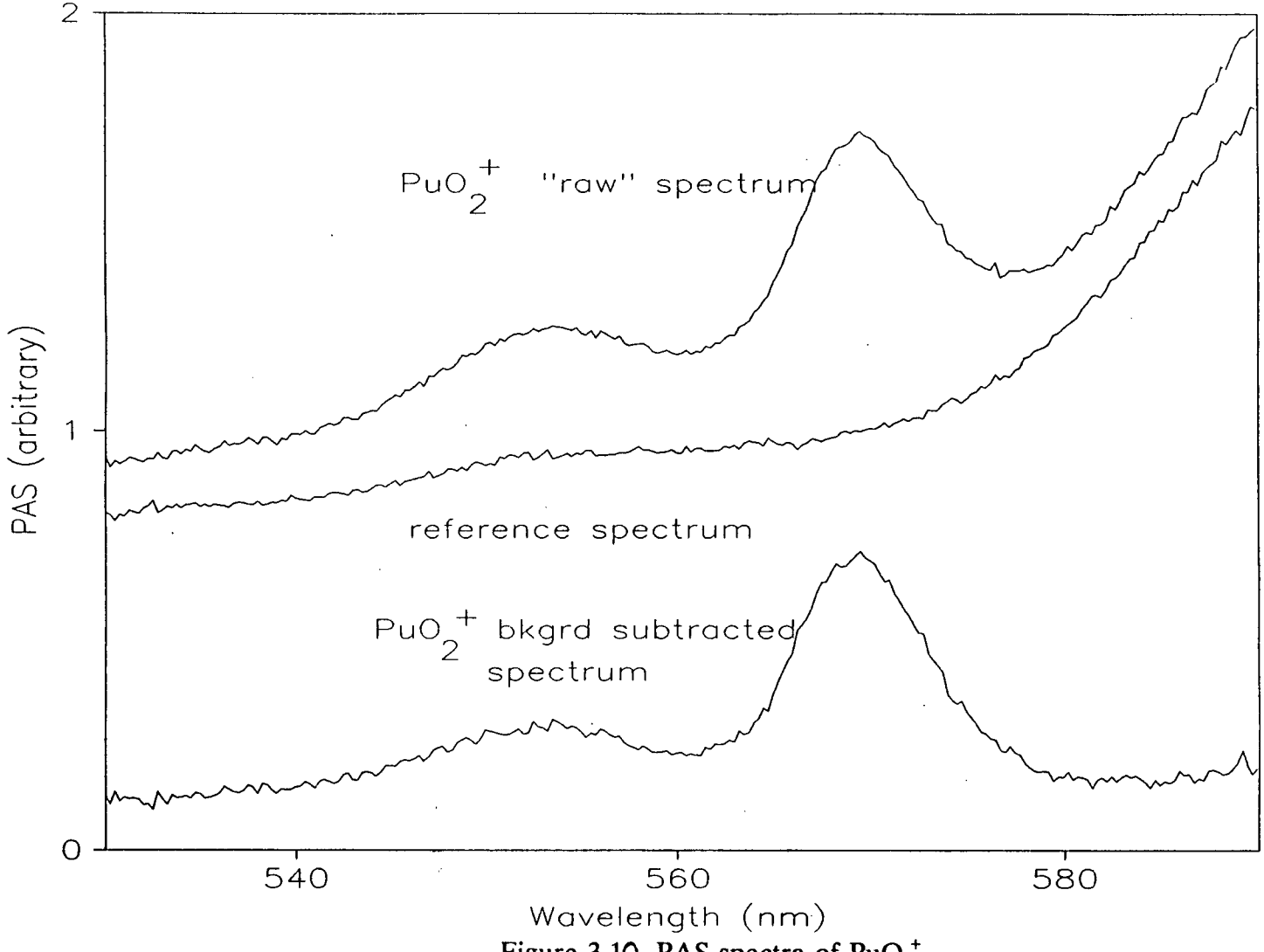

Figure 3.10 PAS spectra of PuO_2^+.

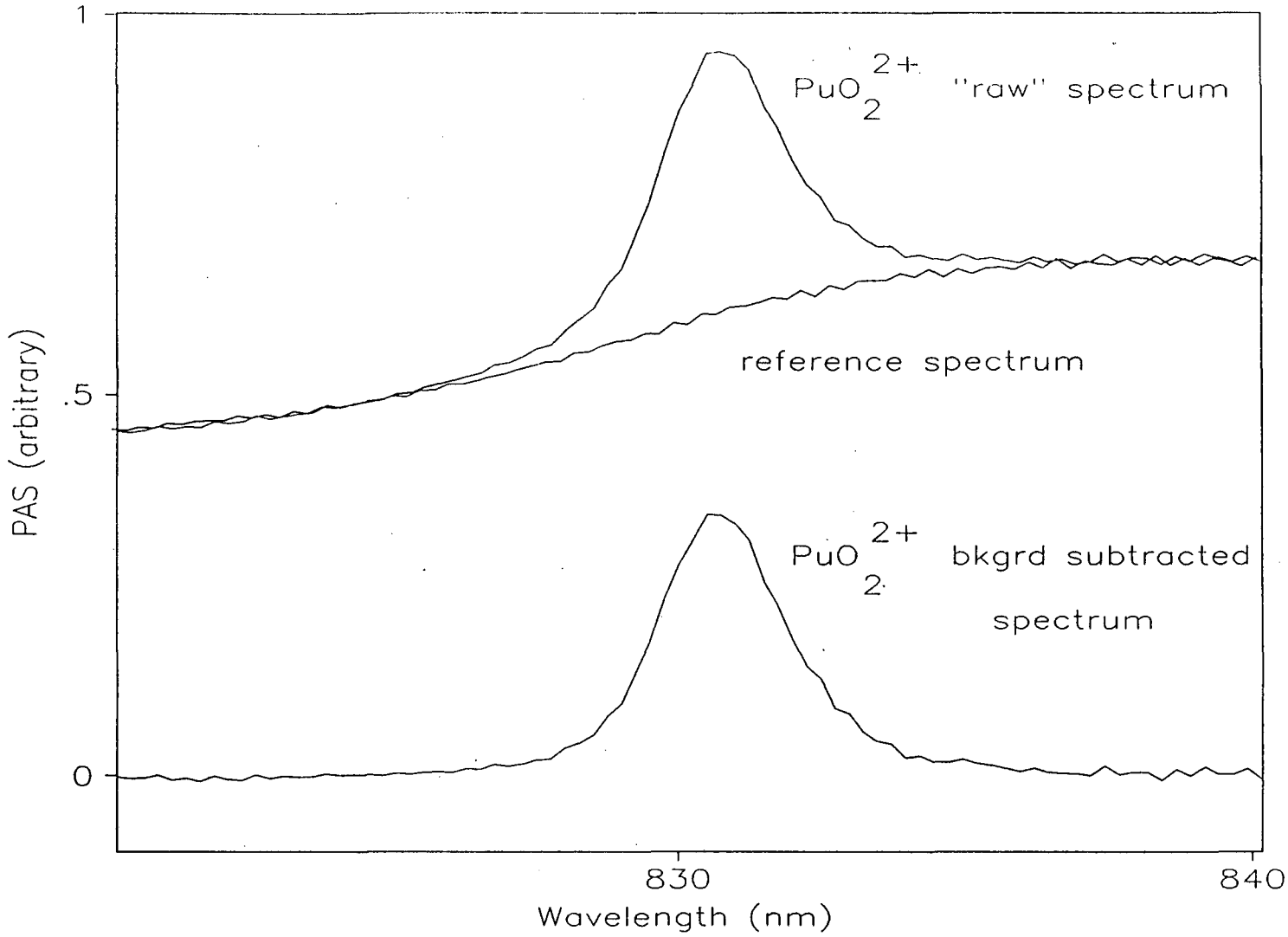

Figure 3.11 PAS spectra of PuO_2^{2+}.

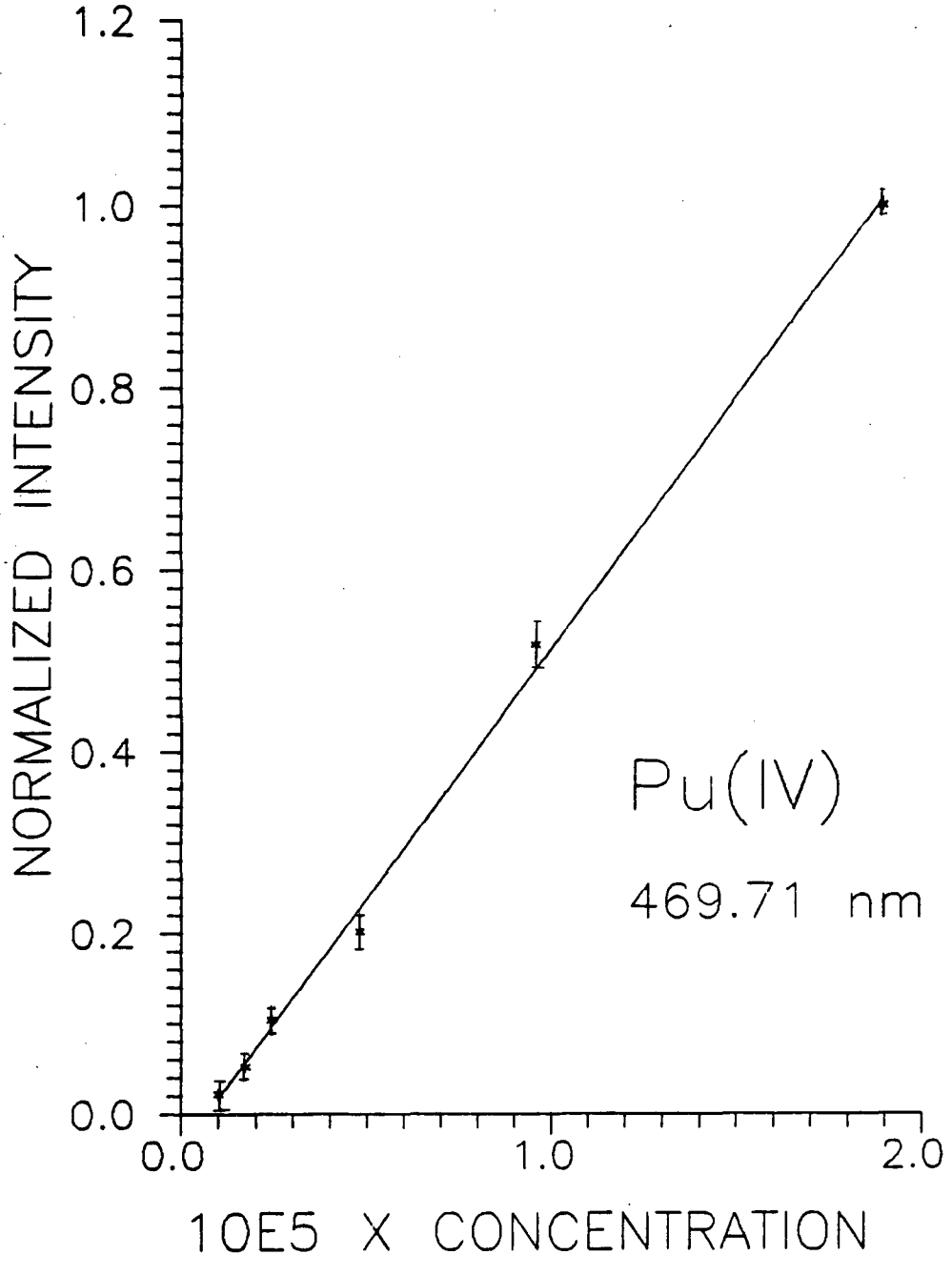

Figure 3.12 Beer's Law plot of Pu^{4+}.

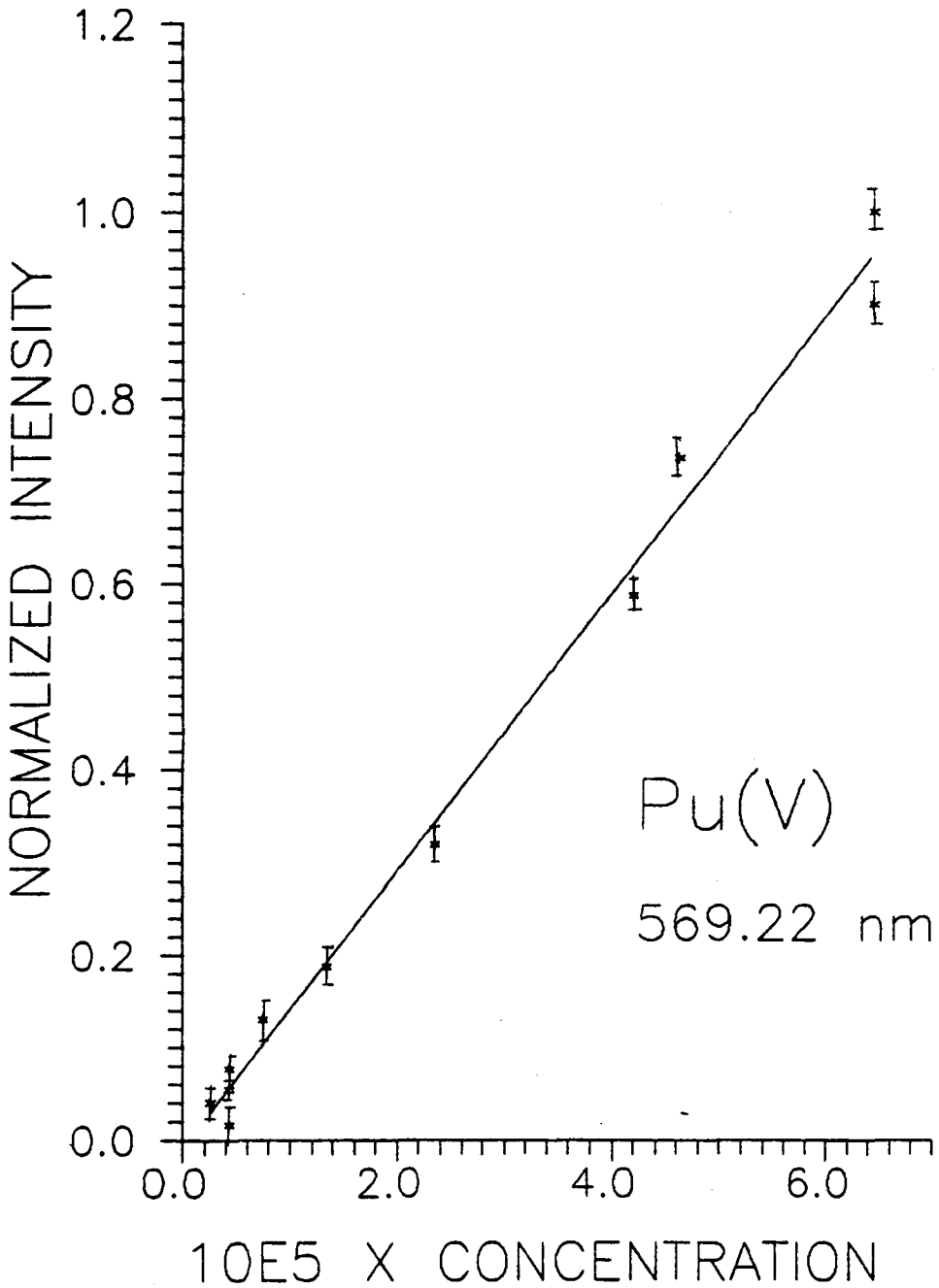

Figure 3.13 Beer's Law plot of PuO_2^+.

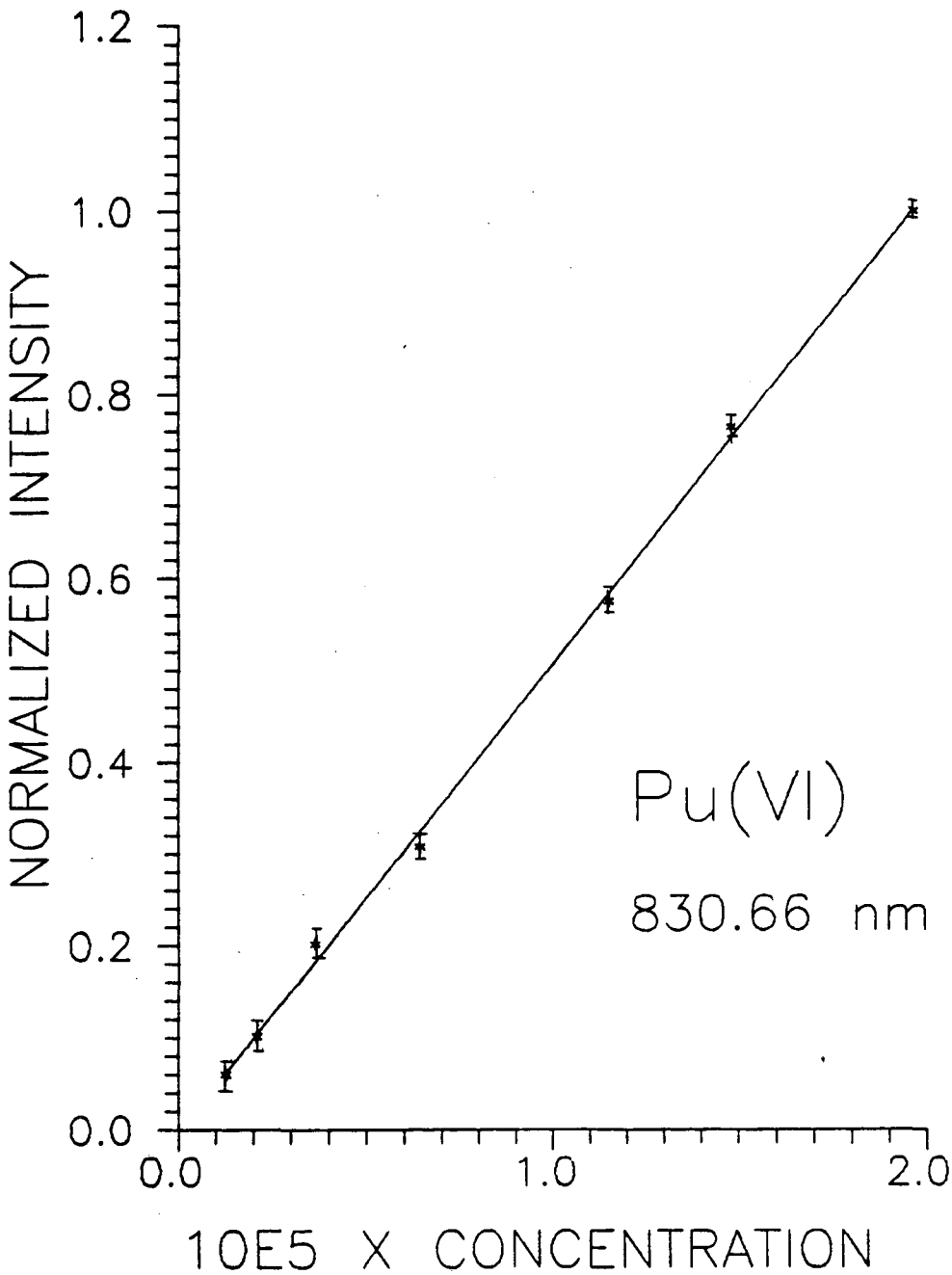

Figure 3.14 Beer's Law plot of PuO_2^{2+}.

Chapter 4

The Spectroscopic Method of Measuring Stability Constants

The objective of equilibrium studies is to design the best model for a given system. This model includes the number of species in solution, the stoichiometry of the complexes formed, the stability constants of the complexation reactions, and molar absorptivities at selected

wavelengths. The overall formation constant of the complex $M_pL_qH_r^{(px-qy-r)}$ is defined by

$$pM^{x+} + qL^{y-} + rH^{+} \rightleftharpoons M_pL_qH_r^{(px-qy-r)} \qquad (4.1)$$

where any hydrogen ion dependence is found in the denominator

$$\beta_{pqr} = [\, M_pL_qH_r^{(px-qy-r)} \,] / [M^{x+}]^p[L^{y-}]^q[H^+]^r \qquad (4.2)$$

For hydrolysis, the complexation reaction is written as

$$pM^{x+} + qL^{y-}\ rH_2O \rightleftharpoons M_pL_q(OH)_r^{(px-qy-r)} + rH^+ \qquad (4.3)$$

Because the hydrogen ion concentration is located in the numerator, the stability constant is distinguished with an *, as shown in Eq. 4.4

$$^*\beta_{pqr} = [\, M_pL_q(OH)_r^{(px-qy-r)} \,] [H^+]^r / [M^{x+}]^p[L^{y-}]^q \qquad (4.4)$$

The spectroscopic data are composed of the absorbance, A, which is a linear function of concentration of a given species at a specified wavelength, λ. The absorbance of a solution is given by Beer's Law, which may be expressed as in Eq. 4.5 as

$$A_{obs} = \epsilon_1 c_1 l + \epsilon_2 c_2 l + \ldots \epsilon_n c_n l \qquad (4.5)$$

where A_{obs} is the observed absorbance at wavelength λ; $\epsilon_1, \epsilon_2, \ldots \epsilon_n$ are the molar absorptivities of species 1, 2, . . . n at wavelength λ;

$c_1, c_2, \ldots c_n$ are the concentrations of species 1, 2, . . . n, respectively, and l is the path length.

An overall picture of the experimental approach is shown in Figure 4.1. Based on the initial estimate for the equilibrium model, spectra are obtained from a series of solutions in which the metal:ligand ratios range from an excess of the metal ion to an excess of the ligand. The data are then processed in a manner consistent with the initial estimate of the equilibrium model. When a bad fit is noted between the experimental and calculated observable, the equilibrium model and experimental plan are modified accordingly.

4.1 Data Analysis: Review of Literature Methods

Numerous algorithms have been developed and adapted for computing stability constants. D. J. Leggett has reviewed the approaches and algorithms reported through 1983 [4.1]. This summary will emphasize the different fundamental concepts, rather than specific algorithms. The "best fit" of formation constants to the observed data may be expressed in terms of the least-squares criterion. The quantity W, the sum of the

squares of residuals, is defined according to Eq. 4.6 as:

$$W = \sum_{k=1}^{m} [Y^k_{obs} - Y^k_{calc}]^2 \qquad (4.6)$$

The Y^k_{obs} are the observed data, the Y^k_{calc} are the values of the objective function defined in general terms as f(x,t). The dependent variable vector, x, includes the formation constants and any other parameters that may be required by the equilibrium model (molar absorptivities, enthalpy of formation, etc.) and/or experimental conditions (concentrations, calibration constants, etc.). The independent vector, t, comprises experimentally determined variables. Therefore, the set of dependent variables that minimizes W will give the "best fit", as shown in Figure 4.2. The approaches used to accomplish this minimization can be broken into several categories, each with their own relative assets and liabilities. In most cases, the tradeoff is based on time versus efficiency. However, the increasing capability and decreasing cost of small computers has allowed the more complex, and often more time consuming, computational methods to become increasingly feasible.

4.1.1 Direct Search and Univariate Methods

Direct search and univariate methods are the simplest methods that have been used. These include grid [4.2-5], star [4.6,7], and composite [4.7] design approaches. The disadvantage of these techniques is that they are slow to converge. Their advantage is the ablity to discover multiple minima in the error surface.

The Fibonacci sequence [4.8] and the Golden Section [4.9] routines have been useful for determination of a single constant, but may not converge for general functions.

The method of Hooke and Jeeves involves a two step process of parameter evaluation followed by movement along the best parameter fit into error space. The Simplex [4.10-12] searching technique of moving an n dimensional figure through error space has become increasingly more popular. It is considered by some to be one of the most efficient pattern search methods currently available [4.13]. Both the Hooke and Jeeves and Simplex methods are slow to converge near the minimum, but their small memory requirements make them ideally suited for small computers.

Methods utilizing quadratic and cubic interpolation have also been used. Quadratic interpolation [4.14] is limited to a one-dimensional search requiring function values only. The cubic method [4.15] is more complicated than the quadratic and requires fewer iterations to locate the minimum.

4.1.2 Least-Squares Methods

4.1.2.1 Newton-Raphson

The Newton-Raphson method, first used by Sillén in his program LETAGROP [4.16], is based on modeling the error surface, W, by a Taylor series. Calculus states that by setting the first-order differential of y = f(x), dy/dx, to zero and solving for x locates the exact minimum (or maximum) of the function. Generalization of this basic premise forms the basis for the gradient method. A column vector x, and its transpose $x^T = (x_1, x_2, \ldots, x_n)$ are used to treat the n parameters. Changes in the parameters are represented by Δx and its transpose $\Delta x^T = (\Delta x_1, \Delta x_2, \ldots, \Delta x_n)$. Transposition of the gradient vector, VW, results in the Jacobian

gradient vector g:

$$g^T = \nabla W = [\, \partial W/\partial x_1, \partial W/\partial x_2, \ldots, \partial W/\partial x_n \,] \qquad (4.7)$$

The symmetric matrix of second order partial differentials of W is known as the the Hessian:

$$H = \begin{vmatrix} \frac{\partial^2 W}{\partial x_1^2} & \frac{\partial^2 W}{\partial x_1 \partial x_2} & \cdots & \frac{\partial^2 W}{\partial x_1 \partial x_n} \\ \frac{\partial^2 W}{\partial x_2 \partial x_1} & & & \\ \vdots & & & \vdots \\ \frac{\partial^2 W}{\partial x_n \partial x_1} & & & \frac{\partial^2 W}{\partial x_n^2} \end{vmatrix} \qquad (4.8)$$

If the first and second order derivatives exist and can be evaluated, then the Taylor expansion of the function can be used to minimize the function. A positive definite Hessian matrix and all zero elements in the Jacobian vector represent the minimum. If the function, W(x), is quadratic, then the Taylor expansion is exact and the minimum can be evaluated directly. For the general case, the error fuction is assumed to be approximated by a parabola near the minimum, as shown in Figure 4.3. Therefore, truncation of the Taylor series gives:

$$W \approx W(x_o) + g^T\Delta x + 1/2\Delta x^T H\Delta x \qquad (4.9)$$

Partial differentiation and setting the equation to zero give:

$$\Delta x = -H^{-1}g \qquad (4.10)$$

where Δx indicates the movement required to approach the minimum of Eq. 4.10. One reexpands about the point $x_o + x$. If this is a true minimum in W, then the algorithm has converged. If not, another iteration is carried out.

4.1.2.2 Gauss-Newton Method

If $Y^k_{calc} = \sum a_{ki}x_i$, then the solution can be obtained from a linear least-squares analysis. This is generally not the case and the objective function is modeled by a Taylor series.

$$f_k(x) = f_k(x_o) + \sum \partial f_k/\partial x_i \, \Delta x_i + \ . \ . \ . \qquad (4.11)$$

The k^{th} residual resulting from the initial x, x_o is expressed as:

$$R_k^o = Y^k_{calc}(x) - f_k(x_o) \approx \sum_i \partial f_k/\partial x_i \, \Delta x_i \qquad (4.12)$$

The summation is expanded, truncated, and rearranged to fit a form suitable for linear least-squares analysis. Substitution of $H = 2A^TA$ into

Eq. 4.10 gives the solution having the form

$$\Delta X = [\,2A^TA]^{-1}A^TR \qquad (4.13)$$

where ΔX provides information regarding movement toward the minimum [4.17]. Again, replacement of x_o with $x_o + \Delta x$ either yields the minimum or the point of departure for the next iteration.

An adaptation of the Gauss-Newton method has been suggested by Leveberg [4.18] and Marquardt [4.19]. They acknowledge that a steepest descent method is more appropriate away from the minimum while the Gauss-Newton iteration converges more rapidly near the minimum. An adjustable parameter, Ω, has been introduced into the Gauss-Newton least-squares increment such that:

$$\Delta x = -[\Omega I + A^TA]^{-1}A^Tf \qquad (4.14)$$

where I is the identity matrix used for the purpose of scaling. By continually updating the value of Ω, the algorithm is able to choose between the two minimization schemes.

4.2 Stability Quotients from Absorbance Data (SQUAD)

The program Stability Quotients from Absorbance Data (SQUAD) was used to calculate the best values for the stability constants of the proposed equilibrium model by employing a nonlinear least-squares approach. The program is completely general in scope, having the capability to calculate stability constants for the general complex system $M_pM'_pL_qL'_qH_r$, where p, p′, q, q′ ≥ 0 and r is positive for protons, negative for hydroxide ions, or zero. Therefore, the same program may be used to study acid-base equilibria for ligands that are weak acids (or bases); M_pL_q; mixed-ligand (or mixed-metal) complexes; protonated or hydroxy complexes. SQUAD was originally designed to process absorbance data from aqueous solutions. However, recent modification permit the analysis of data from any type of solution.

SQUAD evolved from a number of earlier programs. Nagano and Metzler [4.3] developed the program PITMAP implementing a FORTRAN coding of Sillen's twist matrix algorithm [4.20] and using the concept of "two-level adjustment of common and group parameters" [4.21].

PITMAP was extensively modified by Thompson [4.22], but still required recoding of the species concentration subroutine for each new model tested. This problem was alleviated by incorporating the subroutine COGSNR, from SCOGS [4.23], into PITMAP [4.24]. Unsatisfactory experiences with this new version of PITMAP led to SCOGS being rewritten in subroutine form, one set of routines for the Gauss-Newton least-squares algorithm and another set to solve the mass balance equations. When a sum of squares of residuals subroutine was added, which incorporated Cramer's method for solving a system of linear equations, SQUAD was born [4.6]. Extensive use of this version of SQUAD uncovered the problem of the calculation of negative molar absorptivities. This difficulty was overcome by replacing Cramer's algorithm with a multiple regression (MR) and a nonnegative linear least-squares algorithm (NNLS) [4.27]. MR or NNLS can be used at the users discretion to solve the Beer's law equations.

References

4.1 Leggett, D. L.: "Computational Methods for the Determination of Formation Constants", Plenum Press, New York (1985).

4.2 Izatt, R. M., Eatough, D., Snow, R. L. Christensen, J. J.: Computer Evaluation of Entropy Titration Data. Calorimetric Determination of Log β_i, ΔH_i, and ΔS_i Values for the Silver(I) and Copper(II) Pyridine Systems, J. Phys. Chem. 72, 1208-1213 (1968).

4.3 Nagano, K., Metzler, D. E.: Machine Computation of Equilibrium Constants and Plotting of Spectra of Individual Ionic Species in the Pyridoxal System, J. Am. Chem. Soc. 89, 2891-2900 (1967).

4.4 Leussing, D. L.: Schiff Base Complexes. A Numerical Study of the Nickel(II)-Pyruvate-Glycinate System Using a High Speed Computer, Talanta 11, 189-201 (1964).

4.5 Natansohn, S., Krugler, J. I., Lester, J. E., Chagnon, M. S., Finocchiaro, R. S.: Stability Constants of Complexes of Molydbate and Tungstate Ions with o-Hydroxy Aromatic Ligands.J. Phys. Chem. 84, 2972-2980 (1980).

4.6 Leggett, D. J. and McBryde, W. A.: General Program for the Computation of Stability Constants for the Absorbance Data, Anal. Anal, Chem. 47, 1065-1070 (1975).

4.7 Hahn, G. J.: "Statistics" Eastern Analytical Symposium (R. F. Hirsch, ed.), The Franklin Institute Press, Philadelphia, PA (1978).

4.8 Kieffer, J. J.: Sequential Minimax Search for a Maximum, Proc. Am. Math. Soc. 4, 269-282 (1970).

4.9 Gans, P. and Irving, H. M. N. H.: The Calculation of Stability Constants of Weak Complexes from Spectrophotometric Data, J. Inorg. Nucl. Chem. 34, 1885-1890 (1972).

4.10 Spendley, W, Hext, G. R, Himsworth, F. R.: Sequential Applications of Simplex Designs in Optimization and Evolutionary Operation, Technometrics 4, 441-461 (1962).

4.11 Nelder, J. A. and Mead, R.: A Simplex Method for Function Minimalization, Comput. J. 7, 308-313 (1965).

4.12 Deming, S. N. and Parker, L. R.: A Review of Simplex Optimization in Analytical Chemistry, Crit. Rev. Anal. Chem. 7, 187-202 (1978).

4.13 Walsh, G. R.: "Methods of Optimizations", Wiley, New York (1975).

4.14 Powell, M. J. D.: An Efficient Method for Finding the Minimum of a Function of Several Variables withour Calcualtiong Derivatives, Comput. J. 7, 155-162 (1964).

4.15 Davidon, W. C.: "Variable Metric Method for Minimization, AEC(US) Research and Development ANL-5990 (Rev. 2)", Argonne Nat'l Lab., Argonne, IL (1966).

4.16 Dyrssen, D., Ingri, N., Sillén, L. G.: "Pit-Mapping"--A General Approach for Computer Refinement of Equilibrium Constants, Acta Chem. Scand. 15, 694-696 (1961).

4.17 Anton, H.: "Elementary Linear Algebra", Wiley, New York (1977).

4.18 Levenberg, K. A.: A Method for the Solution of Certain Nonlinear Problems in Least Squares, Quart. Appl. Math. 2, 164-168 (1944).

4.19 Marquardt, D. W.: An Algorithm for Least Squares Estimation of Nonlinear Parameters, J. Soc. Indust. Appl. Math. 11, 431-441 (1963).

4.20 Ingri, N. and Sillen, L. G.: High-Speed Computer as a Supplement to Graphical Methods III.Acta Chem. Scand. 18, 1085-1098 (1964).

4.21 Sillen, L. G. and Warnqvist, B.: High-Speed Computer as a Supplement to Graphical Methods 6. A Strategy for Two-level LETAGROP Adjustment of Common and "Group" Parameters. Some Features that Avoid Divergence. Acta Chem. Scand. 31, 315-339 (1968).

4.22 Thompson, J. A.: Ph.D. thesis, Univ. of Waterloo, Dept of Chem. (1970).

4.23 Sayce, I. G.: Computer Calculations of Equilibrium Constants of Species Present in Mixtures of Metal Ions and Complexing Agents, Talanta 15, 1397-1411 (1968).

4.24 Leggett, D. J. and McBryde, W. A. E.: Metal Ion Interaction of Picoline-2-Aldehyde Thiosemicarbazone, Talanta 22, 781-789 (1975).

4.25 Leggett, D. J.: Numerical Analysis of Multicmponent Spectra, Anal. Chem. 49, 276-281 (1977).

4.26 Tobias, R. S. & Yasuda, M.: Computer Analysis of Stability Constants in Three-Component Systems with Polynuclear Complexes. Inorg. Chem. 2, 1307-1310 (1963).

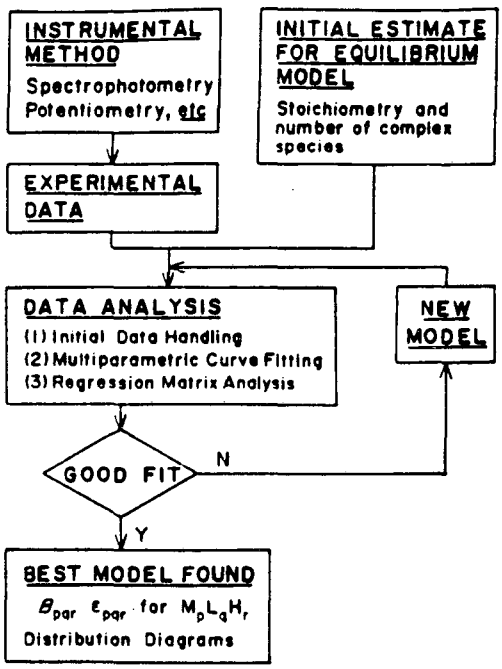

Figure 4.1 Overall scheme for equilibrium model studies.

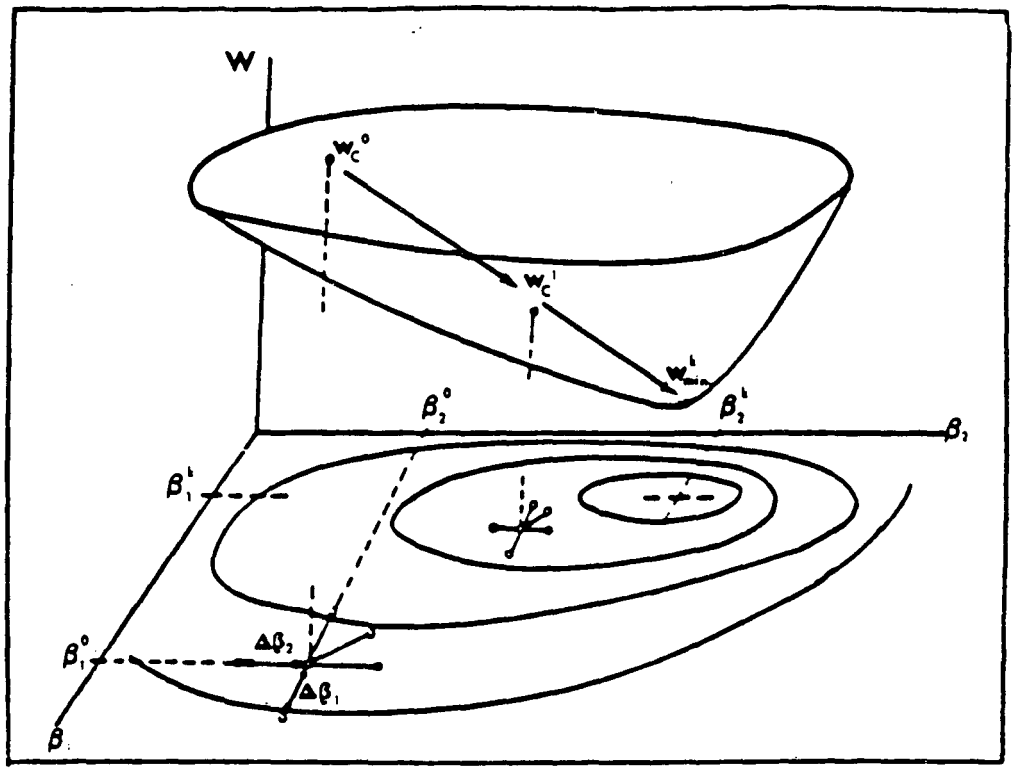

Figure 4.2 Graphical representation of a systematic search of the error suface, W.

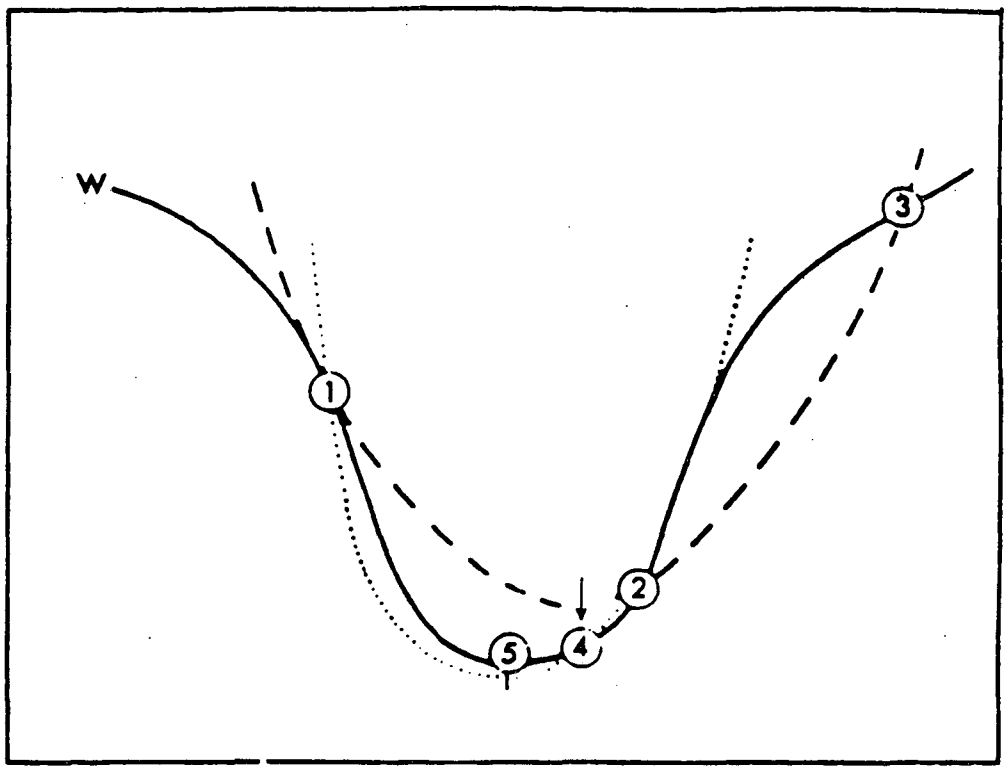

Figure 4.3 Convergence to a minimum by parabolic interpolation. A parabola (- - -) is drawn through the three original points 1, 2, 3 on the given function (_____). The function is evaluated at the parabola's minimum, 4, which replaces point 3. A new parabola (. . .) is drawn through points 1, 4, 2. The minimum of this parabola is at 5, which is close to the minimum of the function.

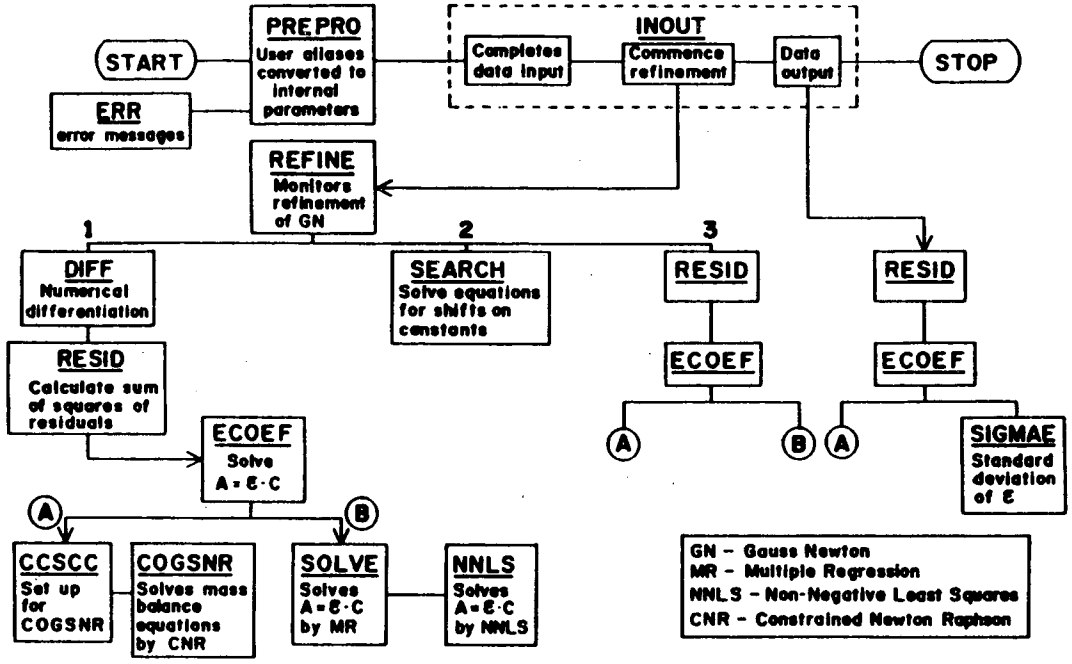

Figure 4.4 A block diagram for the computer program SQUAD showing the interrelationships of the various subroutines.

Chapter 5

Hydrolysis of PuO_2^+

By definition, hydrolysis refers to the reaction of anything with water. In inorganic chemistry, the word has been primarily applied to cations which form soluble hydroxide or oxide complexes and, to a lesser extent, hydroxide and oxide precipitates. Hydrolysis reactions are common to most cations because most metal atoms form strong bonds to oxygen and the OH^- ligand is always present in water at concentrations which can be varied over an unusually wide range (>1 to $<10^{-14}$ M) as a result of the small self-dissociation constant of water [5.1]:

$$Q_w = [H^+]\,[OH^-] \approx 10^{-14} \qquad (5.1)$$

Hydrolytic reactions are often written as in Eq. 5.2

$$mM^{z+} + yH_2O \rightleftharpoons M_m(OH)_n^{(mz-n)+} + nH^+ \qquad (5.2)$$

where the overall formation constant for a hydrolysis product is defined by Eq. 5.3

$$*\beta_{mn}(I) = \{\,[M_m(OH)_n^{(mz-n)+}]\,[H^+]^n\,\} / \,[M^{z+}]^m \qquad (5.3)$$

where I indicates the ionic strength of the solution and the subscript m is omitted for mono nuclear complexes.

However, a more realistic description would be to consider the hydrolysis reaction as the acid dissociation of the metal-ion hydrates, as shown in Eq. 5.4

$$M(H_2O)_n^{z+} \rightleftharpoons M(H_2O)_{n-1}(OH)^{(z-1)+} + nH^+ \qquad (5.4)$$

As is generally the case with metal-aquo ions, those of plutonium act as acids, splitting off protons from the coordinated water molecules. Their strength as acids increases strongly with the charge on the central atom and the size of the ionic radii. For example, trivalent plutonium is a much weaker acid than most other metal ions of this charge, because of its large

ionic radius [5.2]. However, the charge of the tetravalent ions is high enough to turn its hydrates into quite strong acids, in spite of its large radius. In fact, Pu^{4+} polymerizes in aqueous solutions at a pH below 1. Metal-aquo ions of penta- and hexavalent plutonium are too acidic to exist in aqueous solution. Therefore, even at extremely high acidities, these ions are hydrolyzed to the metal dioxides, PuO_2^+ and PuO_2^{2+} ions, respectively. The charge on the central atom of these rod-shaped ions is considerably higher than the net ionic charge [5.3,4]. In the case of PuO_2^+, the charge is not high enough to make the hydrate a very strong acid. However, the acid properties of PuO_2^{2+} ions are quite significant. Therefore, plutonium metal ion acidity increases in the following order: $PuO_2^+ < Pu^{3+} \approx PuO_2^{2+} < Pu^{4+}$.

Since hydrolysis is favored for cations of high charge and small size, the actinide ions are classified as hard [5.5-6]. For hard acceptors, the electrostatic attraction between the central ion and the ligand is of crucial importance in their formation, while covalent interactions are subordinate. Even though the ionic radii of the actinides contract across

the series as the f orbitals are filled, actinides with the same oxidation state have chemically similar properties. Therefore, PuO_2^+ should have a hydrolysis constant comparable to that of NpO_2^+. The NpO_2^+ hydrolysis constant has been measured at a variety of ionic strengths; extrapolation to zero ionic strength yields log $*\beta_1(0) = -10.08$ [5.7-11].

5.1 Previous Experiments

In 1949, Kraus and Dam [5.12] reported an upper limit for the PuO_2^+ hydrolysis quotient of log $*\beta_1(3 \times 10^{-3}) < -9.7$. This value was determined from potentiometric titrations. The authors used a PuO_2^+ concentration of approximately 4×10^{-4} M at an ionic strength of 3×10^{-3} M. The reported value was considered an upper limit because of premature precipitation. Kraus and Dam's value is in experimental agreement with the observed behavior of NpO_2^+ and provides insight into the experimental conditions necessary to measure the hydrolysis of PuO_2^+.

5.2 Experimental Procedure

The hydrolysis experiments were conducted under an inert atmosphere of argon in which the CO_2 level was maintained below 20 ppm. The PuO_2^+ concentration ranged from 1.5×10^{-5} to 2.6×10^{-6} M and was measured before and after each spectrum by liquid scintillation counting (LSC) of the alpha activity. The pH range was 3.00 to 10.50. Because the samples had to be passed out of the inert atmosphere box to the photoacoustic spectrometer, each sample was tightly capped and 5×10^{-3} M ammonia or tris(hydroxymethyl)aminomethane buffer was added to maintain constant pH. The ionic strength of all solutions was adjusted to 0.1 M with sodium perchlorate. The pH electrode response was calibrated in terms of the log of the hydrogen ion concentration by titrating a strong acid at 0.1 M ionic strength according to the procedure outlined by Martell [5.13]. For the hydrolysis experiments, $pH_{true} = 0.9804\ pH_{measured} + 0.0591$.

It was necessary to confirm that the buffers were not complexing the PuO_2^+. Therefore, PAS spectra of PuO_2^+ were measured at three different buffer concentrations (2.5×10^{-3}, 5×10^{-3}, and 1×10^{-2} M), while holding

the PuO_2^+ concentration constant at 1 x 10^{-5} M. The pH was approximately equal to the pK_a for each buffer. As shown in Figures 5.1 and 5.2, there is no change in the absorption spectra with changing buffer concentration, indicating that the buffers do not complex the PuO_2^+ under the conditions of these experiments.

The hydrolysis experiments were performed by pre-equilibrating buffer solutions in 0.25 pH unit increments from pH 6.75 to 10.75. An aliquot of PuO_2^+ stock solution was added to a portion of the appropriate buffer solution. The resulting mixture was magnetically stirred and allowed to re-equilibrate (> 2 hours). The sample was then filtered (Millex-G, 200 micron filter) into the cell detection assembly unit; three aliquots were taken for LSC; the pH was remeasured; and the UV-quartz cuvette tightly capped. The PAS spectrum was measured in the previously described system (Section 3.4). A background spectrum was established at each pH value. Upon completion of the PAS measurement, the pH was remeasured and three additional aliquots were taken for LSC. This entire process was repeated for each measurement.

5.3 Results and Discussion

The absorption spectrum of PuO_2^+ in moderately acidic solution features a well-established band at 569 nm with a molar absorptivity of 19 $M^{-1}cm^{-1}$ [5.14,15]. The formation of $PuO_2(OH)$ decreases the molar absorptivity of this peak. This change in absorbance was studied as a function of hydroxide (OH^-) concentration and the hydrolysis constants were determined using non-linear least squares techniques.

The effect of hydrolysis on the absorption spectrum of PuO_2^+ between 530 and 590 nm is shown in Figure 5.3. The pH of the PuO_2^+ solution was increased stepwise from 3 to 10.75 (while the ionic strength was held constant at 0.1 M). Up to pH 8.0, there was no change in the spectrum. Beyond pH 8, the molar absorptivity decreased. At pH 10.00, the total PuO_2^+ concentration dropped to 2.6 x 10^{-6} M, which is near the detection limit of the LIPAS system for PuO_2^+. The samples at pH 10.25 and 10.50 did not contain enough PuO_2^+ in solution for spectra to be recorded. Because of the small spectral changes, replicate experiments were

performed at each pH increment. To improve the signal to noise ratio, the spectra were ensemble averaged with commercially available program Spectra-Calc [5.11]. The SQUAD program was used to calculate the stability constants from the spectroscopic data. As described in Chapter 4, SQUAD minimizes the squared differences between the measured and calculated absorbance values. The calculated absorbances are derived from the Beer-Lambert law and the speciation model defined by the experimentalist.

The hydrolysis equilibria are described by Eq. 5.5

$$PuO_2^+ + n\,H_2O \rightleftharpoons PuO_2(OH)_n^{1-n} + [H^+]^n \qquad (5.5)$$

The overall formation constants for these equilibrium reactions are:

$$*\beta_n(I) = \frac{[\,PuO_2(OH)_n^{\,1-n}\,]\,[\,H^+\,]^n}{[\,PuO_2^+]} \qquad (5.6)$$

Asuming the formation of the first complex only (n=1), analysis of the data gives log $*\beta_1$ (0.1) = -9.73 ± 0.10. When the data were analyzed according to a two-complex model, there was no improvement in the uncertainty of the first complex constant or the residuals from the

differences betwen the observed and calculated absorbances. Therefore, only a single hydroxy complex appears to be formed under the conditions of this experiment.

To obtain the thermodynamic hydrolysis constant, the above value must be corrected to infinite dilution. Several methods have been described in the literature. They include the Debye-Hückel equations [5.17] , the Davies equation [5.18], the Pitzer and Brewer B method [5.19, the Brønsted-Guggenheim-Scatchard approach [5.20-23], the Pitzer virial coefficient method [5.24] and the Baes and Mesmer equations [5.1] The specific ion interaction theory (S.I.T.) in the form of the Brønsted-Guggenheim-Scatchard approach was applied to the values measured in this work as recommended by the Nuclear Energy Agency (NEA) of the Organization of Economic Cooperation and Development (OECD) [5.25]. The S.I.T. theory is based on the Debye-Hückel term, which is the dominant term in the expression for the activity coeffients in dilute solution. The Debye-Hückel term accounts for electrostatic, non-specific long-range interactions. At higher concentrations, short range, non-electrostatic interactions have to also be taken into account.

This is done by adding an ionic strength dependent term to the Debye-Hückel expression.

There are two basic assumptions in the specific ion interaction theory. The first assumption is that the activity coefficient γ_j of an ion j of charge z_j in the solution of ionic strength I_m may be described by Eq. 5.7

$$\log \gamma_j = -z_j^2 D + \sum_k \epsilon_{(j,k,Im)} m_k \qquad (5.7)$$

where D is the Debye-Hückel term:

$$D = \frac{A\sqrt{I_m}}{(1 + Ba_j\sqrt{I_m})} \qquad (5.8)$$

In Eq. 5.8, A and B are temperature dependent constants, and a_j is the effective diameter of the hydrated ion j. The values of A and B as a function of temperature are listed in Table 5.1.

In general, values of a_j (in Å) are 3 to 4, 4 to 6, 9, 11, and 4.5 to 7 for univalent, divalent, trivalent, tetravalent, and organic ions, respectively. The specific ion interaction theory uses $Ba_j = 1.5$ Å, because this value has empirically been found to minimize the variation of j with I.

The summation in Eq. 5.7 extends over all ions k present in solution. By design, the concentrations of the ions of the background electrolyte are very much larger than those of the reacting species. Therefore, the ions forming the ionic medium give the main contribution to the value of the activity coefficient for the reacting ions. This fact makes it possible to simplify the summation in Eq. 5.7 so that only ion interaction coefficients between the participating ionic species and the ionic medium are included.

Table 5.1: Debye-Hückel constants [5.25]

temperature (°C)	A	B(x10^{-8})
0	0.4913	0.3247
5	0.4943	0.3254
10	0.4976	0.3261
15	0.5012	0.3268
20	0.5050	0.3276
25	0.5091	0.3283
30	0.5135	0.3291
35	0.5182	0.3299
40	0.5231	0.3307
45	0.5282	0.3316
50	0.5336	0.3325
55	0.5392	0.3334
60	0.5450	0.3343
65	0.5511	0.3352
70	0.5573	0.3362
75	0.5639	0.3371

The second assumption in the specific ion interaction theory is that the ion interaction coefficients $\epsilon_{(j,k,Im)}$ are zero for ions of the same charge sign and for uncharged species. The rationale behind this assumption is as follows. Since the ion interaction coefficient describes specific short-range interactions, it must be small for ions of the same

charge because electrostatic repulsion keeps them far apart. This assumption holds to a lesser extent for uncharged species.

Ion interaction coefficients for simple ions can be obtained from tabulated data of mean activity coefficients of strong electrolytes or from the corresponding osmotic coefficients. Ion interaction coefficients for complexes can either be estimated from the charge and size of the ion or determined experimentally from the variation of equilibrium constant with ionic strength. Ion interaction coefficients may vary slightly with ionic strength. However, the extent of this variation depends on the charge type and is small for 1:1, 1:2, and 2:1 electrolytes for molalities less than 3.5 M. Therefore, the concentration dependence of ion interaction coefficients can be neglected in this work. This point was emphasized by Guggenheim [5.23], who has presented much experimental evidence supporting this assumption.

For the equilibrium

$$PuO_2^+ + H_2O \rightleftharpoons PuO_2(OH) + H^+,$$

the S.I.T. expression is

$$\log {}^*\beta_1(0) = \log {}^*\beta_1(I) - \Delta(z^2)D + \Delta\epsilon m \qquad (5.9)$$

where D is the Debye-Hückel term at 25°C, m is the molality of the solution, $\Delta\epsilon$ and $\Delta(z^2)$ are the differences in the interaction coefficients and the squared ionic charges, respectively. Using

$$\Delta z^2 = z^2_{PuO2+} - z^2_{H+} = 0$$

and

$$\Delta\epsilon = \epsilon(H^+,ClO_4^-) - \epsilon(PuO_2^+, ClO_4^-) = -0.03 \pm 0.08$$

and $\Delta\epsilon_{(m)} = -0.003 \pm 0.008$.

where $\epsilon(H^+,ClO_4^-) = 0.14 \pm 0.02$ and $\epsilon(PuO_2^+, ClO_4^-) = 0.17 \pm 0.08$. The value for $\Delta\epsilon$ was calculated from the information in the ion interaction coefficient tables listed in Appendix 2, which were tabulated from the values published by Ciavatta [5.26] and Riglet, Robouch, and Vitorge [5.27]. Substituting the above equations and our experimental value for log $*\beta_1(0.1)$ of -9.73 ± 0.10 in Eq. 5.9, we obtain log $*\beta_1(0) = -9.73 \pm 0.10$. Based on this thermodynamic hydrolysis constant, the species distribution of PuO_2^+ at infinite dilution was calculated. The results are shown in Figure 5.4.

References

5.1 Baes, C. F. and Mesmer, R. E.: The Hydrolysis of Cations, Wiley and Sons, New York (1976).

5.2 Arrland, S.: Solution Chemistry and Kinetics of Ionic Reactions. In: Chemistry of the Actinides, (J. J. Katz, L. R. Morss, G. T. Seaborg, eds), 1988

5.3 Bell, J. T.: Continuities in the Spectra and Structure of the Actinyl Ions. J. Inorg. Nucl. Chem. 31, 703-710 (1969).

5.4 Madic, C., Begun, G. M., Hobart, D. E., and Hahn, R. L.: Raman Spectroscopy of Neptunyl and Plutonyl Ions in Aqueous Solution: Hydrolysis of Np(VI) and PU(VI) and Disproportionation of Pu(V). Inorg. Chem. 23, 1914-1921 (1984).

5.5 Ahrland, S., Chatt, J. and Davies, N. R.: Q. Rev. Chem. Soc. 12, 265-276 (1958).

5.6 Pearson, R. G.: Hard and Soft Acids and Bases, HSAB, Part 1. J. Chem. Educ. 45, 581-587, 643-648 (1968).

5.7 Patil, S. K.: Aqueous Coordination Complexes of Neptunium. Coord. Chem. Rev. 25, 133-171 (1978).

5.8 Schmidt, K. H.: A Pulse Readiolysis Study of the Reduction of Np(V) by Hydrated Electrons. J. Inorg. Nucl. Chem. 42, 611-615 (1980).

5.9 Bidoglio, G., Tanet, G., and Chatt, A.: Study of Neptunium(V) Carbonate Complexes under Geological Repository Conditions. Radiochim. Acta 38, 21-26 (1985).

5.10 Lierse, C., Treiber, W. and Kim, J. I.: Hydrolysis Reaction of Neptunium(V). Radiochim. Acta 38, 27-28 (1985).

5.11 Maya, L.: Hydrolysis and Carbonate Complexation of Dioxoneptunium(V) in 1M $NaClO_4$ at 25°C. Inorg. Chem. 22, 2093-2095 (1983).

5.12 Kraus, K. A. and Dam, J. R.:Hydrolytic Behavior of Plutonium(V). In: The Transuranic Elements, IV-14B. (Seaborg, Katz, & Manning, eds.) McGraw Hill, New York, pp 478-499 (1949).

5.13 Martell, A. E. & Motkaitis, R. J.: The Determination and Use of Stability Constants, Chapter 4, VCH, New York (1988).

5.14 Gevantman, L. H. & Kraus, K. A.: Chemistry of Plutonium (V). Stability and Spectrophotometry. In: ref [12], pp 500-518.

5.15 Cohen, D.: The Absorption Spectra of Plutonium Ions in Perchloric Acid Solutions. J. Inorg. Nucl. Chem. 18, 211-218 (1961).

5.16 Spectra Calc, Galactic Indus. Corp., 395 Main St., Salem, New Hampshire (1988).

5.17 Debye, P. & Hückel, E.: Phyzik Z. 24, 334 (1923); 25, 97 (1924).

5.18 Davies, C. W.: J. Chem. Soc.2093 (1938).

5.19 Pitzer, K. S. & Brewer, L.: Thermodynamics (2^{nd} Ed.) New York Mac Graw-Hill (1961).

5.20 Brønsted, J. M.: Studies of Solubility: IV. The Principle of Specific Interaction of Ions. J. Am. Chem. Soc. 44, 877-898 (1922).

5.21 Brønsted, J. M.: Calculation of the Osmotic Activity Functions of Uni-valent Salts. J. Am. Chem. Soc. 44, 938-948 (1922).

5.22 Scatchard, G.: Concentrated Solutions of Strong Electrolytes. Chem. Rev. 19, 309-327 (1936).

5.23 Guggenheim, E. A.: Applications of Statistical Mechanics, Clarenden Press, Oxford (1966).

5.24 Pitzer, K. S.: Thermodynamics of Electrolytes: I. Theoretical Basis and General Equations. J. Phys. Chem. 77,268 (1973).

5.25 Grenthe, I. & Wanner, H.: Guidelines for the Extrapolation to Zero Ionic Strength. OECD Nuclear Energy Agency, Data Bank, report NEA-TDB-2, F-91191 Gif-sur-Yvette, France (1988).

5.26 Ciavatta, L.: The Specific Interaction Theory in Evaluating Ionic Equilibria. Ann. Chim. (Rome) 70, 551-567 (1980).

5.27 Riglet, C., Robouch, P., and Vitorge, P.: Standard Potentials of MO_2^{2+}/MO_2^{+} and M^{4+}/M^{3+} Systems for Np and Pu. Radiochim. Acta 46, 85 (1989).

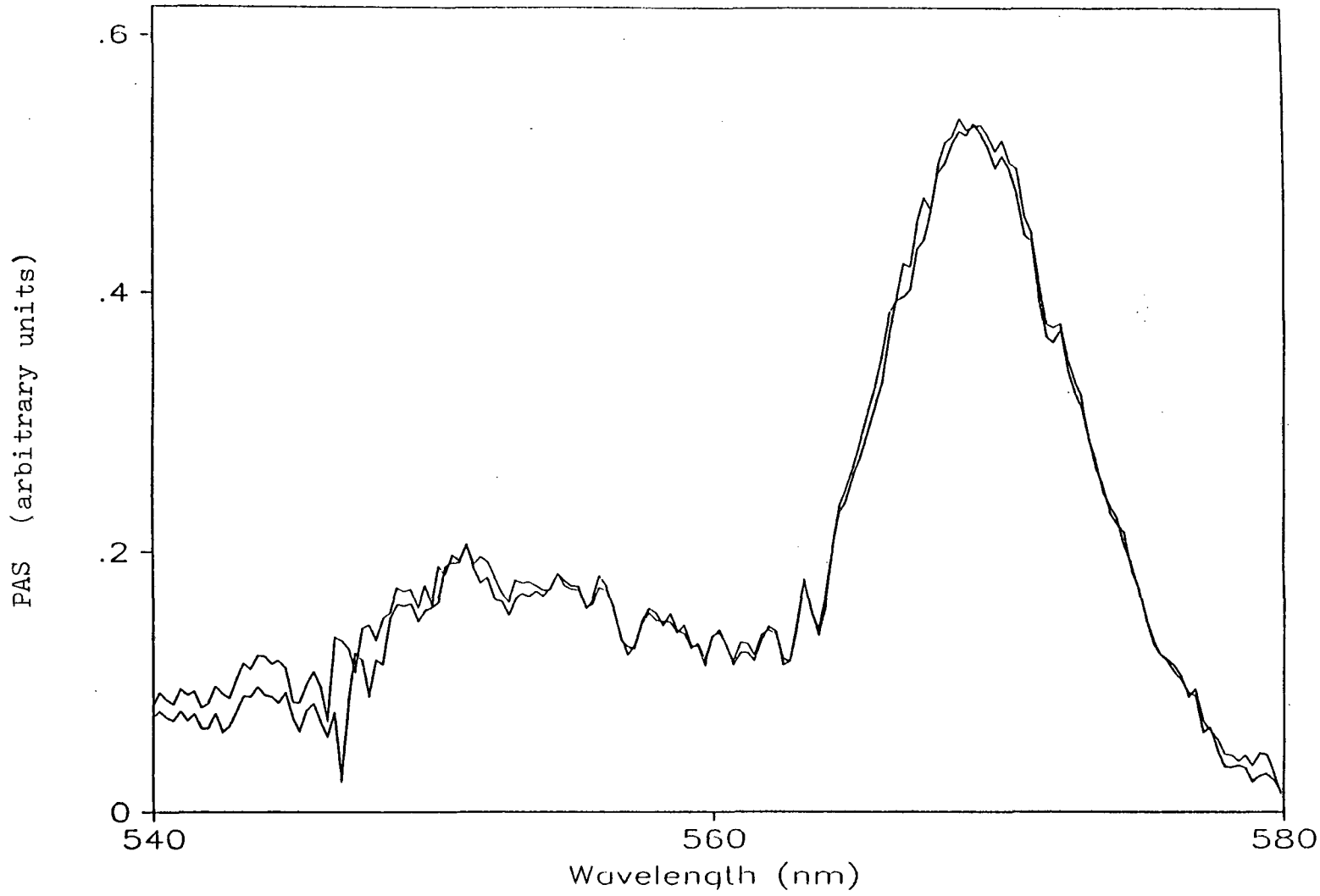

Figure 5.1 PAS spectra of PuO_2^+ in the two extreme buffer conc., 2.5E-3 & 1E-2 M NH_3.

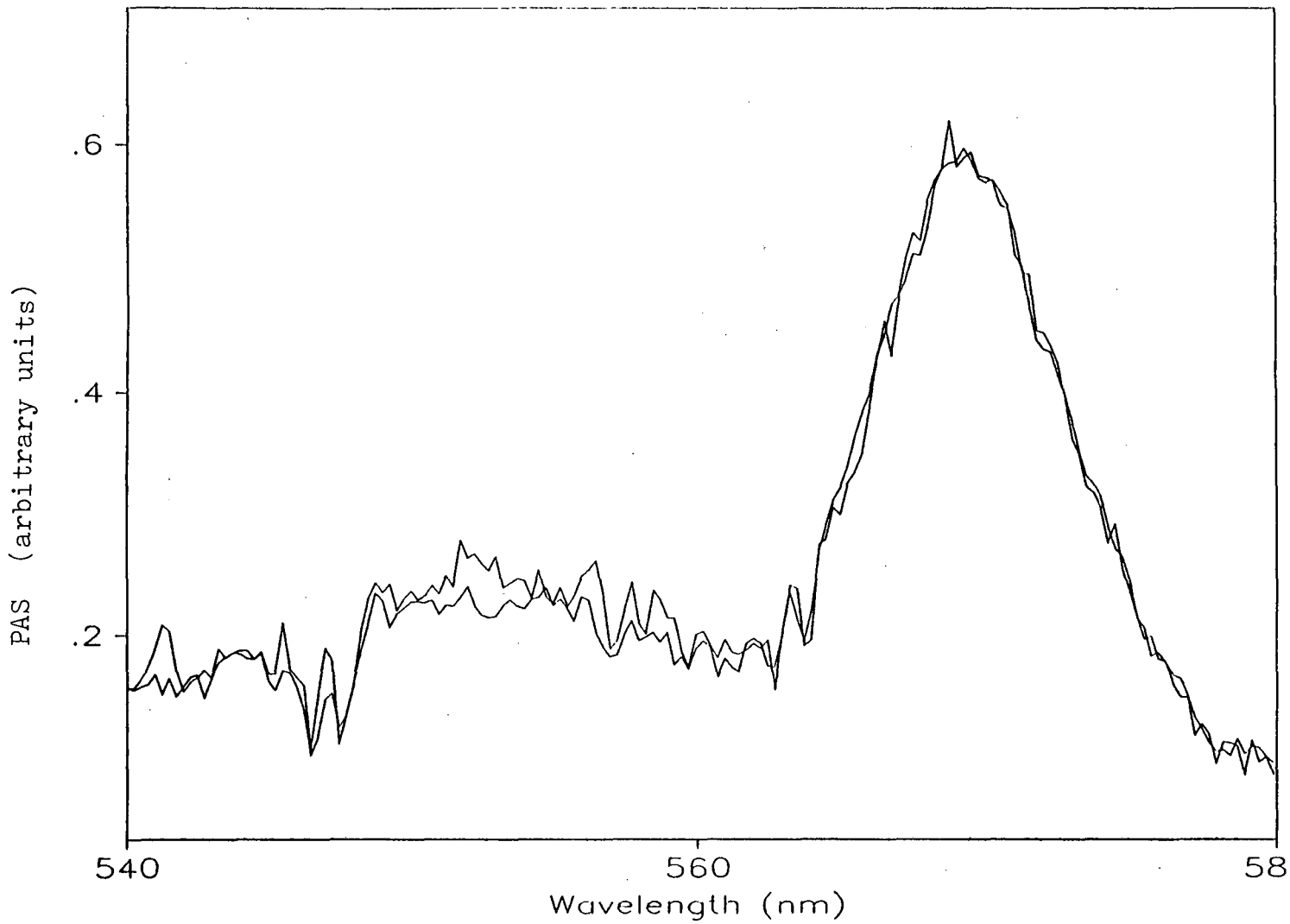

Figure 5.2 PAS spectra of PuO_2^+ in the two extreme buffer conc., 2.5E-3 & 1E-2 M 'tris'

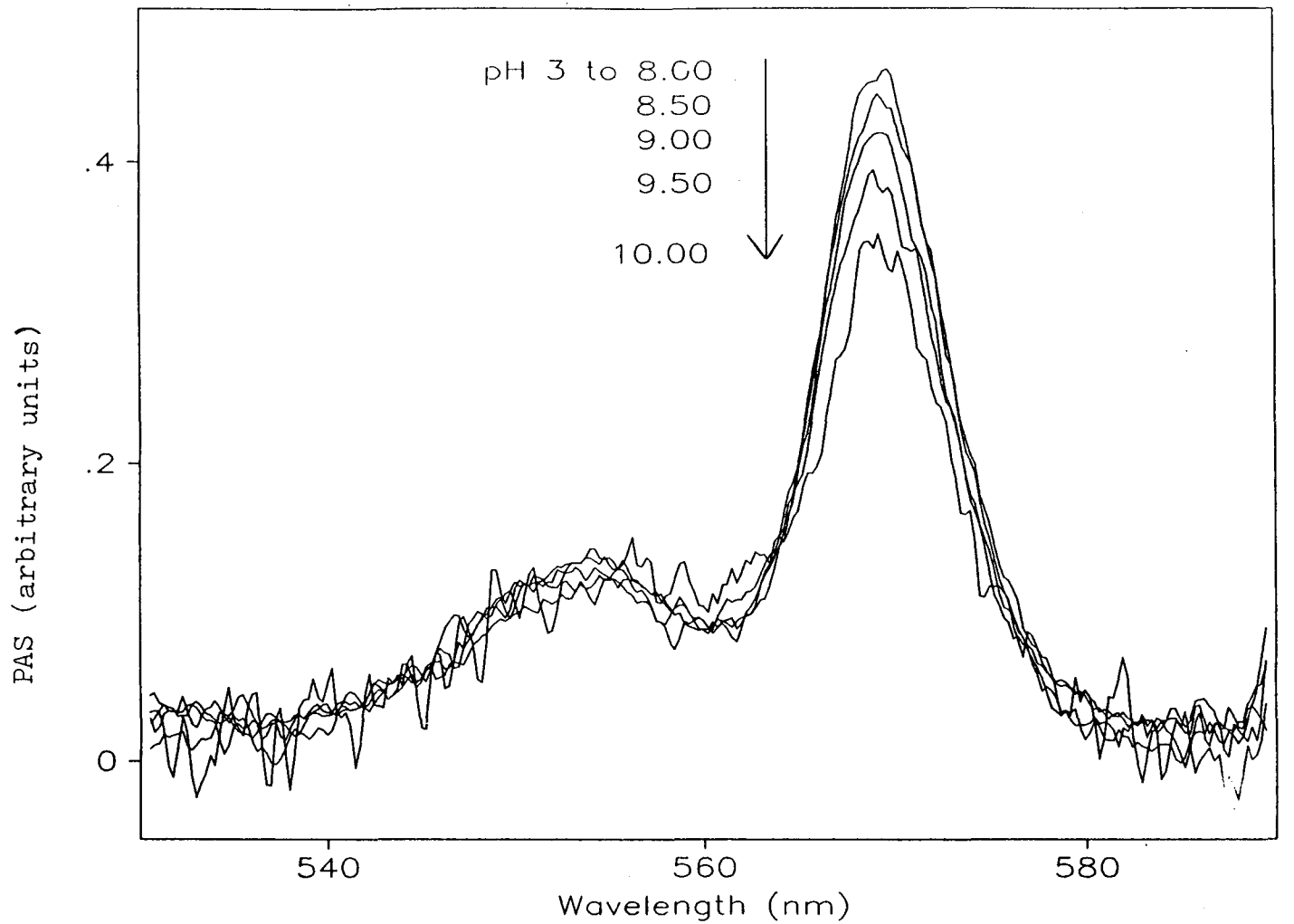

Figure 5.3 Effect of hydrolysis on the PAS spectrum of PuO_2^+.

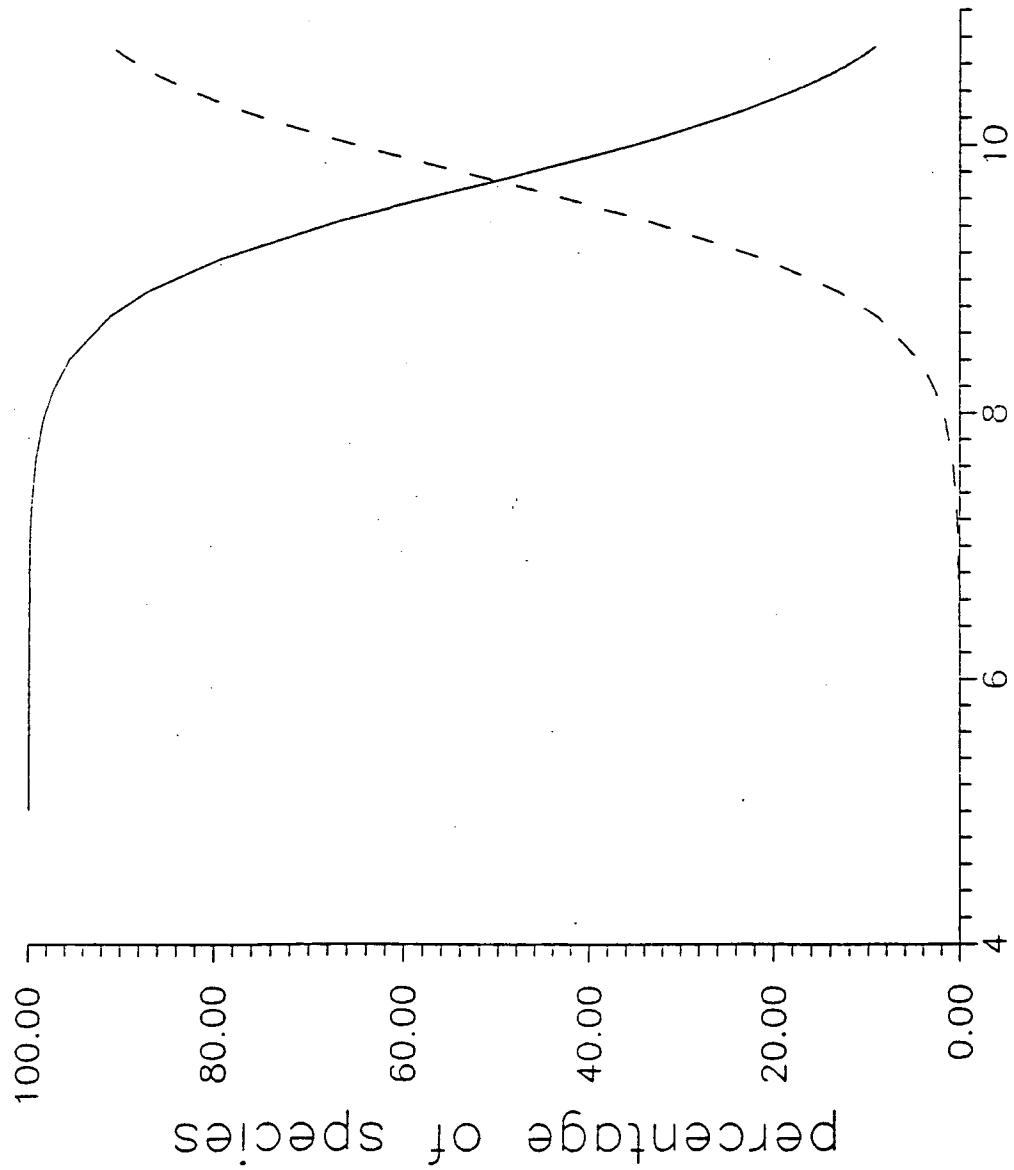

Figure 5.4 Species distribution of PuO_2^+ (——) and $PuO_2(OH)$ (- - -) at I=0.0M.

Chapter 6

Carbonate Complexation of PuO_2^+

Carbonate and bicarbonate are common inorganic anions found in many natural waters. There are two primary reasons for their presence: absorption of carbon dioxide from the atmosphere and/or dissolution of carbonate minerals. The formation of stable carbonate and bicarbonate complexes is a relatively unique characteristic of the lanthanides and actinides [6.1-3]. With the exception of Mg, Ca, Ba, Co, and Pb, most

other elements do not form complexes with carbonate and bicarbonate [6.4]. Actinide carbonate complexes are stronger than their bicarbonate counterparts and are important because they extend the chemistry of the actinides into neutral and alkaline solutions. Consequently, oxidation states are stabilized which were essentially unobtainable in acid solutions. However, the study of actinide carbonate systems is complicated because there are three potential complexing anions in solution: CO_3^{2-}, HCO_3^-, and OH^-.

6.1 The Carbonate-Bicarbonate System

In the carbonate system, there are five equilibrium reactions which must be considered:

$$H_2O \rightleftharpoons H^+ + OH^- \qquad K_w = [H^+]\,[OH^-] \tag{6.1}$$

$$2CO_{2(g)} + H_2O \rightleftharpoons (H_2CO_3)_{aq} + (CO_2)_{aq} \qquad K_{P12} = \frac{[H_2CO_3]_{aq}\,[CO_2]_{aq}}{[P_{CO2}]^2} \tag{6.2}$$

$$CO_{2(g)} + H_2O \rightleftharpoons H^+ + HCO_3^- \qquad \frac{K_1 = [H^+]\,[HCO_3^-]}{P_{CO2}} \tag{6.3}$$

$$HCO_3^- \rightleftharpoons H^+ + CO_3^{2-} \qquad K_2 = \frac{[H^+]\,[CO_3^{2-}]}{[HCO_3^-]} \tag{6.4}$$

$$(H_2CO_3)_{aq} + (CO_2)_{aq} + H_2O \rightleftharpoons 2H^+ + 2HCO_3^- \qquad K_{12} = \frac{[H^+]^2\,[HCO_3^-]^2}{[H_2CO_3]_{aq}[CO_2]_{aq}} \tag{6.5}$$

Table 6.1 lists the literature values for K_{P12}, K_{12}, and K_2 at zero ionic strength. K_1 is not listed, since it is simply the product of K_{P12} and K_{12}.

Table 6.1 Equilibrium Constants for the CO_2-HCO_3^--CO_3^{2-} System at I = 0.0 M, T = 25°C, and p = 1 atm [6.1]

Reaction	-log (K)	Reference
K_{P12}		
$2CO_{2(g)} \rightleftharpoons (H_2CO_3)_{aq} + (CO_2)_{aq}$	1.466 ± 0.002	6.2,3
K_{12}		
$(H_2CO_3)_{aq}+(CO_2)_{aq}+H_2O \rightleftharpoons 2H^+ + 2HCO_3^-$	6.351	6.2
	6.355	6.4
	6.352	6.5
	6.343	6.6
	6.365	6.7
	6.382	6.8
K_2		
$HCO_3^- \rightleftharpoons H^+ + CO_3^{2-}$	10.329	6.5
	10.337	6.4
	10.330	6.9
	10.328	6.8

The equilibrium constants can be corrected to different ionic strengths by applying the S.I.T. method with the zero ionic strength values from Table 6.1 and the interaction coefficients from Appendix 2. As you will recall from Chapter 5, the S.I.T. expression is

$$\log \beta(I) = \log \beta(0) + \Delta(z^2)D - \Delta\epsilon m.$$

The equilibrium constants are listed as a function of ionic strength in Table 6.2.

Table 6.2 Equilibrium constants for the CO_2-HCO_3^--CO_3^{2-} system as a function of ionic strength in $NaClO_4$ solutions at 25°C

Equilibrium	Ionic strength								
	0	0.10	0.20	0.50	1.00	1.50	2.00	3.00	4.00
K_w	14.00	13.80	13.77	13.77	13.83	13.93	14.05	14.32	14.63
K_1	7.82	7.62	7.59	7.57	7.61	7.69	7.78	8.00	8.25
K_2	10.33	9.90	9.80	9.67	9.59	9.57	9.57	9.60	9.67
K_{12}	6.35	6.15	6.12	6.10	6.14	6.22	6.31	6.53	6.78
K_{P12}	1.47	1.47	1.47	1.47	1.47	1.47	1.47	1.47	1.47

6.2 Experimental Procedure

The carbonate complexation experiments were conducted under a partial CO_2 pressure of 0.1 or 0.5 atm. The controlled atmosphere was supplied by gas cylinders containing an analyzed mixture of CO_2 and argon which varied less than 1% from one cylinder to another. The PuO_2^+ concentration was targeted for 1.0×10^{-5} M and confirmed by alpha liquid scintillation counting (LSC) as previously described. The pH electrode response was calibrated in terms of the logarithm of the hydrogen ion concentration ($pCH = -\log [H^+]$) by titrating a strong acid at 0.5 M ionic strength according to the same procedure used for the hydrolysis experiments (Section 5.2). At 0.5 M ionic strength, $pH_{true} = 0.9866\ pH_{measured} + 0.2093$. The CO_3^{2-} concentration ranged from 3.18×10^{-6} to 4.39×10^{-3} M, which corresponded to a pH variation from 6.25 to 7.85. The ionic strength was adjusted to 0.5 M with sodium perchlorate.

The carbonate complexation experiments were performed by pre-equilibrating sodium bicarbonate solutions with the appropriate amount of sodium perchlorate at desired "pH" values between 6.25 and 7.85. An aliquot of PuO_2^+ stock solution was added to a portion of the

carbonate-bicarbonate solution. The resulting mixture was magnetically stirred and allowed to re-equilibrate (≥ 2 hours). The sample was then filtered (Millex-G, 200 micron filter) into the cell detection assembly unit; three aliquots were taken for LSC; the pH was remeasured; and the UV-quartz cuvette tightly capped. Upon completion of the PAS measurement, the pH was remeasured and three additional aliquots were taken for LSC. This entire process was repeated for each measurement.

6.3 Results and Discussion

The change in the absorption spectrum of PuO_2^+ as the concentrations of the carbonate, bicarbonate, and hydroxide were changed is shown in Figure 6.1. The possibility of hydroxy complexation was eliminated by conducting the experiments at pH values below 8, where we have shown PuO_2^+ is not hydrolyzed. The pH and partial pressure of CO_2 were varied to distinguish between bicarbonate and carbonate complexation. As shown in Table 6.1, the carbonate-bicarbonate equilibrium is described by $pK_1 = 7.57$ and $pK_2 = 9.67$ at 0.5 M ionic strength. At partial CO_2 pressures

of 0.1 and 0.5 atm, the pH was controlled so that the CO_3^{2-} concentration remained constant while the HCO_3^- concentration varied, and conversely, the HCO_3^- concentration was held constant while the CO_3^{2-} was varied. As shown in Figures 6.3 and 6.4, spectral changes only occur when there is a change in the CO_3^{2-} concentration.

The PuO_2^+--CO_3^{2-} complexation reaction was studied in a $[CO_3^{2-}]$ range of 3.18×10^{-6} and 4.39×10^{-3} M, at a PuO_2^+ concentration of approximately 1×10^{-5} M. At the highest carbonate concentration, a second peak emerged between 555 and 570 nm. The spectroscopic data were analyzed by the same procedure as in the hydrolysis experiment. The PuO_2^+--CO_3^{2-} complexation equilibria are descrtibed by Eq. 6.6

$$PuO_2^+ + n\ CO_3^{2-} \rightleftharpoons PuO_2(CO_3)_n^{1-2n} \qquad (6.6)$$

where the corresponding stability constants are given by

$$\beta_n(I) = \frac{[\ PuO_2(CO_3)^{1-2n}]}{[\ PuO_2^+\ ]\ [\ CO_3^{2-}]^n} \qquad (6.7)$$

The single complex equilibrium model gives log $\beta_1(0.5) = 4.60 \pm 0.03$. As with hydrolysis, there was no evidence for a second complex.

Since there is no interaction coefficient available for the $PuO_2(CO_3)^-$--Na^+ pair, the value for ϵ ($NpO_2(CO_3)^-$--Na^+) of -0.23 ± 0.09 was used [6.11]. NpO_2^+ is a suitable model compound, since it has the same oxidation state and approximately the same ionic radius as PuO_2^+ [6.12]. To calculate the thermodynamic stability constant for the equilibrium

$$PuO_2^+ + CO_3^{2-} \rightleftharpoons PuO_2(CO_3)^-,$$

the experimental value for log $\beta_1(0.5)$ of 4.60 ± 0.03 was inserted in the S.I.T. expression (described in Chapter 5) where D is obtained from Eq. 5.7 and Table 5.1 at 25°C:

$$\log \beta_1(0) = \log \beta_1(I) - \Delta z^2 D + \Delta \epsilon m \qquad (5.8)$$

where

$$\Delta z^2 = z^2_{PuO2(CO3)-} - z^2_{PuO2+} - z^2_{CO32-} = -4$$

and

$$\Delta \epsilon = \epsilon(PuO_2(CO_3)^- \text{--} Na^+) - \epsilon(Na^+, CO_3^{2-}) - \epsilon(PuO_2^+, ClO_4^-)$$

$$= -0.23 \pm 0.09 - (-0.05 \pm 0.03) - (0.17 \pm 0.08)$$

$$= -0.35 \pm 0.12$$

and $\Delta \epsilon m = -0.175 \pm 0.06$

to obtain $\log \beta_1(0) = 5.12 \pm 0.07$. From this constant, the species distribution of PuO_2^+ was calculated as a function of the CO_3^{2-} concentration, and the results are shown in Figure 6.4.

References

6.1 Palmer, D. A. & Van Edik, R.: Chem. Rev 83, 651 (1983).

6.2 Berg, R. L, & Vanderzee, C. E.: J. Chem. Thermodyn. 10, 1113 (1978).

6.3 Huat, S. G. C., Masson, M., Ringner, B.: J. Chem. Thermodyn. 4, 283 (1972).

6.4 Peiper, J. C. & Pitzer, K. S.: J. Chem. Thermodyn. 14, 613 (1982).

6.5 Harned, H. S. & Davis, R. Jr.: J. Am. Chem. Soc. 65, 2030 (1943).

6.6 MacInnes, D. A. & Belcher, D.: J. Am. Chem. Soc. 55, 2630 (1933).

6.7 Read, A. J.: J. Sol. Chem. 4, 53 (1975).

6.8 Ryzhenko, R. N.: Geokhimiya 151 (1963).

6.9 Millero, F. J.: Geochim. Cosmochim. Acta 43, 1651 (1979).

6.10 Martell, A. E. & Motekaitis, R. J.: The Determination and Use of Stability Constants, VCH, New York, Chapt. 4 (1988).

6.11 Riglet, C.: The Chemistry of Neptunium and other Actinides in Cabonate Solution, Ph. D. Thesis, University of Paris 6 (1989).

6.12 Katz, J. J., Morss, L. R., Seaborg, G. T.: Summary and Comparative Aspects of the Actinide Elements. In: Chemisty of the Actinides, (JJ Katz, LR Morss, GT Seaborg, eds.), Chapter 14 (1988).

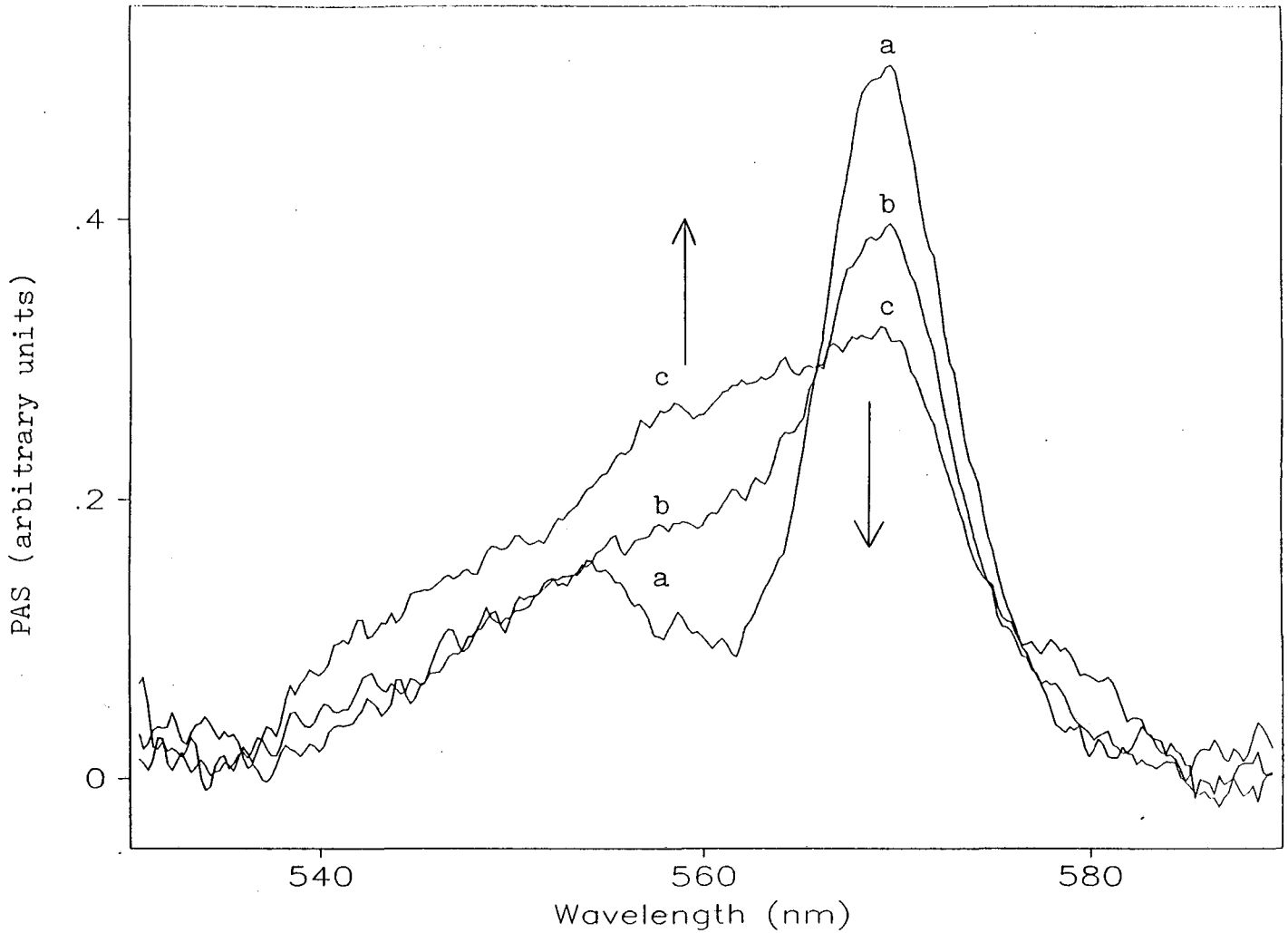

Figure 6.1 Effect of carbonate complexation on PAS spectrum of PuO_2^+ (1 x 10^{-5} M), where the CO_3^{2-} concentration is a=3.18 x 10^{-6}, b=4.81 x 10^{-5}, & c=4.39 x 10^{-3} M.

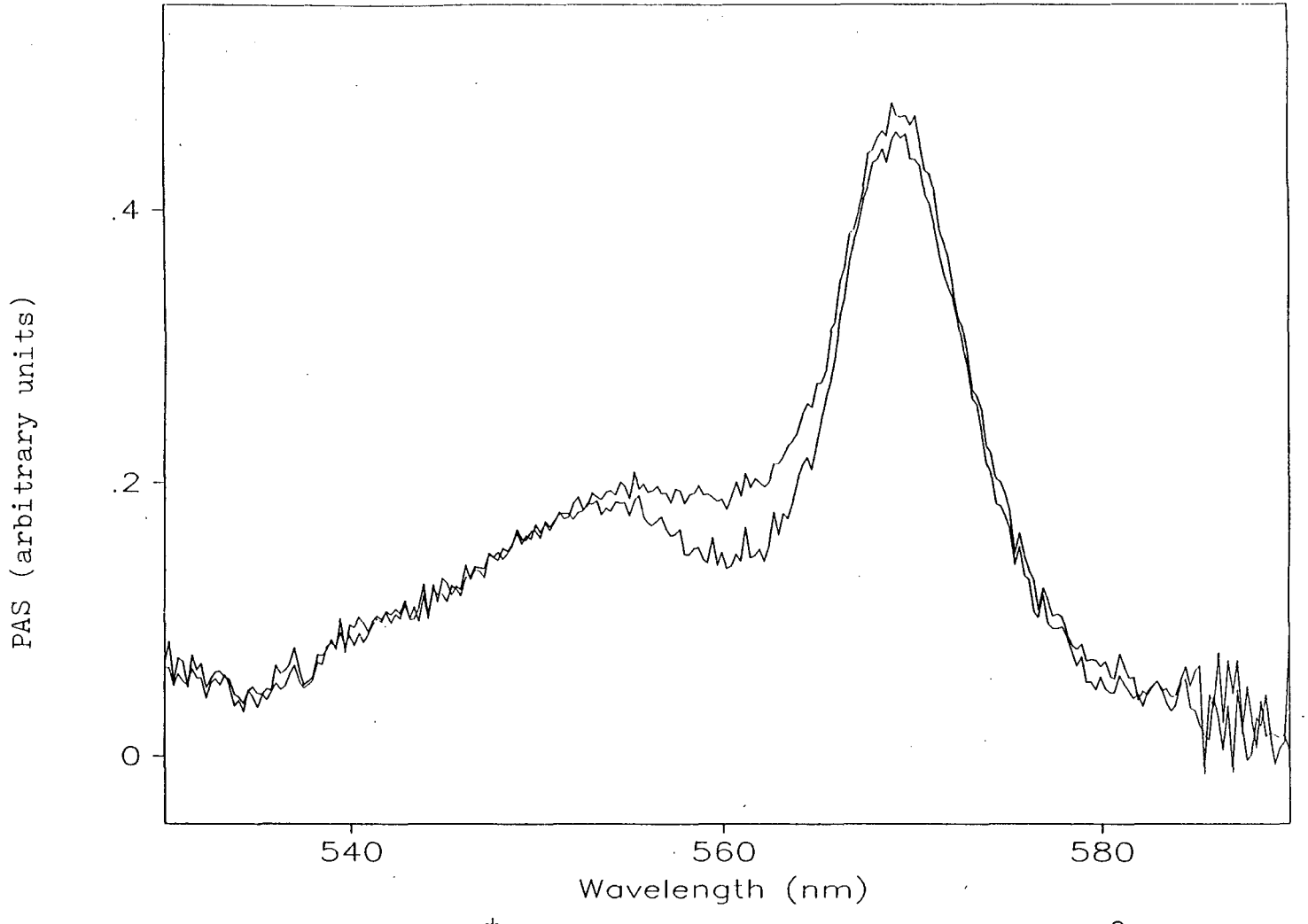

Figure 6.2 PAS spectra of PuO_2^+ in the same HCO_3^- conc. (9.749×10^{-3}M) and varied CO_3^{2-} conc. (1.09×10^{-6} and 5.50×10^{-4} M).

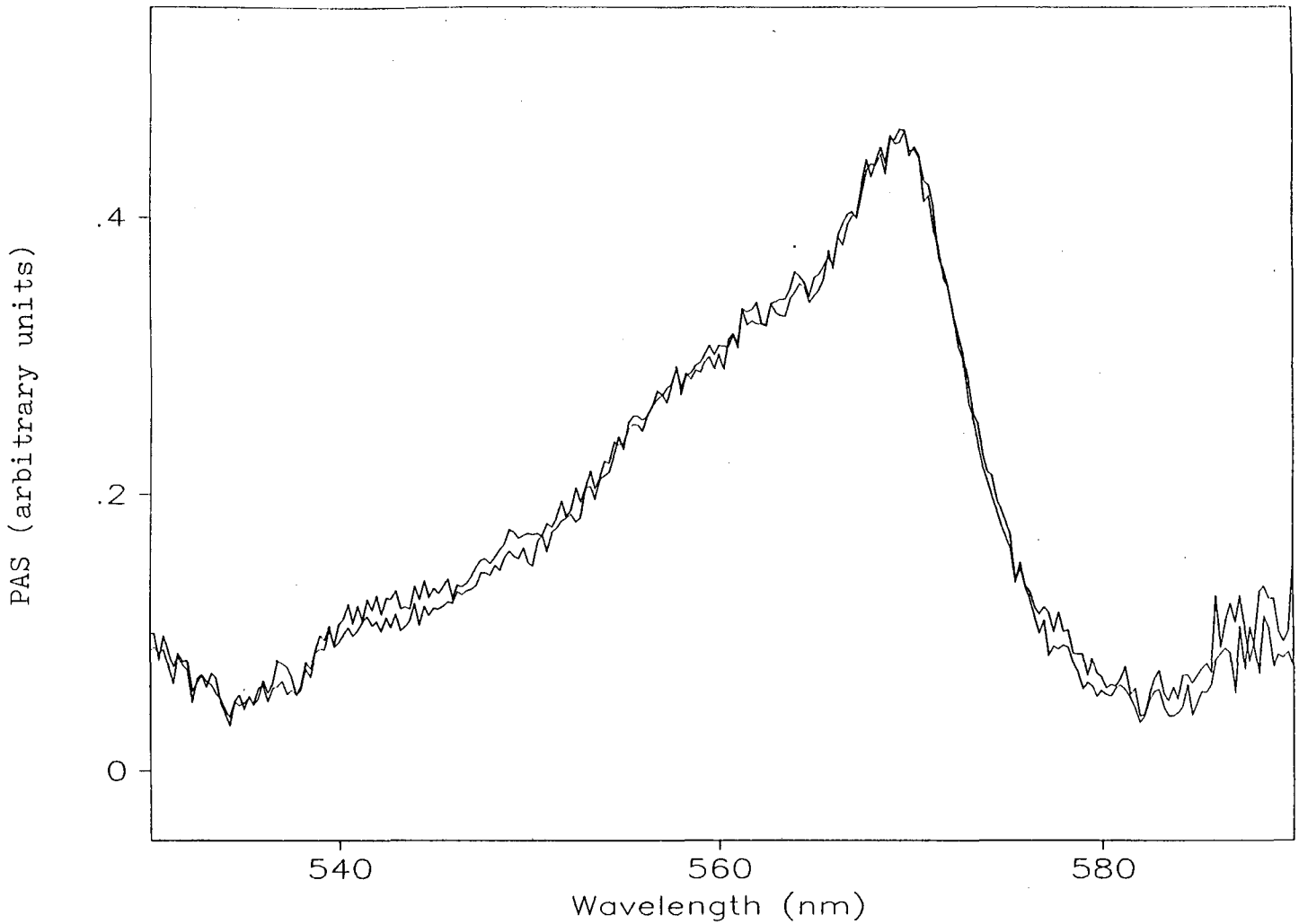

Figure 6.3 PAS spectra of PuO_2^+ in varied HCO_3^- concentration (6.17 x 10^{-2} and 0.1379 M) and the same CO_3^{2-} concentration (2.19 x 10^{-4} M).

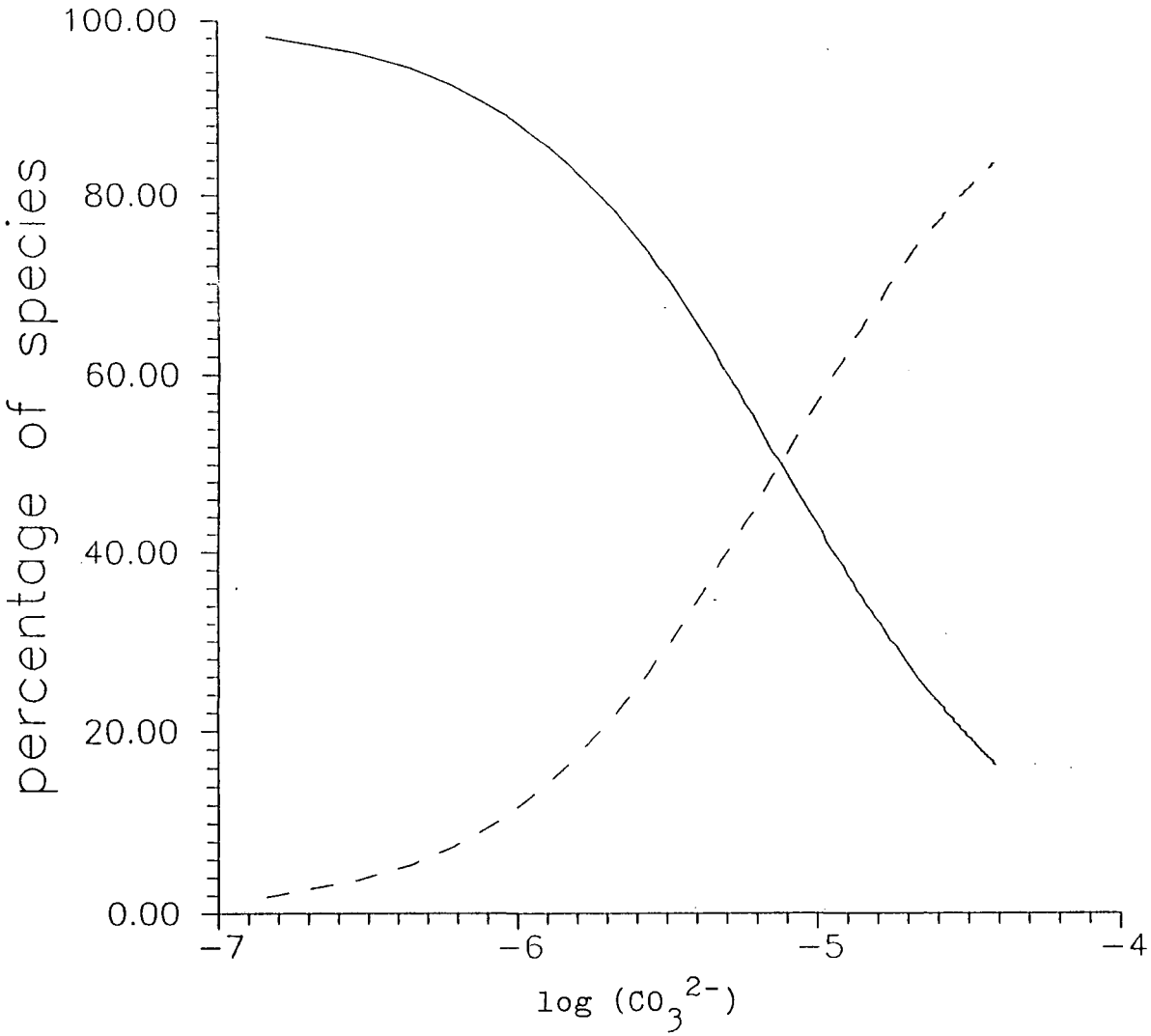

Figure 6.4 Species distribution of PuO_2^+ (——) and $PuO_2(CO_3)^-$ (- - -) at I=0.0 M.

Chapter 7

Conclusions

The thermodynamic hydrolysis and carbonate complexation constants calculated from this work can be combined with the oxidation-reduction potentials of plutonium to obtain the Eh versus pH diagrams shown in Figures 7.1-3. These diagrams give a summary of plutonium species that can exist under a wide variety of values of pH, Eh, and partial pressures of CO_2 possible in environmental systems. The stability constants and redox potentials used to caluculate the diagrams are listed in Tables 7.1 and 2.1, respectively. The natural waters in the vicinity of

Yucca Mountain at the Nevada Test Site have a pH range of 6.9 to 7.7 and an Eh range of 600 to 800 mV and are therefore best represented by Figure 7.3. As shown in Figure 7.3, at least 60% of the soluble species in solution exist as PuO_2^+ between pH 5 and 8 when the solution potential (Eh) ranges from +590 to 950 mV. The first carbonate complex of PuO_2^+ ($PuO_2(CO_3)^-$) is the principal species between pH 8 to 9 when the solution potential ranges from 475 to 700 mV. The exsistence of $PuO_2(CO_3)^-$ is also important to the prediction of the migration behavior of plutonium. The cationic species PuO_2^+ is converted to the anionic species $PuO_2(CO_3)^-$, which will significantly alter the ion exchange behavior of plutonium through the overpack around the canister and the geological medium itself. The calculated speciation behavior in Figures 7.1-7.3 agrees with the experimental results discussed in Chapter 1. The thermodynamic stability constants calculated in the current research help characterize potential radioactive waste repository sites and will be added to the thermodynamic data base.

Table 7.1 Complexation constants and solubility products of PuO_2^+.

	log ß(I), *ß(I), or K_S(I)		
Complex	I=1 M	I=0.1M	I=0
$PuO_2(OH)$		-9.73 ± 0.10	-9.73 ± 0.10
$PuO_2(OH)_{(S)}$	-9.4		-8.9
$PuO_2(CO_3)^-$		4.60 ± 0.04	5.10 ± 0.06
$PuO_2(CO_3)_2^{3-}$	6.7		6.2
$PuO_2(CO_3)_3^{5-}$	8.6		5.3
$Na\ PuO_2(CO_3)_{(S)}$	-10.4		-11.4
$Na_3\ PuO_2(CO_3)_{2(S)}$	-12.7		-15.0

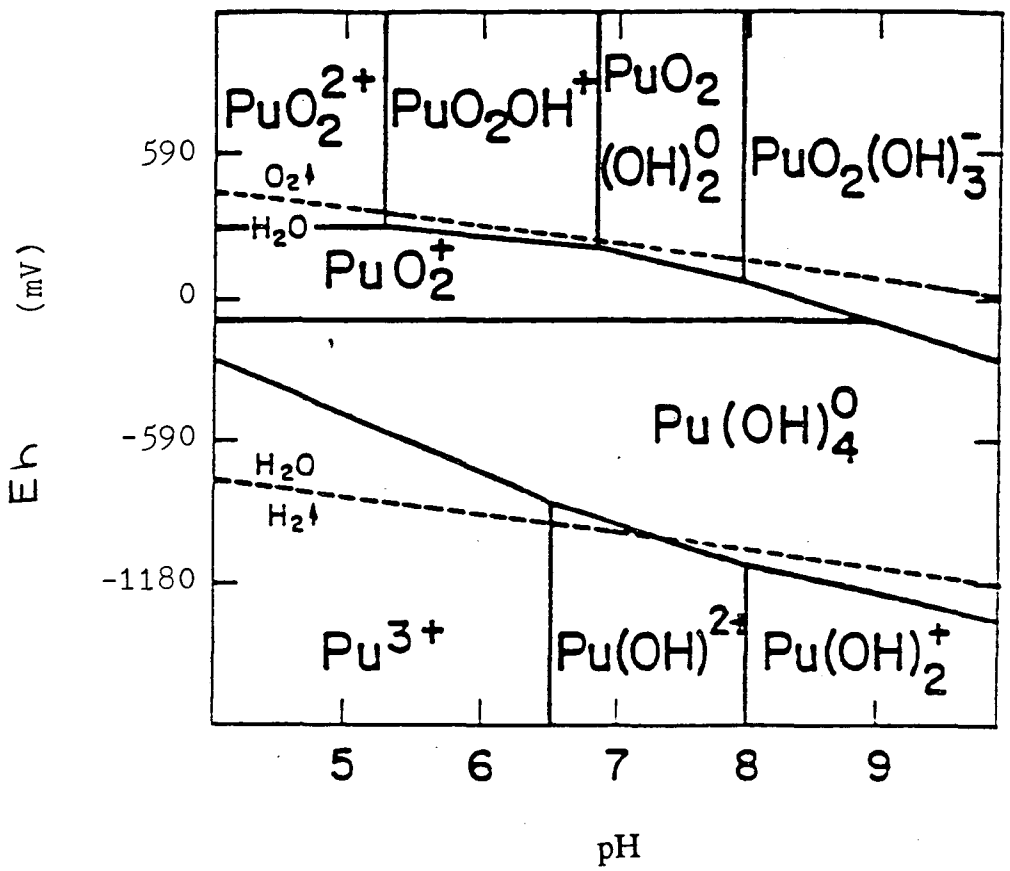

Figure 7.1 Eh vs pH diagram for Pu speciation at zero ionic strength and $P_{CO_2} = 0$.

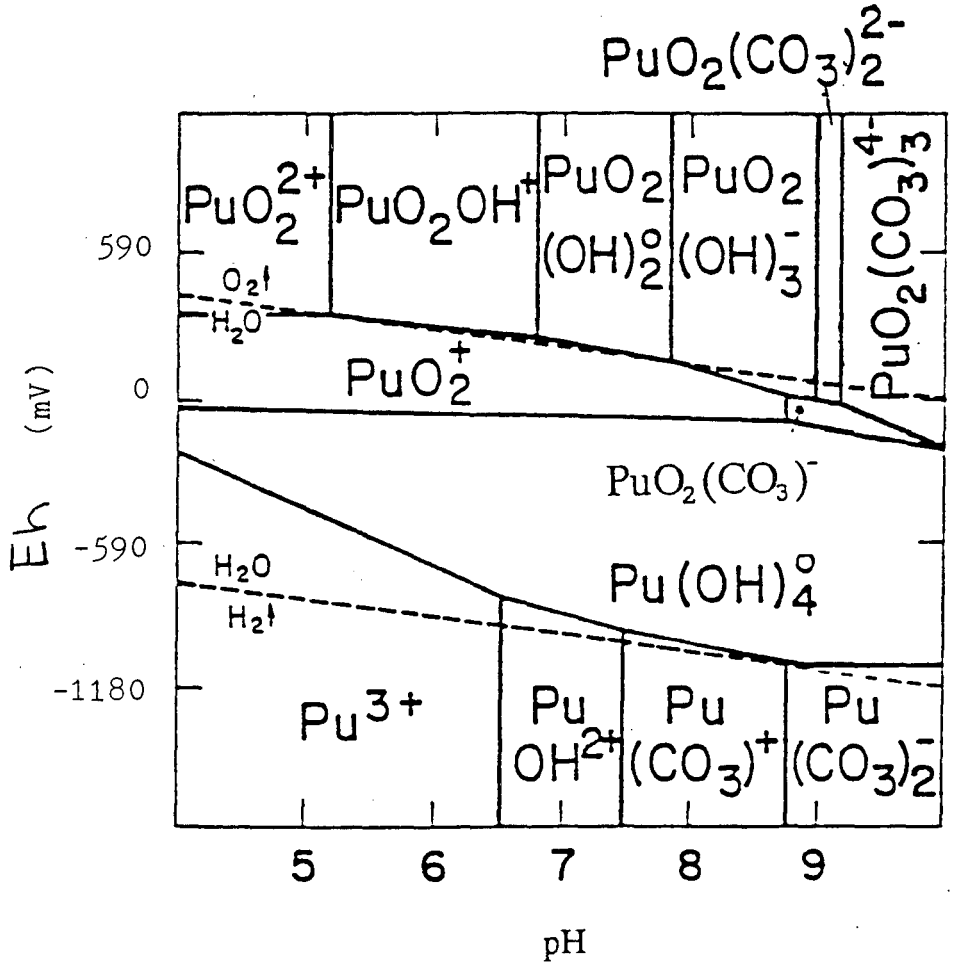

Figure 7.2 Eh vs pH diagram for Pu speciation at zero ionic strength and $pCO_2 = -3.5$.

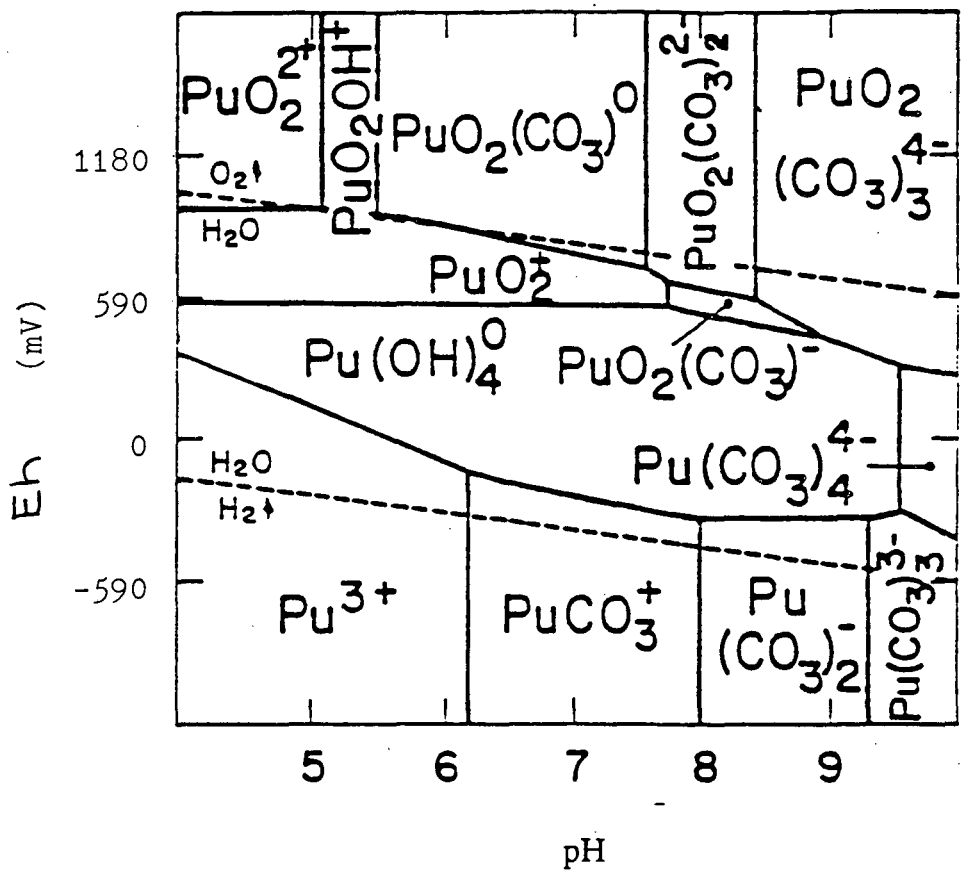

Figure 7.3 Eh vs pH diagram for Pu speciation at zero ionic strength and $pCO_2 = -2$.

Appendix 1 SQUAD

SQUAD employs the two-level adjustment of parameters suggested by Sillen [4.22]. The strategy used is shown in Figure 4.4.

The subroutines DIFF, RESID, ECOEF, CCSCC (and GOGSNR), and SOLVE are called by the subroutine REFINE. Route 1, route 2, and then route 3 are followed, in order, during a single refinement cycle. Once convergence has been achieved, control passes back to the data output section of the subroutine INOUT for postrefinement printouts. The algorithms in SQUAD are well-tried versions of familiar procedures, that have been used in many chemically oriented computational applications. However, the coding of SQUAD is structured such that any of the algorithms may be replaced by newer, more effecient numerical methods.

For each absorbance value $A_{i,k}$, the equation

$$A_{i,k} = \sum [\text{species}]_{i,j} \times \epsilon_{j,k} \qquad (4.15)$$

where $[species]_{i,j}$ is the concentration of the j^{th} species in the i^{th} solution (spectrum) and $\epsilon_{j,k}$ is the molar absorptivity of the j^{th} species at the k^{th} wavelength. SQUAD computes the values of the overall formation constant(s) which minimizes the sum of the squares residuals between the ovserved and calculated absorbance values, according to Eq. 4.16

$$W = \sum (A^{obs}_{i,k} - A^{calc}_{i,k})^2 \qquad (4.16)$$

The subroutines of SQUAD are breifly described below. The main program starts by initializing I/O unit numbers and maximum sizes for all execution-time dimensioned arrays. Subroutine PREPRO is then called to perform the majority of the data input and input file error checking. Next, control passes to INOUT, completes data input, and then begins the refinement cycle of the formation constants by a single call to REFINE.

Subroutine DIFF and SEARCH. Numerical differentiation, employing Stirling's central difference algorithm, is performed by DIFF. The increment for differentiation is fixed at 0.5% of each

constant. The Jacobian and Hessian matrices are developed within DIFF. They are solved by search yielding the shifts to be applied to those formation constants being refined. The correlation matrix is also calculated at this time.

Subroutine RESID. This routine acts a a service routine, during numerical differentiation step in the Gauss-Newton algorithm, and to accumulate W, the squared sum of residuals. The routine also controls the solution of Beer's law for the current set of formation constants, calling subroutine ECOEF for this purpose.

Subroutines ECOEF and SIGMAE. For a given set of formation constants ECOEF first calls CCSCC, which will return the concentrations of complexed and uncomplexed species in solution. At this point, ECOEF prepares arrays for the solution of the linear equations (Beer' Law) by SOLVE. Prior to calling SOLVE, the absorbance array is "corrected" for those species having known molar absorptivities. This process includes the formation of a new absorbance matrix, $A_{i,k}^{unknown}$ from $[A_{i,k}^{total} - A_{i,k}^{known}]$, where $A_{i,k}^{known}$ is the absorbance calculated

from know molar absorptivities and the appropriate species concetrations calculated by CCSCC. Once the molar absorptivities have been calculated they are inserted back into the total molar absorptivity array. $A_{i,k}^{calc}$ is then obtained and, consquently, W. When convergence is achieved, a final call is made to ECOEF at the entry point. Thereby, SIGMAE determines the standard deviations of the calculated molar absorptivities.

Subroutines CCSCC and COGSNR. These two routines are used to calculate the concentrations of all species in solution, as defined by the equilibrium model. The total concentration of each component, the pH of the solution (if applicable), and current set of formation constants are input data for these routines.

CCSCC operates as a bookkeeping and control routine for COGSNR. The latter routine solves the mass balance equations, solution by solution, using a constrained Newton-Raphson procedure. The coding of COGSNR used in SQUAD is a generalized version of that originally presented by Tobias and Yasuda [4.28].

Subroutine SOLVE. Once the concentrations of all species for the current set of constants have been calculated, and the absorbance matrix corrected, then control passes to subroutine SOLVE. At this point, one of two algorithms is selected to solve the overdetermined set of simultaneous equations. For most datat sets, the traditional approach of multiple regression (MR) may be employed. However, in certain situations, the nonnegative linear least-squares (NNLS) may be invoked, where the solution vector is constrained to be equal to or greater than zero.

Subroutine SEARCH. When the matrix on nonlinear least-squares equations is complete, control returns to REFINE and then to SEARCH, where these equations are solved according to the Gauss-Newton algorithm. The result gives the shifts to be applied to the refining constants. Checks are made to ensure that these shifts do not exceed preset limits, and if so, the shifts are adjusted accordingly. The covariance matrix is also calcualted at this point.

Finally, control passes back to REFINE, where the progress of refinement is determined. If convergence has been attained, then the program returns to INOUT and begins the output. Otherwise, another refinement cycle begins.

Subroutine INOUT. INOUT completes the data input and call subroutine REFINE. Once convergence has been achieved, INOUT controls the output of results. First tables of all concentrations for all species and solutions are printed, followed by the calculated molar absorptivities together with their standard deviations.

Appendix 2 Tables of ion interaction coefficients

Table A2.1 Ion interaction coefficients $\epsilon(j,k)$ for anions j with k = Li^+, Na^+, and K^+, taken from references 5.25-27. The uncertainties represent 95% confidence level.

j ↓ k →	Li^+	Na^+	K^+
OH^-	-0.02 ± 0.03	0.04 ± 0.01	0.09 ± 0.01
F^-		0.02 ± 0.02	0.03 ± 0.02
Cl^-	0.10 ± 0.01	0.03 ± 0.01	0.00 ± 0.01
Br^-	0.13 ± 0.02	0.05 ± 0.01	0.01 ± 0.02
I^-	0.16 ± 0.01	0.08 ± 0.02	0.02 ± 0.01
HF_2^-		-0.09 ± 0.04	
ClO_3^-		-0.01 ± 0.02	
ClO_4^-	0.15 ± 0.01	0.01 ± 0.01	
BrO_3^-		-0.06 ± 0.02	
SCN^-		0.05 ± 0.01	-0.01 ± 0.01
HSO_4^-		-0.01 ± 0.02	
HCO_3^-		-0.03 ± 0.02	
$NpO_2(CO_3)^-$		-0.23 ± 0.09	
NO_2^-	0.06 ± 0.04	0.00 ± 0.02	-0.04 ± 0.02
NO_3^-	0.08 ± 0.01	-0.04 ± 0.03	-0.11 ± 0.04
$B(OH)_4^-$		-0.07 ± 0.05	
$H_2PO_4^-$		-0.08 ± 0.04	
$HCOO^-$		0.03 ± 0.01	
CH_3COO^-	0.05 ± 0.01	0.08 ± 0.01	0.09 ± 0.01
$SiO(OH)_3^-$		-0.08 ± 0.03	
$Si_2O_2(OH)_5^-$	-0.08 ± 0.04		

Table A2.1 (continued)

j k → ↓	Li^+	Na^+	K^+
SO_3^{2-}		-0.08 ± 0.05	
SO_4^{2-}	-0.03 ± 0.04	-0.12 ± 0.06	-0.06 ± 0.02
CO_3^{2-}		-0.05 ± 0.03	0.02 ±0.01
$S_2O_3^{2-}$		-0.08 ± 0.05	
HPO_4^{2-}		-0.15 ± 0.06	
CrO_4^{2-}		-0.06 ± 0.04	-0.08 ± 0.04
$Si_2O_2(OH)_2^{2-}$		-0.09 ± 0.15	
$Si_2O_3(OH)_4^{2-}$		-0.15 ± 0.06	
$UO_2(CO_3)_2^{-}$		-0.09	
PO_4^{3-}		-0.25 ± 0.03	-0.09 ± 0.02
$Si_3O_6(OH)_3^{3-}$		-0.25 ± 0.03	
$Si_3O_5(OH)_5^{3-}$		-0.25 ± 0.03	
$Si_4O_7(OH)_5^{3-}$		-0.25 ± 0.03	
$Si_3O_3(OH)_{13}^{3-}$		-0.25 ± 0.03	
$NpO_2(CO_3)_2^{3-}$		-0.35 ± 0.15	
$Am(CO_3)_3^{3-}$		-0.1	
$P_2O_7^{4-}$		-0.26 ± 0.05	-0.15 ± 0.05
$Fe(CN)_6^{4-}$			-0.17 ± 0.03
$UO_2(CO_3)_3^{4-}$		-0.02	
$U(CO_3)_4^{4-}$		-0.02	
$UO_2(CO_3)_3^{5-}$		-0.63 ± 0.20	
$NpO_2(CO_3)_3^{5-}$		-0.62 ± 0.18	
$U(CO_3)_5^{6-}$		-0.20 ± 0.11	
$(UO_2)_3(CO_3)_6^{6-}$		-0.39	

Table A2.2 Ion interaction coefficients $\epsilon(j,k)$ for cations j with k = Cl^-, ClO_4^-, and NO_3^-, taken from references 5.25-27. The uncertainties represent 95% confidence level.

j k → ↓	Li^+	Na^+	K^+
H^+	-0.12 ± 0.01	0.14 ± 0.02	0.07 ± 0.01
NH_4^+	0.01 ± 0.01	-0.08 ± 0.04	-0.06 ± 0.03
H_2gly^+	-0.06 ± 0.02		
Ag^+		0.00 ± 0.01	
Cu^+		0.11 ± 0.01	
$CdCl^+$		0.25 ± 0.02	
$CdSCN^+$		0.31 ± 0.02	
$HgCl^+$		0.19 ± 0.02	
UO_2^+	0.13	0.28 ± 0.08	
NpO_2^+		0.26 ± 0.08	
PuO_2^+		0.17 ± 0.08	
AnO_2^+		0.23 ± 0.10	
$LaCO_3^+(AmCO_3^+)$		0.26 ± 0.08	
$Th(OH)_3^+(AmO_2OH^+)$		0.26 ± 0.08	
UO_2F^+		0.29 ± 0.05	
UO_2Cl^+		0.31 ± 0.04	
UF_3^+		0.00 ± 0.05	
Mg^{2+}	0.19 ± 0.02	0.33 ± 0.03	0.17 ± 0.01
Ca^{2+}	0.14 ± 0.01	0.27 ± 0.03	0.02 ± 0.01
Ba^{2+}	0.07 ± 0.01	0.15 ± 0.02	-0.28 ± 0.03
Mn^{2+}	0.13 ± 0.01		
Co^{2+}	0.16 ± 0.02	0.34 ± 0.03	0.14 ± 0.01
Ni^{2+}	0.17 ± 0.02		
Cu^{2+}	0.08 ± 0.01	0.32 ± 0.02	0.11 ± 0.01

Table A2.2 (continued)

j ↓ k →	Cl^-	ClO_4^-	NO_3^-
Zn^{2+}		0.33 ± 0.03	0.16 ± 0.02
Cd^{2+}		0.09 ± 0.02	-0.02 ± 0.01
Hg_2^{2+}		0.09 ± 0.02	-0.02 ± 0.01
Hg^{2+}		0.34 ± 0.03	-0.01 ± 0.01
Pb^{2+}		0.15 ± 0.02	-0.20 ± 0.12
UO_2^{2+}	0.21 ± 0.02	0.46 ± 0.03	0.24 ± 0.03
$FeOH^{2+}$ ($AmOH^{2+}$) ($ThOH^{2+}$)		0.38	
$FeSCN^{2+}$		0.45	
$YHCO_3^{2+}$		0.39 ± 0.04	
UF_2^{2+}		0.03 ± 0.01	
$U(NO_3)_2^{2+}$		0.58 ± 0.13	
Al^{3+}	0.33 ± 0.02		
Cr^{3+}	0.30 ± 0.03		0.27 ± 0.02
Fe^{3+}		0.56 ± 0.03	0.42 ± 0.08
La^{3+} (Am^{3+})	0.22 ± 0.02	0.47 ± 0.03	
La^{3+} Lu^{3+}		0.47 0.52	
Be_2OH^{3+} ($ThOH^{3+}$)		0.50 ± 0.05	
$Be_3(OH)_3^{3+}$	0.30 ± 0.05	0.51 ± 0.05	0.29 ± 0.05
UCl^{3+}		0.79 ± 0.11	
UNO_3^{3+}		0.75 ± 0.10	

Table A2.2 (continued)

j ↓ k →	Cl^-	ClO_4^-	NO_3^-
Th^{4+}	0.25 ± 0.03		0.11 ± 0.02
U^{4+}		0.84 ± 0.10	
Np^{4+}		0.84 ± 0.10	
Pu^{4+}		1.03 ± 0.10	
An^{4+}		0.88 ± 0.14	
$Fe_2(OH)_2^{4+}$		0.82	
$Y_2CO_3^{4+}$		0.80 ± 0.04	

LAWRENCE BERKELEY LABORATORY
UNIVERSITY OF CALIFORNIA
INFORMATION RESOURCES DEPARTMENT
BERKELEY, CALIFORNIA 94720